

Chulalongkorn University

Chula Digital Collections

Chulalongkorn University Theses and Dissertations (Chula ETD)

2023

Evaluation of patient radiation dose and risk of cancer from CT examinations

Saowapark Poosiri
Faculty of Medicine

Follow this and additional works at: <https://digital.car.chula.ac.th/chulaetd>



Part of the [Radiation Medicine Commons](#), and the [Radiology Commons](#)

Recommended Citation

Poosiri, Saowapark, "Evaluation of patient radiation dose and risk of cancer from CT examinations" (2023). *Chulalongkorn University Theses and Dissertations (Chula ETD)*. 10321.
<https://digital.car.chula.ac.th/chulaetd/10321>

This Thesis is brought to you for free and open access by Chula Digital Collections. It has been accepted for inclusion in Chulalongkorn University Theses and Dissertations (Chula ETD) by an authorized administrator of Chula Digital Collections. For more information, please contact ChulaDC@car.chula.ac.th.

Evaluation of patient radiation dose and risk of cancer from CT examinations



Mrs. Saowapark Poosiri

A Dissertation Submitted in Partial Fulfillment of the Requirements

for the Degree of Doctor of Philosophy in Medical Physics

Department of Radiology

Faculty of Medicine

Chulalongkorn University

Academic Year 2023

การประเมินปริมาณรังสีและการประเมินความเสี่ยงของการเป็นมะเร็งในผู้ป่วยที่ตรวจด้วย
เครื่องเอกซเรย์คอมพิวเตอร์



วิทยานิพนธ์นี้เป็นส่วนหนึ่งของการศึกษาตามหลักสูตรปริญญาวิทยาศาสตรดุษฎีบัณฑิต
สาขาวิชาฟิสิกส์การแพทย์ ภาควิชารังสีวิทยา
คณะแพทยศาสตร์ จุฬาลงกรณ์มหาวิทยาลัย
ปีการศึกษา 2566

Thesis Title	Evaluation of patient radiation dose and risk of cancer from CT examinations
By	Mrs. Saowapark Poosiri
Field of Study	Medical Physics
Thesis Advisor	Associate Professor Anchali Krisanachinda, Ph.D.
Thesis Co Advisor	Assistant Professor Kitiwat Khamwan, Ph.D.

Accepted by the Faculty of Medicine, Chulalongkorn University in Partial
Fulfillment of the Requirement for the Doctor of Philosophy

..... Dean of the Faculty of Medicine
(Associate Professor Chanchai Sittipunt, M.D.)

DISSERTATION COMMITTEE

..... Chairman
(Professor Franco Milano, Ph.D.)

..... Thesis Advisor
(Associate Professor Anchali Krisanachinda, Ph.D.)

..... Thesis Co-Advisor
(Assistant Professor Kitiwat Khamwan, Ph.D.)

..... Examiner
(Associate Professor Yothin Rakvongthai, Ph.D.)

..... Examiner
(Assistant Professor Taweap Sanghangthum, Ph.D.)

..... External Examiner
(Professor Kosuke Matsubara, Ph.D.)

เสาวภาคย์ ภูศิริ : การประเมินปริมาณรังสีและการประเมินความเสี่ยงของการเป็นมะเร็งในผู้ป่วยที่ตรวจด้วยเครื่องเอกซเรย์คอมพิวเตอร์. (Evaluation of patient radiation dose and risk of cancer from CT examinations) อ.ที่ปรึกษาหลัก : รศ. ดร.อัญชลี กฤษณจินดา, อ.ที่ปรึกษาร่วม : ผศ. ดร.กิตติวัฒน์ คำวัน

การตรวจวินิจฉัยทางการแพทย์ด้วยเครื่องเอกซเรย์คอมพิวเตอร์ (ซีที) มีปริมาณการส่งตรวจที่เพิ่มมากขึ้น และเป็นสาเหตุหลักของการได้รับรังสีที่เพิ่มขึ้นของผู้ป่วย ความเสี่ยงของการเป็นมะเร็งจากการตรวจด้วยซีที ขึ้นอยู่กับปริมาณรังสีที่ผู้ป่วยได้รับ วัตถุประสงค์ของการศึกษานี้เพื่อประเมินปริมาณรังสีที่ผู้ป่วยได้รับและความเสี่ยงของอุบัติการณ์การเป็นมะเร็งและเสียชีวิตด้วยโรคมะเร็งจากการตรวจด้วยซีทีหลายครั้งในวันเดียวกัน ข้อมูลถูกรวบรวมจากผู้ป่วยที่มีอายุ 15 ถึง 75 ปีที่ได้รับการตรวจด้วยซีที ในระยะเวลาห้าปีตั้งแต่เดือน มกราคม 2018 ถึงเดือน ธันวาคม 2022 จากสองโรงพยาบาลที่เป็นโรงเรียนแพทย์ การประเมินปริมาณรังสียังผลสะสมและปริมาณรังสีที่อวัยวะต่างๆได้รับโดย Radimetrics™ Enterprise Platform ซึ่งจำลองข้อมูลผู้ป่วยด้วยวิธี มอนติ คาร์โล ความเสี่ยงของการเป็นมะเร็ง คำนวณจากรายงานของ Biological Effects of Ionizing Radiation VII (BEIR VII) ซึ่งใช้ค่าปริมาณรังสีที่อวัยวะต่างๆได้รับ, เพศ, อายุที่ได้รับการตรวจด้วยซีที, อายุที่นับปลายชีวิต, และสถิติประชากรของประชากรไทย อัตราการเกิดมะเร็งโดยไม่ได้รับรังสีและข้อมูลความน่าจะเป็นในการมีชีวิต จำนวนผู้ป่วย ที่ได้รับปริมาณรังสียังผลสะสมมากกว่าหรือเท่ากับ 100 มิลลิซีเวิร์ต ในหนึ่งวัน จากการตรวจด้วยซีที มีจำนวน 27 คน, เท่ากับ 0.009 เปอร์เซ็นต์ของจำนวนผู้ป่วย 285,286 ราย ค่าความเสี่ยงสูงสุดของอุบัติการณ์การเป็นมะเร็งในสตรีที่อายุน้อย ได้แก่ มะเร็งเต้านมคือ 82 ต่อ 100,000 คน ปริมาณรังสีที่ด้านมมีค่า 148 มิลลิเกรย์ จากการตรวจด้วยซีทีของช่องท้อง ค่าความเสี่ยงสูงสุดของอุบัติการณ์การเป็นมะเร็งในผู้ชายได้แก่ มะเร็งตับคือ 72 ต่อ 100,000 คน ปริมาณรังสีที่ตับมีค่า 133 มิลลิเกรย์ จากการตรวจซีทีหลายส่วน ที่ปริมาณรังสีต่ำ ค่าความเสี่ยงของอุบัติการณ์การเป็นมะเร็ง ได้แก่ มะเร็งเต้านมในสตรีที่อายุน้อยคือ 23 ต่อ 100,000 คน ในขณะที่ความเสี่ยงการเกิดมะเร็งตับในผู้ชายคือ 22 ต่อ 100,000 คน จากการตรวจหลอดเลือดแดงใหญ่ แม้ว่าความเสี่ยงของอุบัติการณ์การเป็นมะเร็งและการเสียชีวิตจากการเป็นมะเร็งจะน้อยกว่า 100 ต่อ 100,000 คนก็ตาม ไม่ควรละเลยเพราะความเสี่ยงของการเกิดมะเร็งอาจเพิ่มขึ้นในบั้นปลายของชีวิต โดยเฉพาะในผู้ป่วยที่อายุน้อย อายุของผู้ป่วยขณะรับการตรวจด้วยซีที มีความสัมพันธ์เชิงลบกับการเป็นมะเร็งสูงอย่างมีนัยสำคัญทางสถิติ, $p < 0.05$.

สาขาวิชา พัลลิสการแพทย์
ปีการศึกษา 2566

ลายมือชื่อ นิสิต
ลายมือชื่อ อ.ที่ปรึกษาหลัก
ลายมือชื่อ อ.ที่ปรึกษาร่วม

6371013730 : MAJOR MEDICAL PHYSICS

KEYWORD: Computed Tomography, Radiation dose and cancer risk, Cumulative Effective Dose

Saowapark Poosiri : Evaluation of patient radiation dose and risk of cancer from CT examinations. Advisor: Assoc. Prof. Anchali Krisanachinda, Ph.D. Co-advisor: Asst. Prof. Kitiwat Khamwan, Ph.D.

Computed Tomography (CT) examinations have been increasingly requested and become the major sources of patient exposure. The cancer risk from CT scans is contingent upon the amount of organ absorbed dose. This study aims to evaluate the cumulative effective doses (CED) and risk of cancer incidence and mortality from recurrent CT examinations in a single day. The patient data at aged 15 to 75 years old performed CT examinations during the period of five years from January 2018 to December 2022 were collected from two academic centers. The CED and organ doses were evaluated using Radimetrics™ Enterprise Platform from Monte Carlo simulations. Lifetime attributable risk (LAR) was determined following Biological Effects of Ionizing Radiation (BEIR) VII Phase 2 report based on the organ dose, gender, age at exposure, attained age, and demographic statistics of the Thai population (baseline rate of cancer and survival probability data). The number of patients who underwent CT examinations receiving CED 100 mSv and above in a single day was 27, accounting for 0.009 percent of 285,286 CT examinations. The highest LAR for breast cancer incidence in young female was 82 per 100,000 exposed patients with the breast dose of 148 mGy from CT whole abdomen. The highest LAR for liver cancer incidence in male patient was 72 per 100,000 with liver dose of 133 mGy from multiple CT scans. At low dose, the highest LAR for breast cancer incidence in young female was 23 per 100,000 while for liver cancer incidence in male patients was 22 per 100,000 from CTA whole aorta. Even though the LAR of cancer incidence and mortality was less than 100 per 100,000, they should not be neglected, particularly in young patients. The risk of cancer incidence could be increased in later life. The patient age at exposure has a strong negative correlation with LAR for cancer incidence and the statistically significant, $p < 0.05$.

Field of Study: Medical Physics

Academic Year: 2023

Student's Signature

Advisor's Signature

Co-advisor's Signature

ACKNOWLEDGEMENTS

I would like to express my sincere gratitude and appreciation to Assoc. Prof. Anchali Krisanachinda, Ph.D., my thesis advisor, who provided the valuable guidance, inspire me on the research study, consistently support and advise me with unwavering kindness.

My appreciation would be expressed to Asst. Prof. Kitiwat Khamwan, Ph.D., for his kind suggestion and continuous encouragement for my research study.

I would like to express my gratitude to Assoc. Prof. Sivalee Suriyapee for recognizing the value of the research topic and providing support for me to conduct this research work.

I would like to express my gratitude to Professor Franco Milano, Ph.D., who is the Chairman of the dissertation defense, as well as Prof. Kosuke Matsubara, Ph.D., the external examiner, for providing valuable suggestions and comments on this research.

I would like to express my great appreciation to the thesis committees, Assoc. Prof. Yothin Rakvongthai, Ph.D., and Asst. Prof. Taweap Sanghangthum, Ph.D., for their guidance and comments on this research.

I greatly appreciate Sornjarod Oonsiri Ph.D., for providing valuable guidance and knowledge on the Glass dosimeter.

I would like to thank Miss Jirawan Jayuphan and Alan Frederick Geater, Ph.D., Department of Epidemiology, Faculty of Medicine, Prince of Songkla University, for their guidance in the statistical analysis.

I sincerely thank the Department of Radiology, Faculty of Medicine, Prince of Songkhla University for providing scholarship support as well as the scholarship provided by Chulalongkorn University.

Finally, I would like to express my gratitude to my beloved family—my parents and my husband—for providing encouragement and comforting me during my doctoral study.

Saowapark Poosiri

TABLE OF CONTENTS

	Page
ABSTRACT (THAI)	iii
ABSTRACT (ENGLISH)	iv
ACKNOWLEDGEMENTS	v
TABLE OF CONTENTS	vi
LIST OF TABLES	xii
LIST OF FIGURES	xv
LIST OF ABBREVIATIONS AND SYMBOLS	xviii
CHAPTER 1	1
INTRODUCTION	1
CHAPTER 2	6
REVIEW OF RELATED LITERATURE	6
2.1 Theory	6
2.1.1 Sources of radiation exposure	6
2.1.2 Radiation dose quantities	7
2.1.2.1 Exposure	8
2.1.2.2 Absorbed dose	8
2.1.2.3 Equivalent dose	9
2.1.2.4 Effective dose	9
2.1.2.5 Organ dose	10
2.1.2.5.1 Mathematical models to calculate organ dose	10
2.1.2.5.2 Dose monitoring software	12

2.1.3 Computed Tomography	14
2.1.3.1 Historical development of CT scanners	14
2.1.3.2 Clinical applications of CT	15
2.1.3.3 CT dose measurement.....	18
2.1.3.3.1 Computed Tomography Dose Index (CTDI) [3, 22].....	19
2.1.3.3.2 Dose length product (DLP).....	20
2.1.4 Biological effects of ionizing radiation	20
2.1.4.1 Deterministic and stochastic responses	20
2.1.4.2 Radiation-Induced carcinogenesis.....	21
2.1.4.2.1 Burden of cancer	21
2.1.4.2.2 Source of epidemiological data [12].....	23
2.1.4.2.3 CT radiation risk.....	24
2.1.5 Cancer risk models	25
2.1.6 Dose-Response Models	26
2.1.7 BEIR VII report on cancer risk models	31
2.1.7.1 Multiplicative and Additive Risk Models	32
2.1.7.2 Models for estimating cancer risks	33
2.1.7.2.1 Models for estimating all solid cancer risks	34
2.1.7.2.2 Models for female breast cancer	36
2.1.7.3 Lifetime attributable risk (LAR)	37
2.2. Review of related literature	40
CHAPTER 3	44
RESEARCH METHODOLOGY	44

3.1 Research hypothesis	44
3.2 Research questions	44
3.3 Research objectives	45
3.4 Scope of work	45
3.5 Research design	46
3.6 Conceptual framework	46
3.7 Research design model	47
3.8 Expected benefit	48
3.9 Variable measurements	48
3.10 Data collection	48
3.11 Outcome	49
3.12 Statistical analysis	49
3.13 Ethical Consideration	49
CHAPTER 4	52
MATERIALS AND METHODS	52
4.1 Materials	52
4.1.1 Verification of displayed $CTDI_{vol}$	53
4.1.2 Verification of organ dose	54
4.1.3 Patient study: Lifetime attributable risk (LAR)	58
4.2 Methods	61
4.2.1 Verification of displayed $CTDI_{vol}$	61
4.2.2 Verification of organ dose	62

4.2.3 Comparison of the organ dose in Rando phantom and Radimetrics™ Enterprise Platform.....	64
4.2.4 Determination of the Lifetime attributable risk (LAR) of patients	66
4.3 Sample population	70
4.3.1 Target population	70
4.3.2 Sample size determination	70
4.3.3 Sample population and eligible criteria	70
4.4 Statistical analysis	71
CHAPTER 5	72
RESULTS	72
5.1 Verification of the displayed CTDI _{vol}	72
5.2 Verification of organ dose	73
5.3 Comparison of organ doses from measurements and Radimetrics	74
5.4 Patient study on CT examinations	75
5.4.1 Patient radiation dose from CT examinations with CED 100 mSv and above	75
5.4.2 Patient radiation dose from CT examinations with CED below 100 mSv	81
5.4.3 Lifetime attributable risk (LAR) at 5 organs for incident and mortality cancers in high dose.....	82
5.4.4 Lifetime attributable risk (LAR) at 6 organs for incident and mortality cancers in low dose	86
5.4.5 LAR, organ dose and related patient parameters in common CT protocols	88
5.4.6 Risk Model for incident cancer risk from CTA examinations	94
CHAPTER 6	99

DISCUSSION	99
6.1 Verification of the displayed CTDI _{vol}	99
6.2 Verification of organ dose	99
6.3 Patient study on CT examinations	102
6.3.1 Patient radiation dose from CT examinations with CED 100 mSv and above	102
6.3.2 Patient radiation dose from CT examinations with CED below 100 mSv ...	104
6.3.3 Lifetime attributable risk (LAR) at 5 organs for incident and mortality cancers in high dose	105
6.3.4 Lifetime attributable risk (LAR) at 6 organs for incident and mortality cancers in low dose	106
6.3.5 LAR, organ dose and related patient parameters in common CT protocols	109
6.3.6 Risk Model for incident cancer risk from CTA examinations	111
6.4 Limitations	111
CHAPTER 7	113
CONCLUSION	113
RECOMMENDATIONS	116
REFERENCES	117
APPENDIX I	123
Quality Control of Multi-Detector Computed Tomography System	123
APPENDIX II	131
Measurement process of RPLGDs	131
Calibration of RPLGDs	132

APPENDIX III	135
Lifetime attributable risk (LAR).....	135
VITA	150



LIST OF TABLES

Table 2.1: Tissue weighting factors according to ICRP 103	10
Table 2.2: Definition of UNSCEAR DDREF and LSS DDREF ^a	30
Table 2.3: Risk transfer approaches adopted by international organizations.	33
Table 2.4: Summary of BEIR VII preferred risk models	34
Table 2.5: Parameter values for risk models in BEIR VII	35
Table 4.1: Specifications of RPLGD model GD-352M.....	55
Table 4.2: CT scanners at King Chulalongkorn Memorial Hospital	58
Table 4.3: CT scanners at Songklanagarind Hospital.....	58
Table 4.4: 90 RPLGDs inserted in each tissue or organ.	64
Table 4.5: Acquisition parameters and radiation dose for chest and abdomen CT examinations.....	65
Table 5.1: Measured and displayed CTDI _{vol} on the Siemens CT monitor in head and body phantoms.....	72
Table 5.2: Measured and displayed CTDI _{vol} on the GE CT monitor in head and body phantoms.	72
Table 5.3: Measured and displayed CTDI _{vol} on the Canon CT monitor in head and body phantoms.....	73
Table 5.4: Air kerma measurement from 100 RPLGDs	73
Table 5.5: Comparison of organ doses using RPLGD measurement and Radimetrics ..	74
Table 5.6: Patient demography and radiation dose from CT examinations in young patients with the high dose	77

Table 5.7: Patient demography and radiation dose from CT examinations in elder patients with the high dose	77
Table 5.8: Patient demography and organ dose from CT examinations in young patients with the high dose	78
Table 5.9: Patient demography and organ dose from CT examinations in elder patients with the high dose	79
Table 5.10: Patient demography and CED (mSv) from common CT protocols	81
Table 5.11: Mean organ dose (mGy) in common CT protocols from all patients.....	82
Table 5.12: LAR of cancer incidence and mortality from CT examinations for each young patient.....	84
Table 5.13: LAR of cancer incidence and mortality from CT examinations to 7 young patients	84
Table 5.14: LAR of cancer incidence and mortality from CT examinations to 20 elder patients	85
Table 5.15: LAR of cancer incidence and mortality from CT whole abdomen with the high dose.....	85
Table 5.16: Lifetime attributable risk per 100,000 of cancer incidence and mortality of the young patients with both genders in common CT protocols.....	86
Table 5.17: Lifetime attributable risk per 100,000 of cancer incidence and mortality of the elder patients with both genders in common CT protocols	87
Table 5.18: Correlation of patient parameters and LAR in common CT protocols	88
Table 5.19: Correlation of LAR for lung cancer incidence and patient parameters: CT Chest examination	89
Table 5.20: Correlation of LAR for breast cancer incidence and patient parameters: CT Chest examination	89

Table 5.21: Correlation of LAR for liver cancer incidence and patient parameters: CT Abdomen examination	90
Table 5.22: Correlation of LAR for colon cancer incidence and patient parameters: CT Abdomen examination	90
Table 5.23: Correlation of LAR for uterus cancer incidence and patient parameters: Abdomen examination	91
Table 5.24: Correlation of LAR for lung cancer incidence and patient parameters: CTA whole aorta examination.....	91
Table 5.25: Correlation of LAR for liver cancer incidence and patient parameters: CTA whole aorta examination.....	92
Table 5.26: Correlation of LAR for colon cancer incidence and patient parameters: CTA whole aorta examination.....	92
Table 5.27: Correlation of LAR for breast cancer incidence and patient parameters: CTA whole aorta examination.....	93
Table 5.28: Correlation of LAR for uterus cancer incidence and patient parameters: CTA whole aorta examination.....	93
Table 5.29: Univariate linear regression of LAR for lung cancer incidence	96
Table 5.30: Multiple linear regression of LAR for lung cancer incidence	96
Table 6.1: Comparison of the organ doses from Iriuchijima A et al. and our study	100
Table 6.2: Comparison of the organ doses from Guberina N et al. and our study	101
Table 6.3: Correlation of LAR for lung cancer incidence and age at exposure	110
Table 6.4: Correlation of LAR for lung cancer incidence and organ dose	110

LIST OF FIGURES

Figure 2.1: Distribution of the annual percentage of examinations from various imaging modalities in 2009-2018	7
Figure 2.2: Distribution of percentage annual collective effective dose from various imaging modalities in 2009-2018	7
Figure 2.3: Different phantoms implemented in CT-Expo, NCICT, NCICTX, and Virtual Dose [25]	12
Figure 2.4: The stylized phantom and the scan region	13
Figure 2.5: CT image reconstruction techniques	15
Figure 2.6: The patient underwent an abdominal multiphase CT scan [29].	16
Figure 2.7: Diagnosis for Patient A: squamous cell carcinoma; Patient B: non-small cell lung cancer [30]	17
Figure 2.8: Imaging of aortic syndromes including aortic dissection, aortic intramural hematoma, and aortic ulcer [35].	18
Figure 2.9: Global estimate of the number of new cancer cases in 2020 [5].	22
Figure 2.10: The number of new cancer cases in Thailand, 2020	22
Figure 2.11: Possible dose response relationship for radiation-induced cancer and radiation dose [6]	27
Figure 2.12: Dose-response assessment [12]	28
Figure 2.13: Dose-response models of ERR for solid cancer (Left) and leukemia (Right) from cancer incidence data of Japanese A-bomb survivors [6].	30
Figure 2.14: Multiplicative (A) and additive (B) risk models [6]	32
Figure 3.1 The Institutional Review Board (IRB) Certificate, Faculty of Medicine, Chulalongkorn University.	50

Figure 3.2: The Institutional Review Board (IRB) Certificate,	51
Figure 4.1: PMMA head phantom 16 cm (left) and body phantom 32 cm diameters (right).	53
Figure 4.2: Pencil-type ionization chamber RaySafe X2 CT Detector and the electrometer	54
Figure 4.3: Radio-photoluminescence Glass Dosimeter (RPLGD), model GD-352M with filters in capsule (Left), Glass rod (Right)	55
Figure 4.4: Laboratory oven (Carbolite Gero), (Left) and glass dosimeter reader (FGD-1000), (Right)	56
Figure 4.5: Female anthropomorphic Rando phantom (Left), Slab of lung phantom with holes for RPLGD insertion (Right)	56
Figure 4.6: A 6-cc ion chamber Model 10X6-6 and Radcal 9096 electrometer	57
Figure 4.7: Siemens Healthineers radiographic system.....	57
Figure 4.8: The organ dose estimated by the dose monitoring software, Radimetrics™ Enterprise Platform (Bayer HealthCare, Whippany, NJ, USA).....	59
Figure 4.9: The baseline rate of cancer provided by CANCER TODAY, WHO	60
Figure 4.10: Measurement process of RPLGDs	63
Figure 4.11: Set the SDD for the ionization chamber and RPLGDs at 150 cm for the calibration.	64
Figure 4.12: R Studio library development	69
Figure 5.1: Air kerma measurement from 100 RPLGDs	74
Figure 5.2: The comparison of 5 organ doses measured by RPLGD and calculated by Radimetrics.....	75

Figure 5.3: 27 patients with high CED in a single day (15 females and 12 males).	76
Figure 5.4: Organ doses obtained from CT abdomen examination in six patients.	80
Figure 5.5: LAR for incidence (top) and mortality (bottom) of 5 cancer sites from high CT dose for both genders among 27 patients.	83
Figure 5.6: The normal distributed square root form of LAR (Top) and dose in the lung (Bottom)	95
Figure 5.7: Kernel density estimation of residuals follow normal distribution in multiple linear regression analysis (Blue)	97
Figure 5.8: Two-way scatterplot with a linear regression line of LAR for lung cancer incidence	97
Figure 6.1: RPLGDs were inserted into the holes along the central axis of the lungs...	102
Figure 6.2: LAR for lung cancer incidence from CT chest examination	107
Figure 6.3: The LAR for lung cancer incidence per 100,000 persons (BEIR VII)	108
Figure 6.4: LAR for colon cancer incidence from CT abdomen examination	108
Figure 6.5: The LAR for colon cancer incidence per 100,000 persons (BEIR VII)	109

LIST OF ABBREVIATIONS AND SYMBOLS

AR	Absolute risk
BEIR	Biological Effects of Ionizing Radiation
BW	Body Weight
CED	Cumulative effective dose
CI	Confidence Interval
CT	Computed Tomography
CTA	Computed Tomography Angiography
CTDI	Computed tomography dose index
CTDI _{vol}	Volume computed tomography dose index
CTDI _w	Weighted computed tomography dose index
DDREF	Dose and dose rate effectiveness factor
DICOM	Digital Imaging and Communications in Medicine
DLP	Dose-length product
D _{organ}	Dose to a particular organ
E	Effective dose
EAR	Excess absolute risk
ECG	Electrocardiography
EPA	Environmental Protection Agency
ERR	Excess relative risk
H _T	Equivalent dose of tissue
IC	Ionization chamber
ICRP	International Commission on Radiological Protection
ICRU	International Commission on Radiological Units and Measurements
kVp	Kilovoltage Peak
LAR	Lifetime attributable risk

LET	Linear Energy Transfer
LNT	Linear no threshold
LSS	Life Span Study
mAs	milliampere seconds
MC	Monte Carlo
MDCT	Multi-Detector Computed Tomography
mGy	milliGray
mGy.cm	milliGray-centimeter
MPR	Multiplanar reconstruction
mSv	milliSievert
NCRP	National Council on Radiation Protection and Measurements
NUREG	Nuclear Regulatory
PMMA	Polymethyl methacrylate
RDMS	Radiation Dose Monitoring Software
RDSR	Radiation Dose Structured Report
REP	Radimetrics™ Enterprise Platform
RERF	Radiation Effects Research Foundation
RPLGD	Radio-Photoluminescence Glass Dosimeter
RR	Relative Risk
SEER	Surveillance, Epidemiology, and End Results
SPR	Scan projection radiographs
UNSCEAR	United Nations Scientific Committee on the Effects of Atomic Radiation
WED	Water equivalent diameter
WHO	World Health Organization
w_R	Radiation weighting factor
w_T	Tissue weighting factor
μ_{en}/ρ	Mass energy absorption coefficients

CHAPTER 1

INTRODUCTION

The man-made source of ionizing radiation continues to be the most common applications of radiation in medicine, especially in diagnostic imaging modalities including radiography, fluoroscopy, computed tomography (CT), mammography, and interventional radiology [1-3]. The United Nations Scientific Committee on the Effects of Atomic Radiation (UNSCEAR) 2020/2021 [4] reported the distribution of examinations and radiation dose by diagnostic imaging modality worldwide. CT accounts for the majority of radiation exposure related to medical imaging. From 2009 to 2018, CT had been contributed 9.6 percent of all modalities, and the collective effective dose was 61.6 percent.

The National Council on Radiation Protection and Measurements (NCRP) publication 184 [1] reported the trend of CT procedures in the US increased by 20 percent per year. CT examinations had risen consistently since 1993 from 18.3 million, reaching a peak of 85.3 million in 2011 and then stabilizing, slightly decreasing to 73.8 million procedures in 2017. In 2016, the majority of CT examinations were as follows: 26.3 percent for abdomen/pelvis, 18.9 percent for brain, 15.9 percent for chest, and 15.5 percent for angiography-non cardiac. The remaining examinations include neck, spine, extremities, cardiac, and miscellaneous, accounted for 23.4 percent [1, 2]. The evolution of CT systems provided good quality imaging, fast gantry rotation time, and high temporal resolution and became an essential examination for diagnosis in symptomatic patients or screening of asymptomatic patients and follow-up of the disease [3].

Cancer is one of the largest health problems in the world and the leading cause of mortality worldwide. In 2020, the number of cancer mortality was about 9,958,133,

and the new cases of cancer, cancer incidence, was 19,292,789 [4]. Nevertheless, cancer is also the leading cause of death in Thailand. The risk of mortality cancer was 10.2 percent at the age of 75 years old and earlier, while the risk of incidence cancer was 16.4 percent at the age of 75 years old and earlier [5]. The top five of most frequent cancers were lung, liver, breast, colorectal, and cervix uteri [4, 5], excluding non-melanoma skin cancer. Although the causes of the majority of cancers are not well defined, genetic or family history, and lifestyle behavior such as smoking, poor diet, physical inactivity, alcohol, environment, and ionizing radiation appear to be among the significant factors that influence cancer risk [6].

The biological effects of ionizing radiation include the deterministic and stochastic effects. Deterministic effects are observed at the doses above a threshold, with the severity of the effect being greater for a higher dose, such as skin burn and cataracts. The stochastic effects or long-term effects have no threshold, and the severity of the effect is independent of the radiation dose, such as carcinogenesis and genetic effects [7]. The most significant concern in diagnostic imaging is cancer incidence, which occurs many years after exposure. For example, the latent periods of leukemia and solid cancer are 2 and 5 years after exposure respectively. As evidence after the nuclear accidents, those who received radiation exposure resulted in long-term health impacts or cancer [8]. The significant impact of the expansion of imaging procedures, the number of examinations, and the frequency of repeated imaging led to a high cumulative effective dose and increased cancer risk, especially in children and young adult patients [10-12]. The risk of radiation-induced cancer is dependent on the age at exposure, gender, the type of examinations, as well as the organs absorbed dose [12-14]. The BEIR VII affirmed the linear no-threshold model (LNT), which is the association between low-dose exposure and the incidence of solid cancers that are induced by ionizing radiation. The LNT model could be used in radiation protection to estimate

cancer risk, even the small amount of radiation could increase the risk of cancer in later life [7-10].

Risk models had been developed to estimate the risk of radiation-induced cancer incidence and mortality for solid cancer and leukemia. NUREG (1993) developed the risk model based on the assumption that the risk is proportional to the risk coefficient and dose, while BEIR VII (2006), UNSCEAR (2006), ICRP103 (2007), and U.S.EPA (2011) derived the epidemiological data, primary from Japanese atomic bomb survivors [8, 10, 11].

BEIR VII report classified low dose range from close to zero to 100 mSv, and the high dose from more than 100 mSv. Several publications reported that the risk of cancer from ionizing radiation is dependent on the organ dose [1, 2, 19, 20]. At low dose, radiation risk is associated with stochastic effect or cancer induction based on epidemiological data from Japanese atomic bomb survivors. Cancer risks were determined based on either excess relative risk model (ERR) or excess absolute risk model (EAR) adjusted for age at exposure, attained age, gender and organ dose (mGy). The cancer risk assessment of solid cancer incidence and mortality for low LET radiation was derived from the study of acute exposure at high dose and dose rates, then extrapolated to lower dose and dose rates. Consequently, the risk model embedded within the correction factor, the dose and dose-rate effectiveness factor (DDREF). DDREF represents the ratio between risks at high-dose or high-dose rates and low-dose or low-dose rates, BEIR VII report proposed a DDREF of 1.5 [8, 11, 12].

Many publications showed the risk of cancer from various CT protocols, such as the abdomen, chest, head, and heart, were estimated by linear interpolation method as described in BEIR VII table 12D-1,2 [9, 13, 14]. Lim H et al. [15] determined the risk of cancer incidence and mortality from medical radiation imaging using Korean background cancer incidence and mortality. Harbron RW et al. [16] reported cancer

risks attributable to radiation exposure from cardiac catheterizations based on UK background cancer rates. A few studies reported LAR applied to the population based on life table and baseline cancer rate receiving high to low radiation dose [15-18].

The Radiation Effects Research Foundation (RERF) in Japan reported solid cancer has been found in 60 percent of survivors receiving radiation dose less than 100 mSv. In addition, the risk of cancer incidence increased linearly in high dose range when the effective dose exceeded 100 mSv [1, 18-21]. The cumulative effective dose (CED) of 100 mSv and above in a single day become more evidence, particularly from the CT scan of the chest, whole abdomen, and CT angiography [15, 22-24].

The radiation dose from CT scan delivered to the patient should be estimated as several internal organs are sensitive to radiation and the risk of cancer increased. The CED at 100 mSv and above should be investigated in the patients with the recurrent CT examinations. Therefore, the primary objective of this study is to determine the number of patients receiving the CED from recurrent CT examinations at 100 mSv and above in a single day, to identify the procedures, patient characteristics, to estimate the cancer risk and determine factors influenced the risk of cancer using BEIR VII models, based on the organ dose, gender, age at exposure, attained age, and demographic statistics of the Thai population (baseline rate of cancer and survival probability data). The findings of the study lead to quantify the risk of cancer from recurrent CT in Thai patients. The factors affecting the risk of cancer can be used for the justification and optimization of the radiation protection in the recurrent CT patients.

Common CT examinations such as brain, chest, whole abdomen, including CTA whole aorta have been increasingly requested in recent years. The prevalence of the vascular disease has increased significantly worldwide, similar to Thai population. Computed Tomography Angiography (CTA) is commonly used to assess aortic disorders, e.g., dissection or aneurysm, and follow-up patients after surgery or

endovascular aortic repair. Aortic disease has become an established treatment modality with a lifelong follow-up by using CT scan. The recommended standard CTA protocol for follow-up with patients after surgery or endovascular aortic repair is at monthly and then annually for life. Furthermore, the CTA of the whole aorta encompasses several radiosensitive organs in thoracic and abdominal regions such as the lung, breast, red bone marrow, colon, and stomach [7]. Regarding preliminary data gathered from CTA of the whole aorta at King Chulalongkorn Memorial Hospital and Songklanagarind Hospital, the mean effective dose was approximately 30 mSv during the year 2018 to 2022. Even though CT shows many advantages to the patients, the radiation exposure from the recurrent CT is associated with the risk of cancer in the long-term [25-27].

The secondary objectives of this study are to investigate the risk of incidence and mortality cancer using BEIR VII models of patients who underwent common CT protocols, especially CTA whole aorta examination. In addition, to determine parameters that influence radiation dose and risk of cancer based on demographic statistics of the Thai and develop mathematics model/equation to estimate the cancer risk from CTA of an individual patient.

CHAPTER 2

REVIEW OF RELATED LITERATURE

2.1 Theory

2.1.1 Sources of radiation exposure

Human beings are exposed to ionizing radiation from various sources, including background radiation, building materials, medical procedures, consumer products and activities, industrial, educational, and research. The average annual exposure worldwide to natural radiation sources ranges from 1-10 mSv. Radon gas is the primary contributor to background radiation in the United States [1, 8]. UNSCEAR 2006 reported the distribution of annual effective dose per-capita from several sources in the US. The total average annual effective dose per capita from all sources was approximately 5.6 mSv [2].

The majority of radiation exposure of the population, approximately half of the US was attributable to medical exposure, with an annual per capita effective radiation dose value of 3 mSv, and natural background radiation, at 2.4 mSv and approximately 0.14 mSv was from other sources [19]. In the years 2009–2018, the frequency in percentage of conventional diagnostic radiology was 62.6, dental radiology 26.2, CT 9.6, diagnostic nuclear medicine 1.0, and interventional radiology 0.6 of all examinations, as shown in Figure 2.1. The percentage of annual collective effective dose from conventional diagnostic radiology was 23, dental radiology contributed only 0.2, CT accounted for 61.6, while diagnostic nuclear medicine and interventional radiology made up 7.2 and 8.0, respectively [20], as displayed in Figure 2.2.

Although the technological improvement of CT scanners has reduced the radiation dose of individual examinations, the benefit was obtained by the rapid increase of CT examinations. The widespread use of and high contribution of exposure to

medical radiation have raised concerns about potential health risks from CT examinations [21].

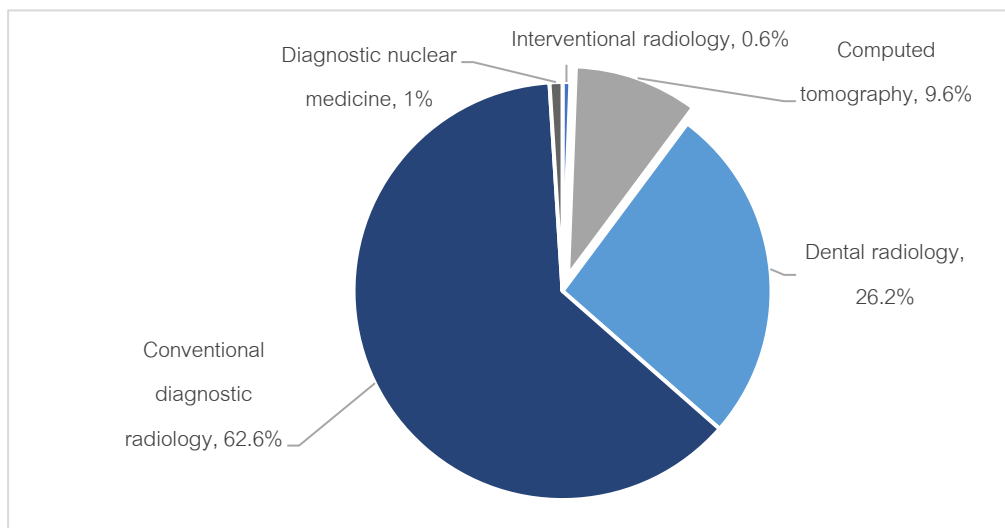


Figure 2.1: Distribution of the annual percentage of examinations from various imaging modalities in 2009-2018

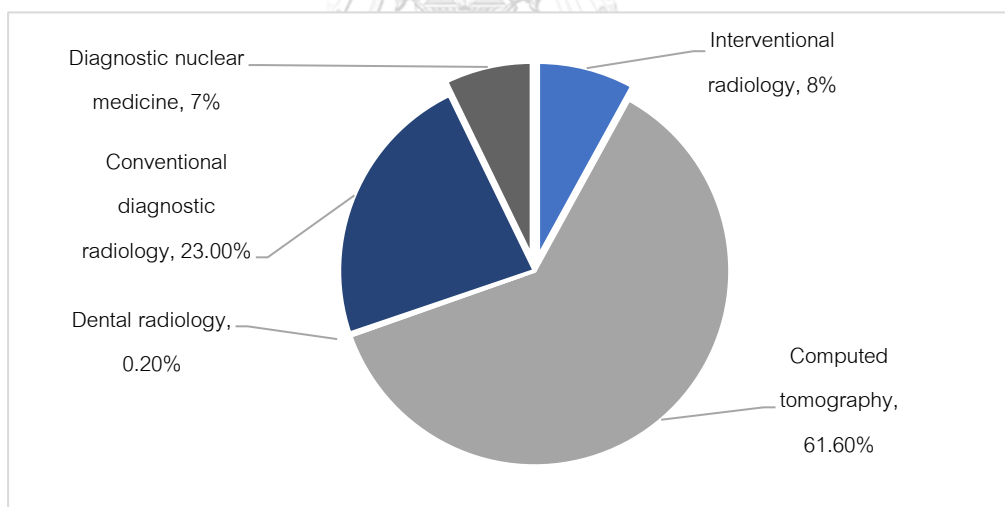


Figure 2.2: Distribution of percentage annual collective effective dose from various imaging modalities in 2009-2018

2.1.2 Radiation dose quantities

The radiation doses to particular organs from CT examination are determined by several factors. The most important are the number of scans, the tube current and scanning time in milliamperere-seconds (mAs), the size of the patient, the axial scan

range, the scan pitch (the degree of overlap between adjacent CT slices), the kilovoltage peaks (kVp), and the specific design of the scanner being used [3]. The following radiation dose quantity and unit will be defined.

2.1.2.1 Exposure

Exposure, X , is defined by the ICRU as the quotient of dQ by dm as in equation 2.1. dQ is the absolute value of the total charge of the ions of one sign produced in air when all the electrons liberated by photons in air of mass, (dm) are completely stopped in air.

$$X = \frac{dQ}{dm} \quad (2.1)$$

Exposure is expressed in the units of charge per mass, coulombs per kg. Exposure is a useful quantity because ionization can be directly measured with air-filled radiation detectors, and the effective atomic numbers of air and soft tissue are approximately the same. Thus, exposure is nearly proportional to dose in soft tissue over the range of photon energies commonly used in radiology. However, the quantity of exposure is limited because it only applies to the interaction of ionizing photons in air [6].

2.1.2.2 Absorbed dose

The quantity absorbed dose, D , is defined as the ratio of the energy, dE , imparted by ionizing radiation per unit mass of irradiated material, dM as in equation (2.2):

$$D = \frac{dE}{dM} \quad (2.2)$$

The SI unit of absorbed dose is gray. Absorbed dose is defined for all types of ionizing radiation, direct and indirect. The absorbed dose would equal the KERMA if the energy imparted to charged particles is deposited locally and the bremsstrahlung produced by the energetic electrons is negligible. For X-rays and gamma rays, the

absorbed dose is calculated from the mass energy absorption coefficient and the energy fluence of the beam.

2.1.2.3 Equivalent dose

Different types of ionizing radiation can produce different magnitudes of stochastic effects or biological damage for the same value of the absorbed dose. For a single type of radiation, R , the equivalent dose, H_T , is the product of a radiation weighting factor, w_R , for radiation R and the organ dose, D_T . For High LET radiations that produce dense ionization tracks cause more biologic damage per unit dose than low LET radiations. High LET has the potential to induce the probability of stochastic effects such as cancer, and therefore assigns a higher radiation weight factor, e.g., w_R of alpha particles at 20 [6, 22]. The SI unit for the equivalent dose is expressed in joule per kilogram with the special name of the Sievert (Sv), as defined by the equation (2.3):

$$H_T = w_R D_{T,R} \quad (2.3)$$

2.1.2.4 Effective dose

The effective dose, E , (Sv) has been defined as a measured of the combined detriment arising from stochastic effects for all organs and tissues in the whole body of an average-sized adult. Effective dose is the sum over all the organs and tissues of the body of the product of the equivalent dose, H_T , to the organ or tissue and a tissue weighting factor, w_T , for that organ or tissue. E is defined as in equation (2.4)

$$E = \sum w_T H_T \quad (2.4)$$

ICRP Publication 103 determined tissue weighting factors [7] (Table 2.1) based on population studies on cancer induction and genetic effects, which are averaged over age and sex for a particular population. The effective dose applies to a population, not to a specific individual and should not be used as the patient's dose for assigning risk. Therefore, the effective dose should not be implemented directly to estimate the

detriment of individual medical exposures. However, effective doses are beneficial in comparing procedures with different exposure parameters or populations [6-8, 22].

Table 2.1: Tissue weighting factors according to ICRP 103

Tissue or organ	Tissue weighting factor (w_T)	$\sum w_T$
Bone marrow, colon, lung, stomach, breast, remainder tissues	0.12	0.72
Gonads	0.08	0.08
Bladder, esophagus, liver, thyroid	0.04	0.16
Bone surface, brain, salivary glands, skin	0.01	0.04

2.1.2.5 Organ dose

According to an epidemiological study of the radiation-induced cancer risk for patients undergoing CT examinations, it is essential to estimate the organ dose. The term organ dose can refer to the mean absorbed dose into a particular organ or tissue. Organ dose is computed in unit of mGy and is significantly affected by the anatomy of the patient, the scan region, and the scanner output. The mean absorbed organ dose (D_T) in the specified tissue or organ is determined by the ratio of the energy imparted to the tissue or organ and the mass of the tissue or organ, representing an estimate of the average damage to the organ per unit mass [22]. Organ dose cannot be measured directly on living tissues or organs, but it can be determined using Monte Carlo (MC) methods and anatomically realistic computational anthropomorphic phantoms to simulate CT scans.

2.1.2.5.1 Mathematical models to calculate organ dose

Mathematical models were designed to simulate standard patients and establish conversion factors for the calculation of organ dose. Many software applications, for instance, Monte Carlo (MC) methods, MCNPX, ImPACT, CT-Expo Virtual Dose, and NCICT were designed to determine the organ dose from CT scan parameters.

MCNPX implements the Monte Carlo method and can be employed to construct a model of the CT scanner and simulate the transport of ionizing radiation in anthropomorphic phantoms. In contrast to stylized phantoms that are constructed using three-dimensional geometric shapes such as spheres and cylinders, computational anthropomorphic phantoms resemble the anatomical characteristics of actual patients and accurately incorporate the tissue compositions of the body based on established standards or reference datasets [23].

Most of the calculations are based on unrealistic stylized phantoms, such as ImPACT and CT-Expo. CT-Expo (G. Stamm, Hannover and H.D. Nagel, Buchholz, Germany), employs a set of mathematical phantoms, two adult phantoms and two pediatric phantoms (Adam, Eva, Child, and Baby), body surface, and organs are represented by equations. Additionally, it can simulate beam modulation during a CT scan and select in axial and spiral modes. ImPACT software does not include an intrinsic calculation method for the estimation of pediatric organ dose, while supplying a set of adjustment factors that can be used to approximate the effective dose for pediatric patients.

VirtualDose is the first organ dose and effective dose calculator available online that includes realistic phantoms for patients of different ages (including pediatric patients aged 0 to 15), gender, pregnancy stage, or size. NCICT software was developed by National Cancer Institute, Bethesda, USA, using hybrid voxel computational phantoms while NCICTX software hybrid voxel computational phantoms family and provide 100 adult males, 93 adult females, 85 males and 73 females of pediatric, with different mass and height combinations [23-25]. The Figure 2.3 shows different phantoms implemented in CT-Expo, NCICT, NCICTX, and Virtual Dose.

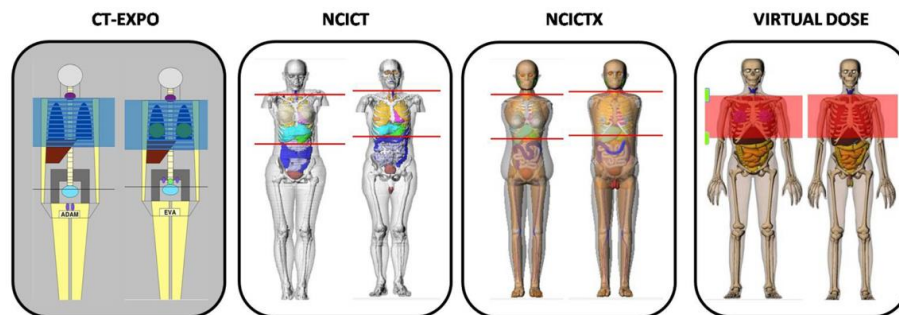


Figure 2.3: Different phantoms implemented in CT-Expo, NCICT, NCICTX, and Virtual Dose [25]

2.1.2.5.2 Dose monitoring software

Radimetrics™ Enterprise Platform (REP), provides organ dose and effective dose derived from Monte Carlo simulation. Monte Carlo simulator consists of three major components, the X-ray source's modeling, the patient phantoms, and the interaction between X-ray photons with the patient. Patients are modeled as stylized phantoms, and organs are represented in simple geometric shapes described in mathematical equations. The dose monitoring software incorporates a library of nine reference phantoms that represent the average of the population. Additionally, it features a set of 45 bariatric phantoms specifically designed to represent individuals with obesity. The reference phantom set includes the original six Christy phantoms, including newborn, 1, 5, 10, 15 years old and adult and 3 pregnancy phantoms.

The mapping of patients to phantoms is determined by factors such as age, gender, weight, effective diameter, or water-equivalent diameter (WED). Effective diameter and water-equivalent diameters are calculated for each slice within the scan region. The average diameter and the standard deviation of the distribution are calculated. The diameter indicator used for selecting phantom is the lesser of the maximum per slice diameter and the average diameter plus two standard deviations. The scan parameters and patient information obtained from Radiation Dose Structured

Report (RDSR), dose sheet, and Digital Imaging and Communications in Medicine (DICOM) to determine which simulation is run under the setup that is the closest to the actual exam. Subsequently, the lookup table derived from this selected simulation is employed. For a given procedure, the total energy deposited in each organ is the sum of the deposited energy from all slices encompassed within the scan region as shown in Figure 2.4.

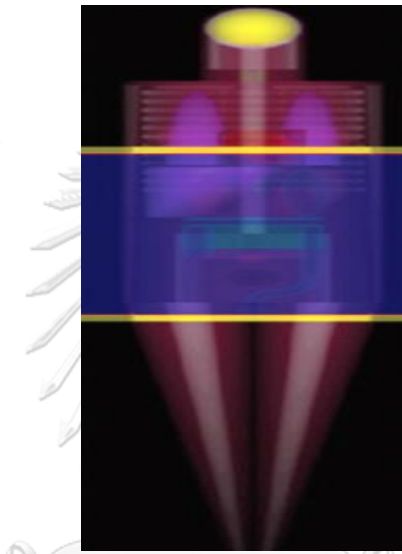


Figure 2.4: The stylized phantom and the scan region

In simulations, the CTDI phantoms are modeled using mathematical descriptions. The measurement of $CTDI_{vol}$ is simulated with the same set of protocols as for the patient phantoms.

The organ dose is determined by the summation of *coeff*, multiplied by the reported $CTDI_{vol}$, as shown in the equation.

$$D_{organ} = \sum_i (coeff \times CTDI_{vol}) \quad (2.5)$$

where *coeff* is the ratio of the simulated organ to the simulated $CTDI_{vol}$, and *i* indicates slice specific values.

2.1.3 Computed Tomography

2.1.3.1 Historical development of CT scanners

After conducting preclinical research and development in the early 1970s, CT was developed rapidly and became into an essential radiological examination of clinical situations. Sir Godfrey Hounsfield invented the first CT scanner in 1972. By the end of 1983, CT technology was already being utilized in medical practice. The first- and second-generation CT scanners utilize the translation-rotation method to acquire CT images. This method data was acquired by the X-ray tube and detector moving in a linear translator pathway and was repeated with small rotational increments. For a third generation CT scanners include a wide fan beam and detectors that rotate slowly, thus requiring multiple breath holds to complete an axial CT exam. The implementation of slip ring technology in 1987 enabled the tube and detectors to rotate continuously. The fourth-generation scanners, with stationary detector rings, were not widely adopted, all current CT scanners are designed as third-generation scanners.

In the early 1990s, spiral CT or helical CT became a new stage in the evolution and further development of CT imaging technology. Spiral Multi-Detector CT (MDCT) was introduced in 1998 and individual detector element was reduced to 0.25 mm per detector element, resulting in an improvement in spatial resolution. Moreover, MDCT is distinguished for high-quality images, fast gantry rotation time, high temporal resolution result in rapid data acquisition, improved volume coverage, and minimized patient movement due to the combination of multiple detector elements. Recent developments in CT imaging have been facilitated by the advent of dual-source, dual-energy CT (DECT). Dual source hardware is a significant technical advancement since it enables exceptionally high pitch and fast rotation speed, reducing acquisition time and improving temporal resolution. Furthermore, DECT uses decomposition methods to separate density from the elemental composition of human materials [6, 26-28].

In the medical field, CT scans are used in adults and children exhibiting symptoms of sickness or injury. Advanced reconstruction algorithms, more potential X-ray tubes, shorter scan times, and the availability of sophisticated visualization tools on workstations and scanners have all contributed to significant improvements in CT image quality. CT scans can be used for multiplanar reconstruction (MPR) in axial, coronal, and sagittal planes, as well as volume rendering (VR), curved multiplanar reformation, and maximum intensity projection (MIP), as shown in the Figure 2.5.



Figure 2.5: CT image reconstruction techniques

2.1.3.2 Clinical applications of CT

Computed Tomography (CT) is one of the most widely used diagnostic imaging modalities in the medical field. It provides detailed cross-sectional images of the body's internal structures to visualize and assess various organs and tissues [26]. The most commonly implemented CT examinations are abdomen and pelvis, chest, head, and CT angiography[1]. The following is a summary of the protocols and clinical indications of the common CT procedures.

2.1.3.2.1 CT abdomen

Abdominal CT is the modality most commonly used to assess abnormalities of the abdominal organs, including the liver, pancreas, and colon, blood vessels, and other

structures within the abdomen. Multiphasic scanning and thinner reconstructed sections provide enhanced characteristics, which facilitate improved diagnosis for detection and characterization of tumors, evaluation of abdominal trauma or assessment of Inflammatory. Tumor characterization is mainly based on lesion contrast uptake in the different enhancement phases.

Early arterial phase at 20 seconds after the injection of contrast media, there is avid enhancement in the arterial vessels but relatively little enhancement of the parenchyma or hyper-vascular lesions. The late arterial phase occurs approximately 30–35 seconds after injection, while the pancreatic parenchymal phase begins at 40–45 seconds after injection. The late arterial phase is optimal for detecting hyper-vascular primary tumor metastatic infiltration, whereas the portal vein phase provides significant pancreas enhancements. The portal venous phase occurs 60-70 seconds post-start of injection with maximum enhancement of the hepatic and still elevated values in the pancreatic parenchyma. The venous phase is advantageous for the detection of tumors with hypo-vascular tumors, for instance, colorectal metastases or pancreatic adenocarcinoma [29], abdominal multiphase CT as illustrated in the Figure 2.6 .



Figure 2.6: The patient underwent an abdominal multiphase CT scan [29].

2.1.3.2.2 CT Chest

CT imaging for chest examinations is vital in diagnosing various lung diseases, such as interstitial lung diseases and pulmonary vascular diseases. The adoption of high-resolution CT scanning of the chest has become more commonly used due to technological advancements. Implementing contrast enhancement protocol involving a delay of 55–90 seconds post-contrast injection. Venous-phase CT scan can demonstrate the visualization of nodes, pulmonary and pleural lesions due to a greater distribution of contrast in the extravascular interstitial space [30, 31]. UNSCEAR 2020/2021 [1] reported the mean effective dose for chest CT scans ranged from 3.7 to 10.1 mSv across various countries. CT chest with contrast enhancement protocol is illustrated in the Figure 2.7.

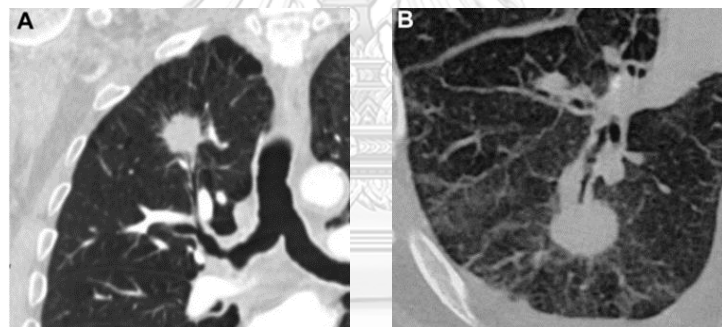


Figure 2.7: Diagnosis for Patient A: squamous cell carcinoma; Patient B: non-small cell lung cancer [30]

2.1.3.2.3 CTA of the aorta

Computed tomography angiography (CTA) of the aorta is a non-invasive imaging technique that is used to visualize blood vessels, including the assessment of aortic aneurysms, dissections, and other vascular conditions, as shown in Figure 2.8. Advancements in MDCT technology provide wide z-coverage and reducing scanning time. Scanning of the entire vascular structure can be routinely completed in a single breath. The pitch factor, table travel per gantry rotation time divided by an x-ray beam

width, is generally set to be less than one, overlapped in slice and can improve visualization of the objects but results in higher patient radiation dose [6, 26, 32]. Arterial contrast enhancement depends on the rate and duration of contrast injection, patient physiology, and the patient's cardiovascular status [33-35].

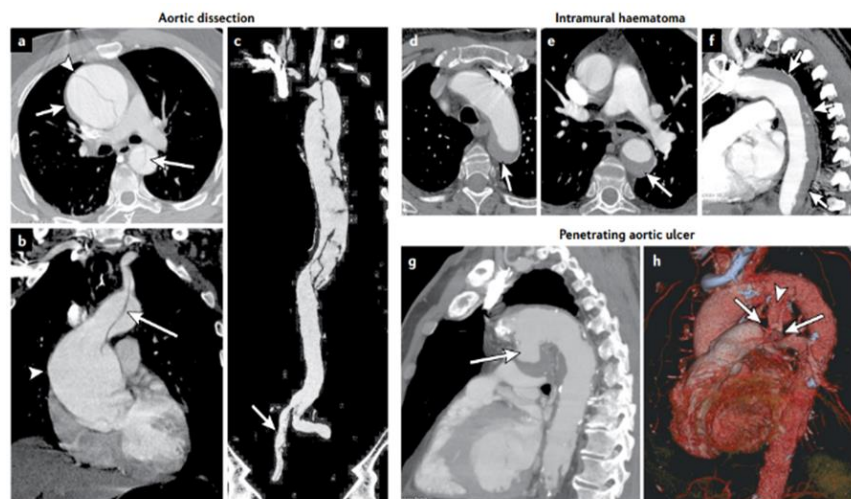


Figure 2.8: Imaging of aortic syndromes including aortic dissection, aortic intramural hematoma, and aortic ulcer [35]

According to cardiac pulsation, the artefact mainly affects the aortic root in non-gated CTA and is more frequently present at slower heart rates. With the launch of electrocardiogram (ECG)-gated, the patient motion artifacts from the aortic root and ascending aorta could be reduced [36, 37]. CTA has increased rapidly in recent years. The hazards from radiation dose and iodine contrast media (CM) are the major concern associated with scanning in multiphasic technique parameter settings (pitch, rotation time and scan length).

2.1.3.3 CT dose measurement

The radiation dose delivered by CT scan is described by CT dose index (CTDI), and dose length product (DLP).

2.1.3.3.1 Computed Tomography Dose Index (CTDI) [3, 22]

CTDI₁₀₀ measurements are taken with a 100-mm-long cylindrical pencil chamber. CTDI₁₀₀ describes as the measurement of the dose distribution in air, D(z), along the z-axis, from a single rotation (axial or sequential) of the scanner with a nominal x-ray beam width, nT. The CTDI₁₀₀ is defined as following equation.

$$CTDI_{100} = \frac{1}{nT} \int_{L=-50mm}^{+50mm} D(z)dz \quad (2.6)$$

The weighted CT dose index, CTDI_w, is calculated by combining center and periphery measurements using 1/3 and 2/3 weighting. CTDI_w is defined as;

$$CTDI_w = \frac{1}{3}CTDI_{PMMA,100,c} + \frac{2}{3}CTDI_{PMMA,100,p} \quad (2.7)$$

Where C_{PMMA,100,c} is measured at the center of PMMA phantom and C_{PMMA,100,p} is the average of measurements taken at four peripheral positions surrounding the phantom.

CTDI_{vol} is a standardized parameter used to measure scanner radiation output, considering the helical scanning, the dose is inversely proportion to helical pitch. Pitch is defined as the ratio of the table translation distance (mm) during a full rotation (360 degrees) of the gantry, and the nominal beam width nT (mm). CTDI_{vol} is defined as following equation.

$$CTDI_{vol} = \frac{CTDI_w}{pitch} \quad (2.8)$$

CTDI_{vol} (mGy) is displayed on the CT scanner console prior to the actual scan. CTDI_{vol} is a metric utilized to assess and compare the radiation doses delivered by various scanning protocols or achieving a specific level of image quality for a particular patient. However, CTDI_{vol} cannot be used as a substitute for patients' dose, either for epidemiological assessments of potential late effects or for deterministic effects [7, 38].

2.1.3.3.2 Dose length product (DLP)

The dose length product (DLP) is the product of the $CTDI_{vol}$ and the length of the CT scan along the patient's z-axis with the unit of mGy.cm, as in the equation.

$$DLP = CTDI_{vol} \times scan\ length \quad (2.9)$$

DLP is an overall radiation dose estimate for standardized phantoms but is not a reliable indicator of patient-specific organ dose [23]. Therefore, the estimation of organ dose, which can be utilized to assess risk and compared to other sources of radiation exposure, necessitates using Monte Carlo simulations.

2.1.4 Biological effects of ionizing radiation

2.1.4.1 Deterministic and stochastic responses

The potential hazard of low LET radiation can be determined from experimental and epidemiological studies. Radiation damage to tissue or organs has been established to be contingent upon several factors, including type of radiation, the sensitivity of different tissues and organs, dose, and the dose rate. The biological effects of radiation exposure can be divided into stochastic and deterministic effects.

The probability of a stochastic effect increasing with dose, but the severity of the effect remains constant. These effects are assumed to exhibit no threshold dose below which they cannot occur, because of damage to a few cells resulting in cancer and heritable effects. Consequently, even low dose radiation can be increased the probability of radiation-induced cancer or genetic effects, specifically, diagnostic radiology, while late effects which are not apparent until years after radiation exposure. On the assumption that the probability of risk increases with the amount of radiation dose and there is no threshold dose below which the magnitude of the risk is zero. This is in accordance with the concept of radiation protection, the objective of which is to keep exposures as low as reasonably achievable (ALARA).

At low dose, the radiation risks are primarily associated with stochastic effects rather than the deterministic effects, the characteristic of higher exposure. At very high dose, the primary biological result is cell death, which appears clinically as degenerative tissue changes that are classified as deterministic effects. These effects are the result of radiation-induced cell loss or damage and occur above dose thresholds, with severity increasing with dose. Deterministic effects may occur mostly after exposure to moderate or high radiation doses within a few hours or days of exposure, for example, an early skin reaction, or may take months or years, e.g., cataracts in the eye lens [6, 8, 12]

2.1.4.2 Radiation-Induced carcinogenesis

2.1.4.2.1 Burden of cancer

Cancer is among the most significant health concerns globally, with about one fifth of world's population and one third of people in many industrialized countries are diagnosed with cancer during their lifetime [12]. Furthermore, cancer is recognized as a significant factor contributing to both morbidity and mortality. In 2020, the global cancer mortality rate is about 9,958,133, and the number of new cases of cancer (cancer incidence) was 19,292,789 (Figure 2.9). The five most common cancers in Thailand, with the exception of nonmelanoma skin cancer, are liver, lung, breast, colon and cervix uteri, as shown in Figure 2.10 [12]. The sources of cancer risk are genetic, family history, lifestyle behaviors such as smoking, poor diet, physical inactivity, alcohol, environment, as well as radiation [6].

According to the assumption of no threshold dose for cancer induction, the ionizing radiation increases the probability of the risk of cancer, and is the most significant somatic delay effect that can occur decades or even years after exposure [6]. Even a single ionization event may theoretically lead to molecular changes in the DNA resulting in malignant transformation and ultimately cancer. An instance can be observed when a person is exposed to a whole-body dose of 3 mGy of low-LET

radiation, resulting in multiple DNA lesions in every cell. Nevertheless, the occurrence of cancer might never arise due to a host of defense mechanisms are initiated following radiation-induced damage to prevent cancer development. These mechanisms include the activation of DNA repair systems; free radical scavenging; cell cycle checkpoint controls; induced apoptosis, and mitotic failure [6].

Estimated number of new cases in 2020, World, both sexes, all ages

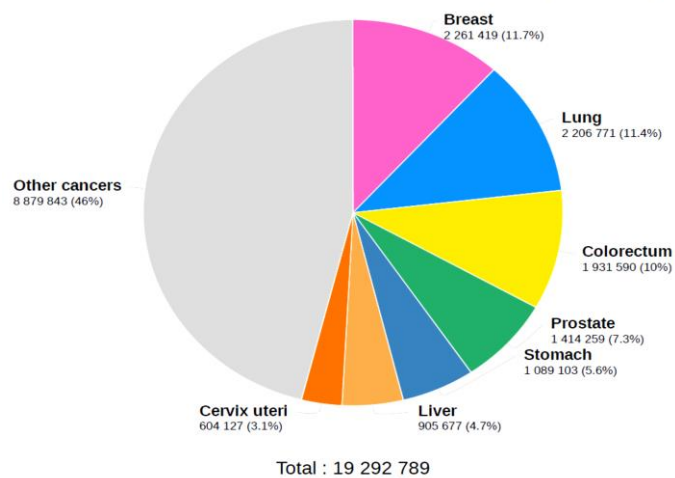


Figure 2.9: Global estimate of the number of new cancer cases in 2020 [5].

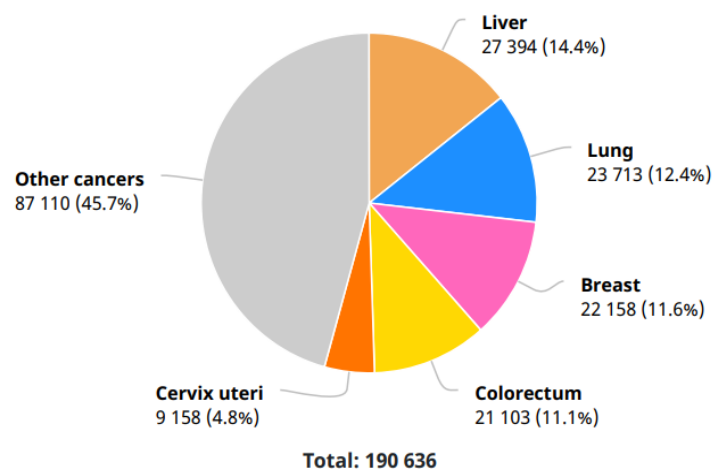


Figure 2.10: The number of new cancer cases in Thailand, 2020

2.1.4.2.2 Source of epidemiological data [12]

Epidemiological investigations on biological effects of low LET radiation depend on four primary sources of population data.

- Life Span Study (LSS) cohort of survivors of the atomic bomb explosions in Hiroshima and Nagasaki.
- Patients who were exposed to radiation during the treatment of various neoplastic and non-neoplastic diseases.
- Persons with occupational exposures.
- Populations with high natural background exposures and environmental exposures.

Analysis of data obtained from the atom-bomb survivors' cohort has significantly influenced current estimates of cancer risks associated with radiation exposure. The population size is large and there is a wide range of doses, from which it is possible to dose-response and the effect of modifying factors, such as age, on cancer induction. However, data at high doses are limited; thus, the analysis included individuals in whom the doses were 2 Gy or less. The demographics of the survivors did not reflect that of a normal Japanese population, as a significant number of adult males were serving in the military. Furthermore, a higher proportion of children and the elderly died shortly after the bombing than did young adults, suggesting the possibility that the survivors may represent a hardier subset of the population.

Another essential uncertainty is the transfer of sites specific cancer risk estimates to the U.S. population, based on results obtained on the Life Span Study (LSS) population, for cancers with substantially different baseline incidence rates.

2.1.4.2.3 CT radiation risk

According to substantial of evidence, the exposure to high levels of ionizing radiation can cause serious illness or death. The evidence from atomic bomb survivors indicates that high doses correlated with other health effects such as heart disease and stroke. While the health risk assessment of the low level of ionizing radiation is based on scientific knowledge from previous radiation incidents. The primary source of epidemiological information is the LSS of the Japanese atomic bomb survivors receiving an acute dose of radiation. BEIR VII Report focused on investigating the health effects of low levels of low linear energy transfer (LET) ionizing radiation. Low-LET radiation, X-ray and gamma rays deposits less energy in the cell along the radiation path at less destructive per radiation track than high-LET radiation. The health effects associated with low LET include cancer, hereditary diseases, and other diseases such as heart disease [8, 11, 12].

Epidemiological studies are particularly important to assess potential human health risks related to radiation exposure. The term risk in radiation epidemiology includes the relative risk, RR, and the absolute risk, AR [6, 8].

Relative Risk, RR, is the ratio of the disease (e.g., cancer) incidence in the exposed population (R_r) to that in the general (unexposed) population (R_o) as in equation (2.10). Relative risk has no units.

$$RR = R_r / R_o \quad (2.10)$$

Excess relative risk (ERR) is the proportional increase in risk over the background absolute risk or baseline incidence, the ratio of the risk in an exposed group to unexposed group (RR) minus one as in equation (2.11)

$$ERR = RR - 1 \quad (2.11)$$

Absolute risk, AR, presumes a constant absolute increase in risk per dose unit, regardless of the baseline risk. AR is the simple rate of disease among a population. In radiation epidemiology, it is a rate such as the number of excess cases per person per Sv per year.

Excess absolute risk (EAR), referred to excess attributable risk, is in terms of the EAR per unit dose. EAR is different in the rate of cancer between the exposed population and comparable non exposed population, as in equation (2.12).

$$EAR = R_r - R_o \quad (2.12)$$

2.1.5 Cancer risk models

The cancer risk models illustrate the variation of the radiation-induced excess risk of a specific type of cancer with the magnitude of the relevant tissue-specific absorbed dose of radiation received. Several organizations; NUREG model (1993), BEIR VII model (2006), UNSCEAR model (2006), ICRP 103 (2007) and U.S. EPA (2011) developed models to estimate the LAR of radiation-induced cancer incidence and mortality as a function of tissue-specific absorbed dose, age and gender of the exposed reference person [10]. Following is a description of the summary risk models:

The NUREG model (1993), developed by the U.S. Nuclear Regulatory Commission, provides cancer risk model for people exposed to radiation resulting from nuclear accidents. The assumption is based on a linear dose-response model, the risk is proportional to the risk coefficient and dose. The NUREG model implements risk coefficients defined as cancer risk per dose unit for cancer risk assessment.

The BEIR VII model (2006) was derived on epidemiological data, primary from Japanese atomic bomb survivors. Risk models of low-LET radiation for estimating the incidence and mortality of cancer in leukemia and solid tumors have been developed as a weighted means of ERR and EAR estimates, and are adjusted for exposure age, attained age, and gender. The leukemia model has a linear exponential term and a

latency period of 2 years. The solid cancer model has a linear term with an estimated DDREF of 1.5 and a latency period of 5 years.

UNSCEAR model (2006), the cancer risk models were derived through regression analyses of the Japanese atomic bomb survivor. The risk model of mortality from leukemia and solid cancers is linear quadratic, and the site of solid cancer is not specified. The risk model for the incidence of solid cancer is linear and has been developed for various cancer sites. The ERR and EAR estimations were modified taking into account of the age at exposure, attained age, and gender.

The ICRP 103 (2007) developed risk models for cancer incidence due to radiation-induced health effects are stressed in relation to the incidence of cancer, rather than cancer-related mortality. The model for leukemia and solid cancer incidence is derived from the Japanese atomic bomb survivor data. The risk model for leukemia is linear quadratic, while the risk model for solid cancers is linear term. Lifetime cancer risk is determined by the LAR and weighted arithmetic mean of ERR and EAR.

The U.S. EPA (2011) developed risk models for cancer incidence and mortality, using the same models as the BEIR VII model. Solid cancer risk models are linear terms, whereas the leukemia risk model is linear quadratic. They developed new risk models for thyroid, kidney, bone, and skin cancers.

2.1.6 Dose-Response Models

Several models have been demonstrated to characterize dose-response relationships of radiation exposure in humans. Dose-response curves (Figure 2.11) have been classified into different shapes: linear no threshold (LNT), linear-quadratic (LQ), and threshold. The two LNT extrapolations show the components of the dose response data, including high dose (black), and low dose (orange). The LQ dose response curve (red) shows a decrease in radiogenic cancer induction effectiveness at lower dose, a higher efficiency at higher dose that eventually flattens out, reflecting dose associated

with substantial cell killing. Based on experimental and epidemiological evidence, it has been observed that the threshold (blue), a threshold model provides the best fit for some cancer e.g., osteogenic sarcoma risk among painters who had substantial internal radium contamination.

The risk models are used to estimate the relationship between the low level of low-LET ionizing radiation and the health effects. BEIR VII Phase 2 describe the linear no-threshold model (LNT), provided the most reasonable description of cancer incidence. ICRP, 2006 described the LNT hypothesis, combined with an uncertain DDREF for extrapolation from high doses, remains a prudent basis for radiation protection at low doses and low dose rates.

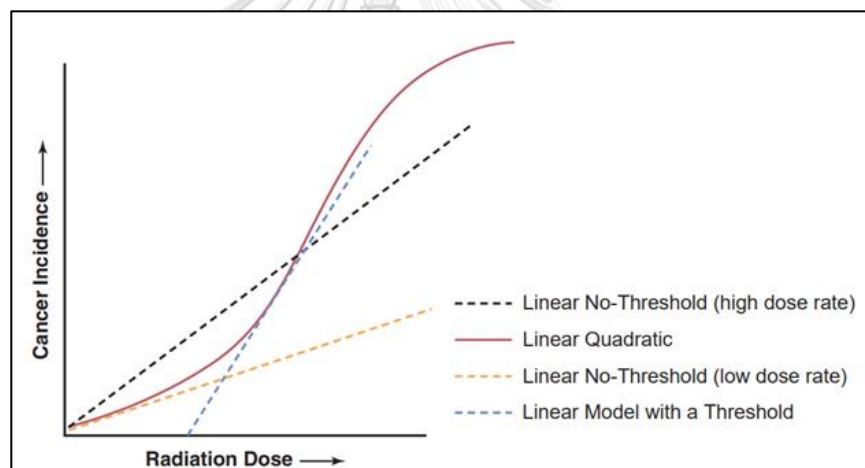


Figure 2.11: Possible dose response relationship for radiation-induced cancer and radiation dose [6]

The majority of the important epidemiologic data on low LET radiation cancer risk is derived from the study of acute exposures. The biological effectiveness of the radiation-induced damage to cells and tissues generally decreases at lower dose and lower dose rates. This effect is due to the ability to repair damage during low dose exposure or high total dose delivered in small dose fractions. Therefore, dose and dose rate effectiveness factor (DDREF) was utilized to convert risk estimates from high-dose and high dose rate exposures to low-dose estimates. DDREF was obtained by utilizing a

Bayesian statistical analysis of the solid cancer incidence data from the A-bomb survivor LSS, along with the results from laboratory animal data.

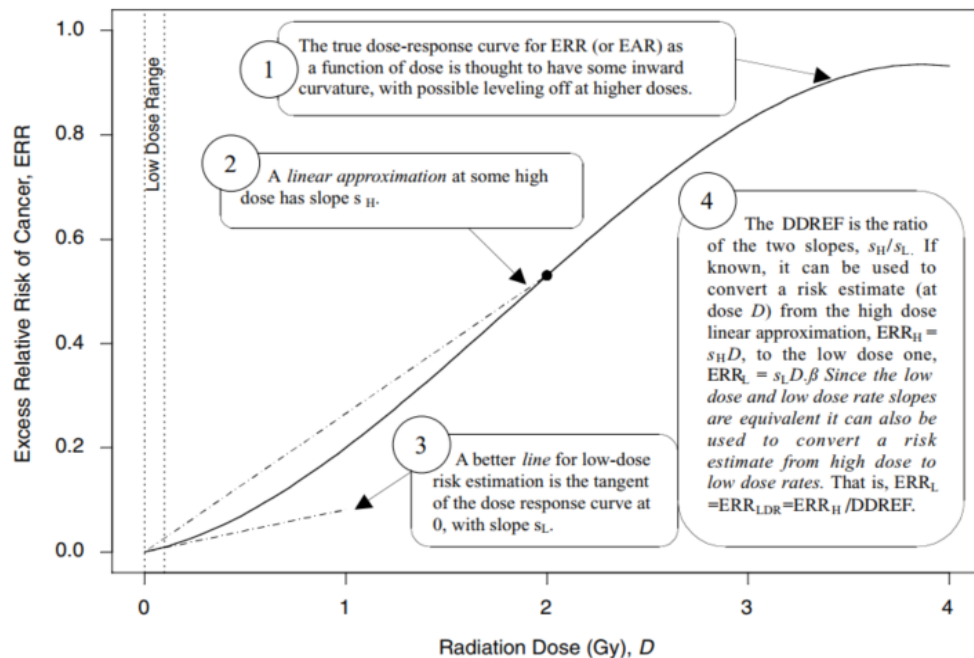


Figure 2.12: Dose-response assessment [12]

Figure 2.12 illustrates a theoretical dose-response curve, in which a linear approximation is employed for low doses, specifically the tangent of the curve at dose zero. Additionally, a linear approximation is utilized based on risk at a specific high dose, which is the line that passes through the origin and the actual dose-response curve at the high dose of 2 Gy. The dose and dose rate effectiveness factor (DDREF) can be determined by the ratio of larger slope (s_H) and the smaller slope (s_L).

An alternative approach is to estimate DDREF by utilizing the degree of curvature of the dose-response for excess cancer after acute irradiation. According to conventional radiobiological theory, the low-dose and low-dose-rate response will be represented by the initial linear (α) term of a linear-quadratic ($\alpha \text{Dose} + \beta \text{Dose}^2$) dose-response. The α and β terms of the acute dose response may be used to provide an estimate of DDREF.

Figure 2.12 shows the line analogous to the “high-dose linear approximation” resulting from linear model estimation with the LSS data. If a certain degree of curvature is presumed, then it is possible to define an LSS DDREF that correctly adjusts LSS linear risk in order to estimate cancer risk at low doses.

If, over some dose range of interest, the dose-response curve can be approximated by a linear-quadratic (LQ) function, $\alpha \text{Dose} + \beta \text{Dose}^2$, then the slope of the high-dose linear approximation (s_H) at a particular high dose (D_H) can be determined by $\alpha + \beta D_H$ (UNSCEAR 1993). The slope of the low-dose linear approximation (s_L) is α , and the DDREF corresponding to D_H is their ratio, $1 + (\beta / \alpha) D_H$. β / α is a numerical quantity that can be used to characterize curvature, which is not tied to particular high dose. This ratio is referred to as the LQ “curvature” and is represented by θ .

If the correct curvature, θ , is determined, define an LSS DDREF using these steps: The LQ model for ERR or EAR is estimated using LSS data, the curvature is constrained to be θ , by fitting the relative risk model $\alpha_{LQ}(\text{Dose} + \theta \text{Dose}^2)$ for fixed θ , with unknown linear component α_{LQ} . A separate linear model is estimated from the same data: with linear component α_L . Thus, LSS DDREF estimates the ratio of the two linear components, α_L / α_{LQ} . The resulting DDREF from the linear model projection can be used to convert risk estimates to the linear component of an estimated LQ model with curvature set by θ .

The two definitions of DDREF that depend on LQ curvature: the UNSCEAR definition, which represents the fixed high-dose DDREF, $\text{DDREF} = 1 + \theta \times \text{high dose}$, and the LSS DDREF, which is determined through the estimation procedure described in the previous paragraph, UNSCEAR definition of DDREF and LSS DDREF corresponding to three values of curvature as shown in Table 2.2.

Table 2.2: Definition of UNSCEAR DDREF and LSS DDREF^a

	UNSCEAR DDREF ^b			LSS DDREF ^c
Curvature (θ , Sv ⁻¹)	High Dose = 1 Sv	High Dose = 2 Sv	High Dose = 3 Sv	
0.5	1.5	2.0	2.5	1.5
1.0	2.0	3.0	4.0	2.1
2.0	3.0	5.0	7.0	3.1

^aFor incidence of solid cancers and based on doses between 0 and 1.5 Sv,

^bDDREF = $1 + \theta \times \text{high dose}$.

^cFrom estimating LQ models forced to have curvature θ .

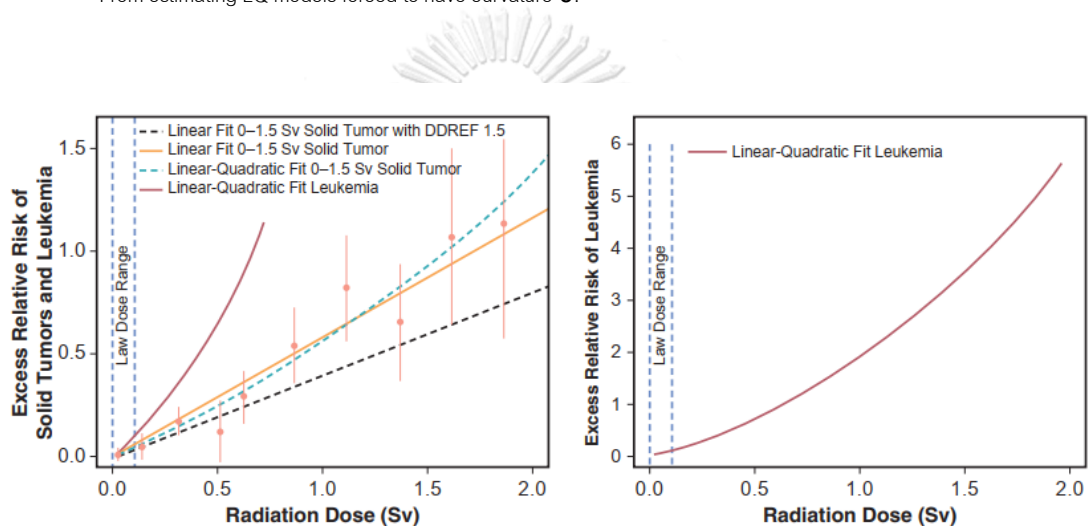


Figure 2.13: Dose-response models of ERR for solid cancer (Left) and leukemia (Right) from cancer incidence data of Japanese A-bomb survivors [6].

BEIR VII presents the point estimates of ERRs of solid cancer incidence (depicted as orange dots). These estimates are averaged across genders and standardized to reflect individuals exposed at the age of 30 who have attained age 60 for specific dose intervals from the A-bomb survivor LSS (Figure 2.13). The orange solid line and the green dashed line represent linear and Linear-Quadratic (LQ) dose-response models, respectively, for the ERR of solid tumors. These models are derived from all subjects with doses ranging from 0 to 1.5 Sv. The BEIR VII committee applied a DDREF of 1.5 to adjust the response observed in the high dose range making it roughly equivalent to the line representing the LNT low-dose response (black dashed line). This

line represents an extension of the linear portion (i.e., zero-dose tangent) of the LQ model.

Within the low-dose range that is relevant to medical imaging and occupational exposure to radiation (dose below 100 mSv). For the solid cancer incidence, the linear quadratic model did not offer the statistically significant improvement in fit, so the linear model was used. The difference between the linear fit to the solid tumor data (represented by a black dashed line incorporating a DDREF of 1.5) and the LQ fit to the same data (represented by a green dashed line) is relatively minor when compared to the 95% confidence intervals. On the left and right sides of the figure, the red lines show the ERR for leukemia that fits best with LQ dose-response model.

The value of the DDREF was derived based on Bayesian statistical analysis of the solid cancer incidence data from the A-bomb survivor LSS, as well as the results from selected laboratory animal data. There was considerable uncertainty in the BEIR VII committee's estimate of a DDREF because the data from the animals was substantial inconsistency and imprecision. Also, the DDREF estimate was particularly sensitive to the selection of the dose range used for estimation, the particular studies chosen for analysis, and the approach used for estimating curvature that is presumed to be the same across all studies.

2.1.7 BEIR VII report on cancer risk models

The BEIR VII committee developed risk models to estimate lifetime risks of cancer incidence and mortality, considering factors such as gender, age at exposure, organ dose, and other factors. The risk models addressing low radiation dose, low-LET (linear energy transfer) radiation, the models are based primarily on data on Japanese atomic bomb survivors. BEIR classified low-dose range of low LET from close to zero to 100 mSv, and high dose from more than 100 mSv. The report provides lifetime risk estimates for cancer incidence and mortality resulting from radiation exposure and applies these models to the U.S. population.

2.1.7.1 Multiplicative and Additive Risk Models

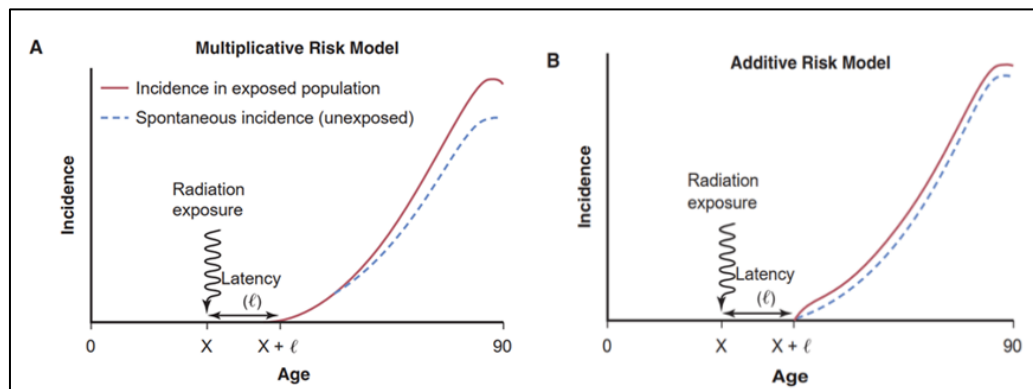


Figure 2.14: Multiplicative (A) and additive (B) risk models [6]

The multiplicative risk model, referred to as the relative risk model, assumes that excess cancer risk increases in proportion to baseline cancer rates. In the multiplicative risk model, the excess risk, after the latent period (ℓ) is a multiple of the natural age-specific cancer risk for a given population which increases with age. The multiplicative risk model predicts the greatest increment in incidence at older ages.

The additive risk mode, referred to as absolute risk model, which assumes that after latent period, the excess cancer rate is constant and independent of the spontaneous population and age-specific natural cancer risk. The additive risk model, in which a fixed incremental increased risk is added to the spontaneous disease incidence, which is assumed to be constant over the remaining lifetime, is depicted in the Figure 2.14.

The multiplicative and additive risk models can be used to transport risk calculated from one population to another population. Due to the majority of radiation risk estimates derived from the LSS of Japanese A-bomb survivors. This issue is particularly critical for radiation risk estimates based on the US population, as the natural incidence of several types of cancer in the U.S. and in Japan is considerably different. For instance, Japan has a 7.5 and a 10-fold greater incidence of stomach and liver cancer, respectively, than the US, despite the US having a three-fold higher case of

breast cancer incidence. Models for breast and thyroid cancer are based on combined analyses that include Caucasian subjects.

BEIR VII estimated risks for solid cancer sites using both relative and absolute risk transport for the U.S. population, a reasonable approach would be to calculate an average of the projections based on the two types of risk models, e.g., a weighted arithmetic or geometric mean. The recommended point estimates are weighted means of estimates obtained under the two models as shown in the Table 2.3.

Table 2.3: Risk transfer approaches adopted by international organizations.

Cancer site	UNSCEAR		BEIR VII	ICRP 103
Leukemia	100% ERR	100% EAR	70% ERR and 30% EAR	100% EAR
Thyroid cancer	100% ERR	100% EAR	100% ERR	100% ERR
Breast cancer	100% ERR	100% EAR	100% EAR	100% EAR
All solid cancers	100% ERR	100% EAR	70% ERR and 30% EAR	50% ERR and 50% EAR

2.1.7.2 Models for estimating cancer risks

As stated by the BEIR VII model for estimating lifetime risks of cancer incidence and mortality by exposure to low-linear energy transfer radiation (LET). Cancer risks are determined based on either excess relative risk (ERR) or excess absolute risk (EAR) models, which are adjusted for age at exposure, attained age, and gender. Risk models are divided into solid cancer and leukemia, models for solid cancers were developed according to the site, such as stomach, colon, liver, lung, breast, prostate, ovary, bladder, thyroid, and others. The risk model for leukemia was derived from the Japanese atomic bomb mortality data from the period 1950 to 2000, and the solid cancers were derived from the Japanese atomic bomb cancer incidence data from 1958 to 1998. In this investigation, BEIR VII provides model parameters for specific organs for each gender and includes a parameter of age at exposure, attained age, and dose and dose rate effectiveness factor (DDREF).

Table 2.4: Summary of BEIR VII preferred risk models

Cancer site	Description	Data sources
Solid cancers	ERR and EAR increase linearly with dose; depends on gender, age at exposure (e), attained age (a)	Excess risk is still observed among atomic bomb survivors more than 50 years after exposure (1958-1998: LSS cancer incidence)
Breast	EAR increases linearly with dose. Effect modifiers: (e, a). Based on analysis of pooled data (Preston et al. 2002b). Breast cancer, the BEIR VII Committee used only an EAR model to quantify risk.	1958-1993 LSS breast cancer incidence derived from Massachusetts TB fluoroscopy cohorts. Rochester infant thymic irradiation cohort
Thyroid	ERR increases linearly with dose. Effect modifiers (s, e). Based on analysis of pooled data (Ron et al. 1995). EAR model not used.	1958-1987 LSS thyroid cancer incidence (Thompson et al. 1994).
Leukemia	ERR and EAR are linear-quadratic functions of dose. Effect modifiers: (s, e, a), time since exposure (t).	1950-2000 LSS cancer mortality (Preston et al. 2004).

2.1.7.2.1 Models for estimating all solid cancer risks

Models for estimating all solid cancer risks, ERR and EAR models are functions of gender, attained age, and age at exposure only for exposure ages under 30 years and are constant for exposure ages over 30, ERR and EAR are shown in equation (2.13).

$$ERR(e, a) \text{ or } EAR(e, a) = \beta_s D \cdot \exp(\gamma e^*) \left(\frac{a}{60}\right)^\eta \quad (2.13)$$

where e is the age at exposure in years, e^* is $(e-30)/10$ for $e < 30$, and equal to zero when $e \geq 30$, and a is attained age in years.

The approach of BEIR VII to quantifying the parameters β_s , γ and η was to use the estimates ERR and EAR models for site-specific cancer. The parameter derived from age-time patterns in radiation-associated risks for solid cancer incidence.

The estimates of β_M and β_F are for male and female, who exposed at age 30 or older at an attained age of 60. γ is equal to the risk decay constant for every decay since radiation exposure. η is the exponent of the ratio between attained age and the reference age at 60 years

For other sites, common values of the parameter γ indicating dependence on age at exposure could be used in all cases. With the ERR models, common values of the parameter indicating the dependence of risks on attained age (η) could be used in all cases except the category “all other solid cancers.” EAR models, it was necessary to estimate the attained age parameter, η , separately for liver, lung, and bladder cancers, which may reflect variation in the pattern of increase with age for site-specific baseline rates, which are shown in Table 2.5.

Table 2.5: Parameter values for risk models in BEIR VII

Cancer Site	No. of Cases	ERR Models				EAR Models			
		β_M^a (95% CI)	β_F^b (95% CI)	γ	η^d	β_M^e (95% CI)	β_F^e (95% CI)	γ	η^d
Stomach	3602	0.21 (0.11, 0.40)	0.48 (0.31, 0.73)	-0.30	-1.4	4.9 (2.7, 8.9)	4.9 (3.2, 7.3)	-0.41	2.8
Colon	1165	0.63 (0.37, 1.1)	0.43 (0.19, 0.96)	-0.30	-1.4	3.2 (1.8, 5.6)	1.6 (0.8, 3.2)	-0.41	2.8
Liver	1146	0.32 (0.16, 0.64)	0.32 (0.10, 1.0)	-0.30	-1.4	2.2 (1.9, 5.3)	1.0 (0.4, 2.5)	-0.41	4.1 (1.9, 6.4)
Lung	1344	0.32 (0.15, 0.70)	1.40 (0.94, 2.1)	-0.30	-1.4	2.3 (1.1, 5.0)	3.4 (2.3, 4.9)	-0.41	5.2 (3.8, 6.6)
Breast	952	—	0.51 (0.28, 0.83)	0	-2.0	—	9.9 ^f (7.1, 14)	-0.51	3.5, 1.1 ^e
Prostate	281	0.12 (<0, 0.69)	—	-0.30	-1.4	0.11 (<0, 1.0)	—	-0.41	2.8
Uterus	875	—	0.055 (<0, 0.22)	-0.30	-1.4	—	1.2 (<0, 2.6)	-0.41	2.8
Ovary	190	—	0.38 (0.10, 1.4)	-0.30	-1.4	—	0.70 (0.2, 2.1)	-0.41	2.8
Bladder	352	0.50 (0.18, 1.4)	1.65 (0.69, 4.0)	-0.30	-1.4	1.2 (0.4, 3.7)	0.75 (0.3, 1.7)	-0.41	6.0 (3.1, 9.0)
Other solid cancers	2969	0.27 (0.15, 0.50)	0.45 (0.27, 0.75)	-0.30	-2.8 (-4.1, -1.5)	6.2 (3.8, 10.0)	4.8 (3.2, 7.3)	-0.41	2.8
Thyroid ^g		0.53 (0.14, 2.0)	1.05 (0.28, 3.9)	-0.83	0				

Table 2.5 displays the parameter in ERR models, at most cancer sites: β_s , and the ERR per Sv at age-at-exposure 30 and attained age 60, tends to be higher for females than males. γ of -0.3 means that the radiogenic risk of cancer at age e falls by about 25% for every decade increase in age-at-exposure up to age 30. η of -1.4 indicates that the ERR is almost 20% lower at attained age 70 than at age 60. As a result, ERR decreases with increasing age-at-exposure (up to age 30) and age attained. In contrast, the EAR models indicate a γ value of -0.41 and η value of 2.8 for almost all

of sites. Therefore, EAR decreases with increasing age at exposure but increases with increasing attained age.

2.1.7.2.2 Models for female breast cancer

BEIR VII Committee has determined models for estimating breast cancer incidence and mortality are those developed by Preston and colleagues (2002a). These models were based on pooled analysis of combined data on breast cancer incidence from several cohorts, including the LSS data for the period 1958–1993, and seven cohorts in which subjects were given radiation treatment for various diseases e.g., tuberculosis, an enlarged thymus, mastitis, benign breast disease, and skin hemangioma. The cohorts consisted of Asians, Europeans, and North Americans, who received either single acute, fractionated, or protracted exposures. Models for both the ERR and the EAR were developed for these cohorts as follows:

Models for Female Breast Cancer, ERR and EAR are shown in equation (2.14) and (2.15)

$$ERR \text{ per Sv} = \beta \left(\frac{a}{60}\right)^{-2} \quad (2.14)$$

where a is attained age. The committee preferred ERR model for estimating risks for U.S. women uses $\beta = 0.51$, β indicates the ERR at an attained age of 60 instead of 50.

BEIR VII EAR model provides a reasonable fit to data from four of the cohorts: the LSS, two cohorts of U.S. tuberculosis patients, and one of the enlarged thymus infant cohorts. The pooled EAR model from Preston and colleagues (2002b) was as follows:

$$EAR = 9.9.D. \exp(-0.05(e - 25))(a/50)^\eta \quad (2.15)$$

where e is age at exposure and a is attained age (years); $\eta = 3.5$ for $a < 50$ and $\eta = 1$ for $a \geq 50$. For the EAR, a typical value of the overall level of risk, 9.9 could be used for all cohorts.

Although the committee utilize both the ERR and EAR models for the computation of lifetime risk assessments. However, the BEIR VII Committee expressed a preference for only utilizing an EAR model in order to quantify risk. With this model, the estimated main effect is more stable because it is based on both LSS and U.S. women. In addition, this model includes both age at exposure and attained age as modifying factors and is thus more comparable to models used for other sites. While it was found that no ERR model fit to the LSS and TB cohorts.

EAR model is dependent on both the age at exposure and the attained age, as described by Equation 2.15. The EAR continues to decrease exponentially with age-at-exposure throughout an individual's lifetime, and the EAR increases with attained age less rapidly after age 50, which is the time of menopause.

2.1.7.3 Lifetime attributable risk (LAR)

The lifetime attributable risk (LAR) is employed to determine the lifetime risk of cancer in the exposed population, which is an accumulation of risk from the initial of radiation. In essence, LAR refers to the risk for cancer induction from exposure during the remaining life for a person taking into account their age and gender. The concept of LAR associated with stochastic health issues is significant relevance for current radiation protection practices [39]. The BEIR VII report utilized LAR to assess the potential risks associated with various cancer sites. This assessment was conducted by employing both an excess absolute risk (EAR) model and an excess relative risk (ERR) model. The LAR for a person exposed to dose D at age-at-exposure, e , the LAR for a specific cancer site at attained-age a , as follows:

$$LAR(D, e) = \sum_a^{a_{max}} M(D, e, a) S(a)/S(e) \quad (2.16)$$

LAR is defined as the summation from a equals $e + L$ to a_{max} , a is attained age (years), a_{max} is maximum age, L is a risk-free latent period (5 years for solid cancers), e is the age at exposure, D is an organ dose, and $S(a)/S(e)$ is the conditional probability of

a person alive and cancer-free at age-at exposure, e , to reach at least an attained age- a . $M(D, e, a)$ is the excessive cancer risk model, which can be calculated using relative risk transport and absolute risk transport based on the excess relative risk (ERR) model and the excess absolute risk (EAR) model.

$M(D, e, a)$ estimates using relative risk transport were based on ERR models as follows:

$M(D, e, a)$ for cancer incidence

$$M(D, e, a) = ERR(D, e, a)\lambda_I(a) \quad (2.17)$$

$M(D, e, a)$ for cancer mortality

$$M(D, e, a) = ERR(D, e, a)\lambda_M(a) \quad (2.18)$$

Where ERR from BEIR VII model, $\lambda_I(a)$ represents sex- and age-specific 1995–1999 U.S. cancer incidence rates from Surveillance Epidemiology, and End Results (SEER) registries, whereas the $\lambda_M(a)$ are sex- and age-specific 1995–1999 U.S. cancer mortality rates.

$M(D, e, a)$ estimates using absolute risk transport were based on EAR models

$M(D, e, a)$ for cancer incidence

$$M(D, e, a) = EAR(D, e, a) \quad (2.19)$$

$M(D, e, a)$ for cancer mortality

$$M(D, e, a) = EAR(D, e, a) \lambda_M(a)/\lambda_I(s, a) \quad (2.20)$$

The estimation of LAR is derived by combining estimates from the excess relative risk (ERR) and excess absolute risk (EAR) transport models on a logarithmic scale, as given by equation 2.21.

$$\log(LAR) = [p(\log(LAR_{ERR}) + (1 - p)\log(LAR)_{EAR}] \quad (2.21)$$

where LAR_{ERR} and LAR_{EAR} are the estimates based on ERR and EAR transport, respectively. The variable p represents is the risk-transfer weight or weighting factor, which reflects the relative strength of belief in the two transport models. For most cancers, a value of 0.7 was taken for p . Exceptions were lung cancer, where $p = 0.3$. This weighting scheme has not been adopted for breast cancer risk estimates that utilize the LAR derived from the EAR model only.

The uncertainty analysis produces an approximate variance for $\log(LAR)$, emanating from the individual variances in LAR_{ERR} and LAR_{EAR} (sampling variability from the estimation of the LSS risk model). The weighting scheme, p , uncertainty of whether absolute risk or excess risk is transportable from Japanese A-bomb survivors to the US population.

To accomplish this, the model above is written more formally depending on parameters in the ERR model, EAR model. ω is risk-transfer weight; and DDREF, as follows.

$$LAR = [(LAR_{ERR})^\omega \times (LAR_{EAR})^{1-\omega}] / DDREF \quad (2.22)$$

where LAR_{ERR} and LAR_{EAR} based on EAR and ERR transport. DDREF is 1.5 (used to estimate the risk of solid tumors).

2.2. Review of related literature

Original studies showed the frequency of individuals receiving CED from recurrent CT examinations at higher than 100 mSv and the evaluation of the cancer risk. The studies have indicated that CED at 100 mSv and above, multiple organs have been found to receive organ dose equal to or above 100 mGy [9]. Rehani MM et al [40] and Suksanchaoen W et al [41] published the frequency of CED at higher than 100 mSv, without the cancer risks attributable to radiation. The finding of studies examining the frequency of individuals receiving CED from CT examinations at 100 mSv and above for five years is not uncommon. Many publications reported the lifetime attributable risk (LAR) of cancer to various CT protocols, which was proposed in BEIR VII. The estimation of LAR was computed using the linear interpolation method described in BEIR VII Table 12D-1,2. In addition, alternative methods for estimating LAR consider the survival function and baseline cancer rate of the population. The literature relevant to our research are described below,

Zewde N et al. [9] - their research published on organ doses and cancer risk assessment in patients exposed to high doses from recurrent CT exams. This study was a retrospective study of 8,956 patients, ages 16–80 years old, who received a cumulative effective dose of ≥ 100 mSv through recurrent CT exams within five years (2013–2017). They used commercial software, Radimetrics™ Enterprise Platform (Bayer HealthCare, Whippany, NJ, USA), which provided several measures of radiation dose from CT, including organ dose and effective dose calculated from Monte Carlo simulations. BEIR VII report was used to estimate lifetime attributable cancer mortality risks (LACMR). They reported organ doses for the age group of 16–44 years, since younger patients have higher radiosensitivity. Overall, the results demonstrated that in patients with CED ≥ 100 mSv, the organ doses were above 100 mGy, and some exceeded 200 mGy. Out of the 8,956 patients, 6.7% were 16–44 years of age, with median organ doses higher than 200 mGy were stomach and liver. LACMR for the 16–

44-years was 0.6 to 0.7 deaths per 100 individuals for males, and 0.8 for females. The mortality estimate figure was highest for age groups 16–54 years with slightly lower values for the higher age group. Except for the highest bracket of 75–84 years, the LACMR values for 55–74 years are not lower by order of magnitude, and thus one cannot ignore the risks in this age group.

Einstein AJ et al. [42] conducted CT coronary angiography study to determine organ-specific lifetime attributable risks (LARs) of cancer incidence and assess the influence of age, gender, and scanning protocols on the risk of cancer. The assessment of the LAR of cancer incidence was performed by utilizing the organ equivalent dose derived from Monte Carlo simulation (ImpactDose software). The findings of this study indicate that there is a significant variation in risk, which is notably higher for women, younger patients, and for combined cardiac and aortic scans.

Shubayr N et al. [43] reported the estimation of radiation doses and LAR of radiation-induced cancer in the uterus and prostate from abdomen pelvis CT examinations. The organ doses obtained from the NCICT software was used to estimate the LAR of prostate and uterus cancer incidence and mortality. The findings demonstrated that LAR of uterus and prostate cancer incidence was 1.75 ± 1.19 cases and 2.24 ± 1.06 cases per 100,000 persons, respectively. The LAR of cancer mortality rates from uterus and prostate cancers were 0.36 ± 0.22 and 0.48 ± 0.18 cases per 100,000 persons, respectively. A minor increase in risk could help to alleviate concerns regarding well-justified abdomen pelvis CT procedures.

Ghetti C et al. [44] investigated the assessment of LAR from high resolution thorax CT scans during the COVID-19 outbreak. The LAR for lung and major cancers was computed based on the equivalent dose to organs for each patient using a methodology proposed in BEIR VII which considers age and gender. In summary, the results showed that the average LAR of all solid cancers was 2.1 cases per 10,000

patients, while the average LAR of leukemia was 0.2 cases per 10,000 patients. The COVID-19 outbreak caused a substantial increase in thoracic CT exams, and high-resolution low-dose procedure provided low doses and a low LAR risk estimation.

The following research estimates cancer risk and applies it to the population based on a life table data and the baseline cancer rate.

Lim H et al. [15] reported an evaluation of the cancer incidence and mortality risks attributed to diagnostic medical radiation exposure in Korea. The researchers utilized the estimation model developed based on data from the cohort of Japanese A-bomb survivors to estimate the proportions of cancer incidence and mortality in Korea that can be attributable to exposure to low-dose radiation. The risk of cancer incidence and mortality from medical radiation imaging using background cancer incidence and mortality in 2013 were obtained from the Korea Central Cancer Registry and the National Mortality Database provided by the Korean Statistical Information Service, respectively. Additionally, the probability of surviving data was provided by the Korean Statistics Information Service. The EAR and ERR model values can be weighted for obtaining LARs. They use the method in the BEIR VII report that calculates combined estimates using the weighted averages of the logarithmic scale of the estimates obtained from the EAR and ERR models. The researchers assigned a weight of 0.7 to the relative risk transport and a weight of 0.3 to the absolute risk transport. Finally, dose and dose-rate effectiveness factor (DDREF) 1.5 was applied to all the combined estimates. The result show that LAR for cancer incidence for males indicate 0.38 cases of stomach cancer, 0.31 cases of lung cancer, and 0.27 cases of colon cancer per 100,000. For females, the figures are 1.45 cases of thyroid cancer, 0.60 cases of lung cancer, and 0.95 cases of breast cancer per 100,000. The LAR for cancer mortality reveals that lung cancer was the top cause of cancer mortality in both sexes, with a rate of 0.25 per 100,000 for males and 0.40 per 100,000 for females.

Huang B et al. [18] conducted a study to assess the radiation dose and cancer risk resulting from retrospectively and prospectively ECG-gated coronary CTA in a cohort of adult patients from England, the US, and Hong Kong. LAR for the English population was derived using data from the Cancer Registration Statistics England 2005 and United Kingdom Interim Life Tables. The weights of EAR and ERR for the English population were chosen to be the same as those used in the BEIR VII report for the US population, as no weights were suggested for other populations in the BEIR VII report. A DDREF of 1.5 was also used to account for the lower risk of the low-dose radiation. Similarly, LAR for the USA and Hong Kong using baseline cancer and life table data for their population ranging between 20 and 80 years of age. The results show LAR of cancer incidence for a representative 50-year-old subject was calculated for retrospectively ECG-gated CTA to be 0.112% and 0.227% for English males and females, respectively, 0.103% and 0.228% for US males and females, respectively, and was comparatively higher at 0.137% and 0.370% for Hong Kong males and females, respectively.

From the above literature reviews, the radiation dose delivered to the patient had been reported especially the LAR of the internal organs. A few studies have explored the number of patients receiving high doses, CED of 100 mSv and above, in a single day. Therefore, the CED at 100 mSv and above are explored for the patient dose of the recurrent CT examination in our study. Moreover, the LAR of cancer incidence and mortality from CT examinations at high dose and low dose from the common CT procedures, especially in CTA whole aorta are investigated. The cancer risk derived from the risk models described in the BEIR VII report using survival probability data as well as baseline cancer incidence and mortality rates for the Thai population are estimated.

CHAPTER 3

RESEARCH METHODOLOGY

3.1 Research hypothesis

- The percentage of patients receiving CED from recurrent CT in a single day at 100 mSv and above is less than 0.01 per total CT examinations in five years (2018 – 2022) at King Chulalongkorn Memorial Hospital and Songklanagarind Hospital.
- Lifetime attributable risk (LAR) of cancer incidence and mortality of major internal organs are less than 0.3 per 100 or 300 per 100,000 patients receiving CED from recurrent CT in a single day at 100 mSv and above.

3.2 Research questions

- How many patients received CED from recurrent CT in a single day at 100 mSv and above from CT examinations in five years (2018 – 2022) at King Chulalongkorn Memorial Hospital and Songklanagarind Hospital?
- How much is the risk of cancer incidence and mortality of major internal organs for patients receiving CED from recurrent CT in a single day at 100 mSv and above?
- How much is the risk of cancer incidence and mortality for patients who underwent common CT examinations, including CTA of the whole aorta?
- Which parameters influence the risk of cancer?
- What is the risk model for CTA whole aorta examinations?

3.3 Research objectives

3.3.1 Primary objectives

3.3.1.1 To identify the number of patients receiving the CED recurrent CT at 100 mSv and above in a single day, the patients' protocols, patient characteristics, and the percentage of patients for all CT examinations at both hospitals within 5 years (2018-2022).

3.3.1.2 To estimate the risk of cancer, LAR in each target organ and determine parameters that influenced the cancer risk.

3.3.2 Secondary objectives

3.3.2.1 To investigate the risk of cancer, the patient underwent CT common examinations, including CTA of the whole aorta.

3.3.2.2 To determine parameters that influence radiation dose and risk of cancer.

3.3.2.3 To develop model/equation to estimate the cancer risk from CTA of the whole aorta of individual patient.

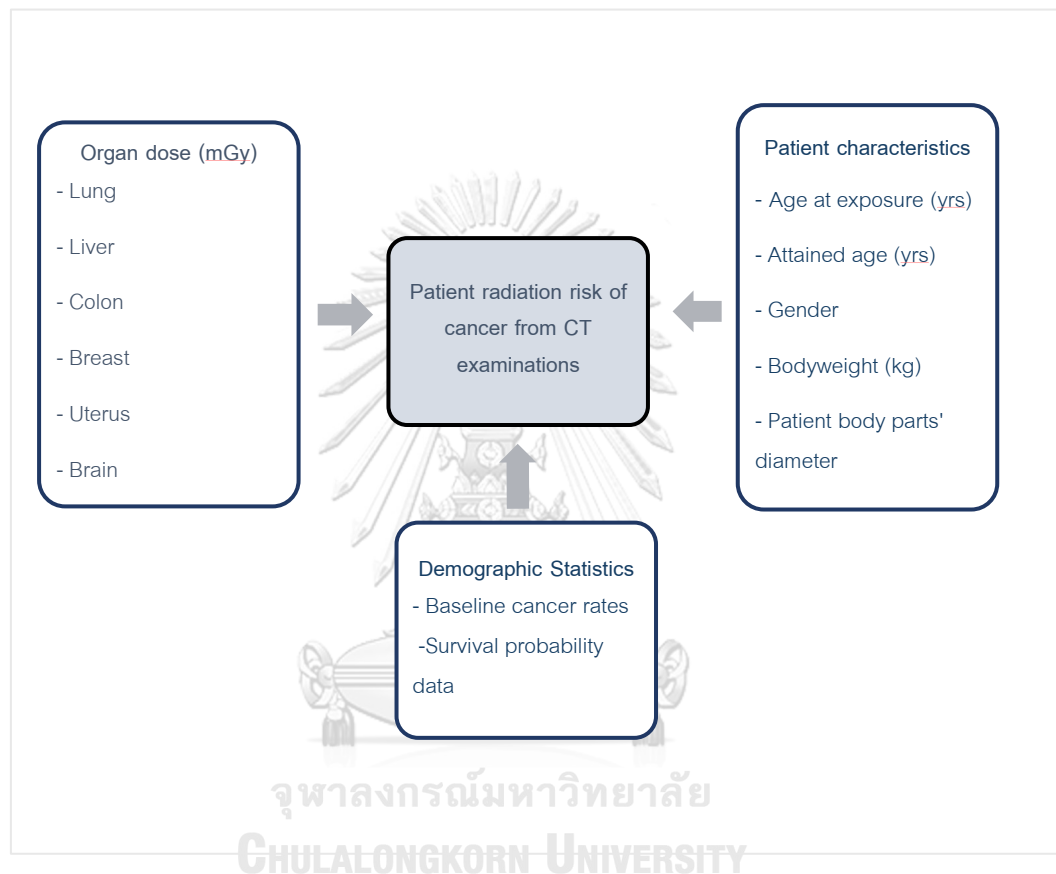
3.4 Scope of work

The scope of this study is to determine the Lifetime Attributable Risk (LAR) of the target organs, which represent the risk of cancer incidence and mortality from CT examinations at high dose, ($CED \geq 100$ mSv) in a single day to low dose, ($CED < 100$ mSv) from the common CT protocols, including CTA of the whole aorta. Refer to the BEIR VII model based on the organ dose, gender, age at exposure, attained age, and demographic statistics of the Thai population (baseline rate of cancer and survival probability data). In addition, a mathematical model derived from multivariate analysis will be developed to assess the cancer risk from CTA of the whole aorta of individual patient.

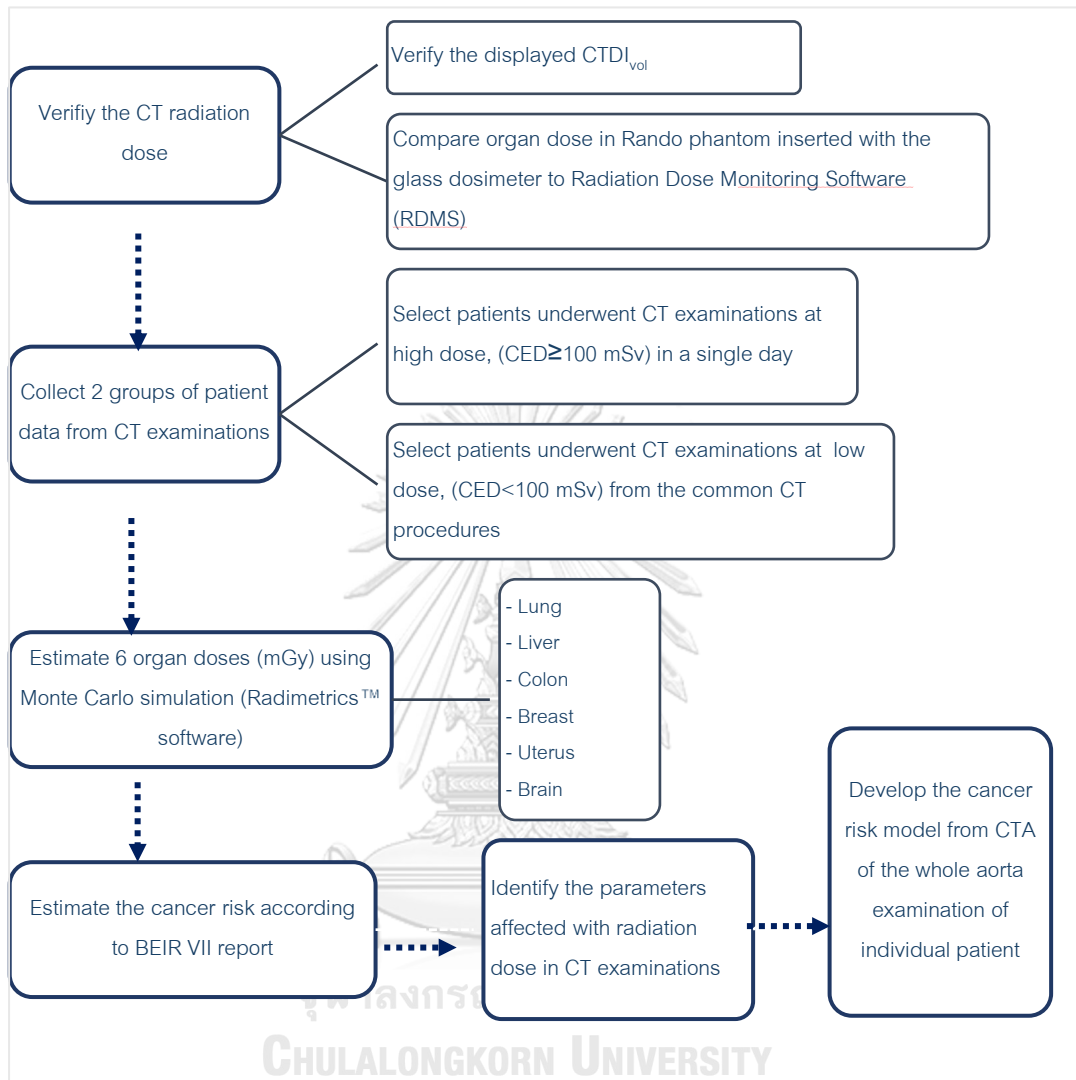
3.5 Research design

This is an observational descriptive research design in a type of retrospective study.

3.6 Conceptual framework



3.7 Research design model



3.8 Expected benefit

- Obtain the number and percentage of patients receiving CED at 100 mSv and above in a single day from total CT Examinations within 5 years at two University hospitals.
- Quantify the risk of cancer from CT examinations at high dose to low dose from the common protocols and identify the impact factors on the radiation dose and cancer risk in different age groups, below 40 years old (young patients), and above 40 years (elder patients). In order to justify and optimize the radiation protection of patients. Using BEIR VII model and demographic statistics: abridged life table data and baseline cancer incidence and mortality rates for the Thai population.
- Obtain the cancer risk model for CTA of the whole aorta examination to estimate the LAR.

3.9 Variable measurements

The independent variables are CT radiation dose, patient characteristics, and demographics of the Thai population.

The dependent variables are the number and percentage of patients receiving CED at 100 mSv and above in a single day and the lifetime attributable risk (LAR).

3.10 Data collection

Data were collected of patients aged 15 to 75 years old who performed CT examinations during the period of five years at two University hospitals. The patient data consists of the age, gender, body weight, body part diameter, patient radiation dose in the effective dose, mSv and organ dose, mGy from the DICOM header and RDMS, Radimetrics™ Enterprise Platform. LAR was estimated by the BEIR VII report including parameters of age at exposure, attained age, organ dose, and dose and dose rate effectiveness factor (DDREF).

3.11 Outcome


The number and percentage of patients who received cumulative effective dose (CED) at 100 mSv and above in a single day, as well as the lifetime attributable risk (LAR) for all CT examinations, are obtained.

3.12 Statistical analysis

Descriptive statistics were used and presented as mean, standard deviation, median, percentage mean, standard deviation, frequency, and range (min-max). A regression model was implemented to analyze the relationship between one or more independent variables and dependent variables.


3.13 Ethical Consideration

This research involved the determination of patient dose and the cancer risk estimation from CT examinations. The patient data had been collected during the period of 5 years from January 2018 to December 2022 in adult patients who underwent CT examinations. The research proposal was approved by the Ethic Committees of the Faculty of Medicine, Chulalongkorn University, and the Faculty of Medicine, Prince of Songkla University, Thailand. The certificates of approval from the Institutional Review Boards (IRB) are shown in Figures 3.1 and 3.2.



INSTITUTIONAL REVIEW BOARD
Faculty of Medicine, Chulalongkorn University
 1873 Rama 4 Road, Pathumwan, Bangkok 10330, Thailand, Tel. 662-256-4493

COA No. 0967/2022
 IRB No. 0404/65



Certificate of Expedited Review Approval
 (COA No. 0967/2022)

The Institutional Review Board of the Faculty of Medicine, Chulalongkorn University, Bangkok, Thailand, has approved the following study which is to be carried out in compliance with the International guidelines for human research protection as Declaration of Helsinki, The Belmont Report, CIOMS Guideline and International Conference on Harmonization in Good Clinical Practice (ICH-GCP)

Study Title : Evaluation of patient radiation dose and risk of cancer from recurrent CT and CT angiography of the aorta

Study Code : -

Principal Investigator : Mrs. Saowapark Poosiri

Affiliation of PI : Department of Radiology,
 Faculty of Medicine, Chulalongkorn University.

Review Method : Expedited


Continuing Report : At least once annually or submit the final report if finished.


Document Reviewed :

1. Research Proposal Version 2 Date 7 July 2022
2. Protocol Synopsis Version 2 Date 7 July 2022
3. Data record form Version 1 Date 3 June 2022
4. Curriculum Vitae and GCP Training

- Mrs. Saowapark Poosiri

- Asst.Prof. Kitiwet Khamwan, Ph.D.
 - Assoc.Prof. Anchali Kisanachinda, Ph.D.

Signature 
 (Emeritus Professor Tada Sueblinwong MD)
 Chairperson
 The Institutional Review Board

Signature 
 (Assistant Professor Patou Tantibirojn MD)
 Member and Assistant Secretary, Acting Secretary
 The Institutional Review Board

Date of Approval : July 18, 2022
Approval Expire Date : July 17, 2023

Figure 3.1 The Institutional Review Board (IRB) Certificate,
 Faculty of Medicine, Chulalongkorn University.

จุฬาลงกรณ์มหาวิทยาลัย
CHULALONGKORN UNIVERSITY

AL-011_TH



คณะกรรมการจริยธรรมการวิจัยในมนุษย์
คณะแพทยศาสตร์ มหาวิทยาลัยสงขลานครินทร์

หนังสือรับรองฉบับนี้ให้ไว้เพื่อแสดงว่า

รหัสโครงการ : REC.65-327-7-2

ชื่อโครงการ : การประเมินปริมาณรังสีและการประเมินความเสี่ยงของการเป็นมะเร็งในผู้ป่วยที่ตรวจด้วยเครื่องเอกซเรย์คอมพิวเตอร์หลายครั้ง และการตรวจหลอดเลือดแดง (Evaluation of patient radiation dose and risk of cancer from recurrent CT and CT angiography of the aorta)

ผู้วิจัยหลัก : เสาวภาคย์ ภูศิริ สาขาวิชารังสีวิทยา คณะแพทยศาสตร์ มหาวิทยาลัยสงขลานครินทร์

ผู้ร่วมวิจัย : กิติวัฒน์ คำวัน ภาควิชารังสีวิทยา คณะแพทยศาสตร์ จุฬาลงกรณ์มหาวิทยาลัย

อัญชลี ฤกษ์จินดา ภาควิชารังสีวิทยา คณะแพทยศาสตร์ จุฬาลงกรณ์มหาวิทยาลัย

เอกสารที่รับรอง :

1. แบบเสนอเพื่อขอรับการพิจารณาจริยธรรมการวิจัยในมนุษย์ เวอร์ชัน 1.0 ฉบับวันที่ 19 สิงหาคม 2565
2. โครงการวิจัยฉบับสมบูรณ์ เวอร์ชัน 2.0 ฉบับวันที่ 20 กันยายน 2565
3. แบบบันทึกข้อมูล เวอร์ชัน 2.0 ฉบับวันที่ 20 กันยายน 2565
4. ประวัติผู้วิจัยและหลักฐานการอบรมจริยธรรมการวิจัย

ได้ผ่านการพิจารณาและรับรองจากคณะกรรมการจริยธรรมการวิจัยในมนุษย์คณะแพทยศาสตร์ มหาวิทยาลัยสงขลานครินทร์ โดยยึดหลักจริยธรรมของประกาศเฮลซิงกิ (Declaration of Helsinki) และแนวทางการปฏิบัติทางคลินิกที่ดี (The International Conference on Harmonization in Good Clinical Practice) โดยบรรจุไว้ในการประชุมคณะกรรมการจริยธรรมการวิจัยในมนุษย์ ครั้งที่ 30/2565 วาระที่ 3.4

ขอให้กวีวิจัยรายงานความก้าวหน้าโครงการวิจัย ทุก 12 เดือน และยื่นต่ออายุก่อนถึงวันหมดอายุอย่างน้อย 30 วัน

ลงชื่อ 

(รศ.นพ.บุญสิน ตั้งตระกูลนิช)

ประธานคณะกรรมการจริยธรรมการวิจัยในมนุษย์
คณะแพทยศาสตร์ มหาวิทยาลัยสงขลานครินทร์

วันที่รับรอง : 23 กันยายน พ.ศ. 2565
หมดอายุ : 22 กันยายน พ.ศ. 2566

คณะกรรมการจริยธรรมการวิจัยในมนุษย์
คณะแพทยศาสตร์ มหาวิทยาลัยสงขลานครินทร์
15 ถนนกาญจนาภิเษย์ อำเภอหาดใหญ่ จังหวัดสงขลา
90110
โทรศัพท์ 074451149, 074451157
โทรสาร 074212900

Ref no. KtV3-t8oS-LcBE-Xprd
มอ 351.7.2/ec.2489

CHULALONGKORN UNIVERSITY

Figure 3.2: The Institutional Review Board (IRB) Certificate,
Faculty of Medicine, Prince of Songkla University

CHAPTER 4

MATERIALS AND METHODS

4.1 Materials

The materials to be used in each section of the experiment are as follows:

4.1.1 Verification of displayed $CTDI_{vol}$

- 1) PMMA phantoms
- 2) Pencil-type ionization chamber and the electrometer

4.1.2 Verification of organ dose

- 1) Radio-Photoluminescence Glass Dosimeter (RPLGD) system
- 2) Anthropomorphic Rando phantom
- 3) Low-dose radiation measuring equipment (ionizing dosimeter)
- 4) General X-ray equipment

4.1.3 Patient study: Lifetime attributable risk (LAR)

- 1) CT Scanners
- 2) Data population and radiation dose determination; DICOM headers, Radimetrics™ Enterprise Platform
- 3) Demographic statistics of Thai population
 - 3.1 Baseline rate of cancer
 - 3.2 Survival probability data
- 4) R Studio software
- 5) Stata software

4.1.1 Verification of displayed $CTDI_{vol}$

1) PMMA phantoms

Two cylindrical phantoms are made of polymethyl methacrylate (PMMA): the body phantom with diameter of 32 cm, and the head phantom, with 16 cm diameter and 15 cm length had been used. There are five holes, one hole located at the center and four holes located peripherally at the 3, 6, 9, and 12 o'clock positions of the phantom, as shown in Figure 4.1.

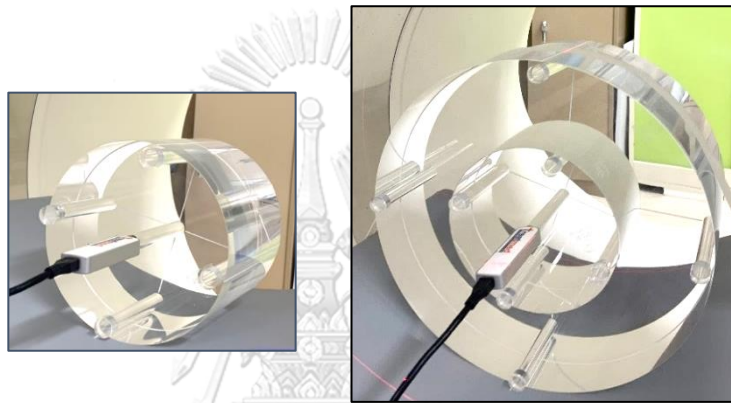


Figure 4.1: PMMA head phantom 16 cm (left) and body phantom 32 cm diameters (right).

2) The pencil-type ionization chamber and the electrometer

The ionization chamber for CT dosimetry is a non-sealed cylindrical chamber with a sensitive length of 10 cm. It was designed to fit in a hole of a PMMA phantom at various locations. The ionization chamber, manufacturer RaySafe Model X2 (Unfors RaySafe AB, Havas, Sweden) with temperature and pressure corrections, was used in this study. The measurement provides the estimation of the CTDI and DLP, in the unit of mGy, and mGy.cm, respectively. The dosimetric quantity was recorded on the digital display. The pencil-type ionization chamber and the electrometer are shown in Figure 4.2.



Figure 4.2: Pencil-type ionization chamber RaySafe X2 CT Detector and the electrometer

4.1.2 Verification of organ dose

1) Radio-Photoluminescence Glass Dosimeter (RPLGD) system

The RPLGD, Dose Ace system, was manufactured by Asahi Techno Glass Corporation (ATGC, Shizuoka, Japan). Glass dosimeter is a type of solid-state dosimeter that relies upon the radio photoluminescent phenomenon of silver-activated phosphate glass. The dosimeter system consists of a rod-shaped silver-activated phosphate glass, a plastic capsule, and an FGD-1000 reader unit.

The RPLGD model GD-352M (Figure 4.3) is equipped with a tin filter to determine the organ dose in the Rando phantom. The tin filter decreases the energy dependence identified in radiation diagnosis within the range of energy below 100 keV and compensates for the high response in low-energy photons. The dimensions of the RPLGD model GD-352M are 1.5 mm in diameter and 12 mm length, the effective atomic number and density are 12.04 and 2.61 g.cm⁻³, respectively. RPLGDs model GD-352M have a wide dose range from 10 μ Gy to 10 Gy with a small fading effect of 0.4% after 100 days, and several repeated readouts [45, 46]. Table 4.1 displays the manufacturer specifications and characteristics of RPLGDs [47]. The annealing process and preheating were conducted using a Laboratory oven (Carbolite Gero) and the accumulated value was read out using an FGD-1000 reader, as shown in Figure 4.4.

Table 4.1: Specifications of RPLGD model GD-352M

Specifications	
Dosimeter element	
Glass element dimensions	1.5x12 mm (cylindrical shape) (with ID and filter)
Weight	Several tens of mg
Measuring range (gamma ray & X-rays)	10 μGy (μSv) to 10 Gy (Sv)
Reader (FGD-1000)	
Display value unit	Gy (Sv)
Display value range	1 μGy (Sv) to 10 Gy (Sv)
Reproducibility, Coefficient of variation (CV)	$\leq 5\%$ (at 100 μGy), $\leq 2\%$ (at 1 mGy)
Continuous reading	20 glass elements
Read-out time	≤ 6 seconds / element



Figure 4.3: Radio-photoluminescence Glass Dosimeter (RPLGD), model GD-352M with filters in capsule (Left), Glass rod (Right)



Figure 4.4: Laboratory oven (Carbolite Gero), (Left) and glass dosimeter reader (FGD-1000), (Right)

2) Anthropomorphic Rando phantom

A female adult anthropomorphic Rando phantom (Alderson Research Labs, Stanford, CA, USA) is made of tissue-equivalent materials, a physical representation of the human body, and simulated the radiation attenuation characteristics [48]. Each phantom slice contains holes plugged with bone-equivalent, soft-tissue-equivalent or lung tissue-equivalent pins enable insertion of RPLGD. The slab phantom was used to determine the organ absorbed dose in the lung, colon, liver, uterus, and breasts, as shown in Figure 4.5.

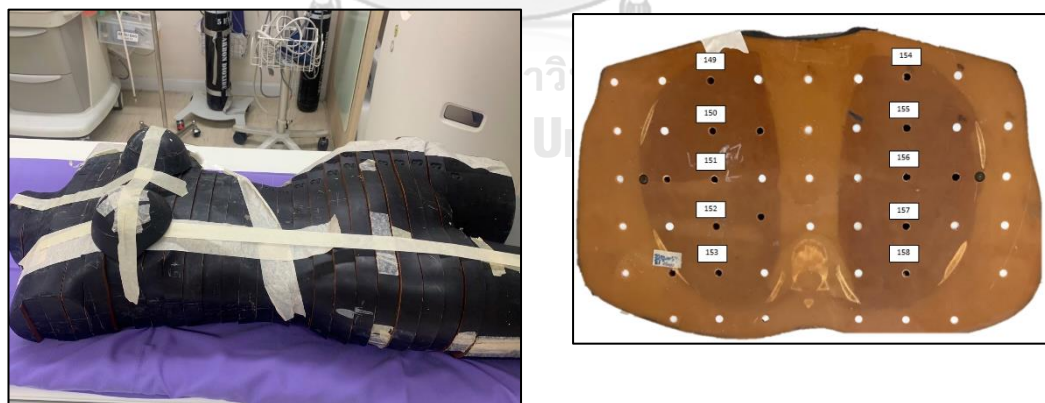


Figure 4.5: Female anthropomorphic Rando phantom (Left), Slab of lung phantom with holes for RPLGD insertion (Right)

3) Low-dose radiation measuring equipment (ionizing dosimeter)

The ionizing dosimeter- an unsealed cylindrical, model 10X6-6, general purpose in beam chamber; Radcal, Monrovia, CA, USA and an electrometer Model9096 (Accu-PRO™) (Figure 4.6) were used to calibrate the RPLGD, with large energy response throughout the diagnostic energy range. The ionizing dosimeter had been calibrated by the Secondary Standard Dosimeter Laboratory (SSDL) in Thailand and considered as the gold-standard for radiation dosimetry.

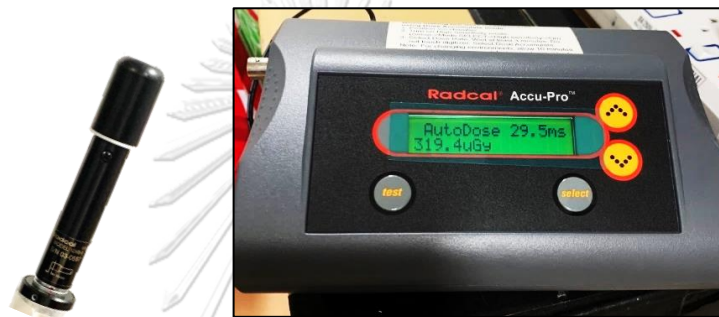


Figure 4.6: A 6-cc ion chamber Model 10X6-6 and Radcal 9096 electrometer (Radcal, Monrovia, CA, USA)

4) General X-ray equipment

A diagnostic imaging system for radiographic, Siemens Healthineers (Model Luminos Argile X-Ray System) is used to calibrate RPLGDs, as shown in Figure 4.7.



Figure 4.7: Siemens Healthineers radiographic system

4.1.3 Patient study: Lifetime attributable risk (LAR)

1) CT Scanners

CT scanners from two academic centers, King Chulalongkorn Memorial Hospital and Songklanagarind Hospital, had been used to acquire and process the medical imaging in this study. CT scanners with details on manufacturer and model, site, and year of installation were displayed in Table 4.2 and 4.3, as followings:

Table 4.2: CT scanners at King Chulalongkorn Memorial Hospital

Manufacturer	Model	Detector Row CT	Year of installation	Number of CT scanners
Siemens Healthineers, Forchheim, Germany	SOMATOM Force dual-source	192	2015	1
GE Healthcare, Milwaukee, WI, USA	Revolution	256	2017	1

Table 4.3: CT scanners at Songklanagarind Hospital

Manufacturer	Model	Detector Row CT	Year of installation	Number of CT scanners
Canon Medical Systems, Otawara, Japan	Aquilion Prime	80	2016	2
Philips Healthcare, Cleveland, OH, USA	Brilliance iCT	256	2016	1
GE Healthcare, Milwaukee, WI, USA	Revolution Apex	256	2017	1

2) Data population and radiation dose determination

The data were collected from adult patients aged 15 to 75 years old who underwent CT examinations for a period of five years from January 2018 to December 2022. The patient data and patient dose were extracted from digital imaging and communications in medicine (DICOM) headers on the Synapse workstation and dose monitoring software, Radimetrics™ Enterprise Platform (Bayer HealthCare, Whippany, NJ, USA).

Radimetrics™ Enterprise Platform provides radiation dose from CT scan, which the organ dose and effective dose were obtained from Monte Carlo simulations. The patients are represented as stylized phantoms, where the organs are modelled using simple geometric shapes described by mathematical equations. The organ dose is calculated from the ratio of the simulated organ dose to the simulated $CTDI_{vol}$ multiplied by the reported $CTDI_{vol}$ [49]. The stylized phantom, along with the scan region and organ dose, resulting from the use of the software are displayed in Figure 4.8.

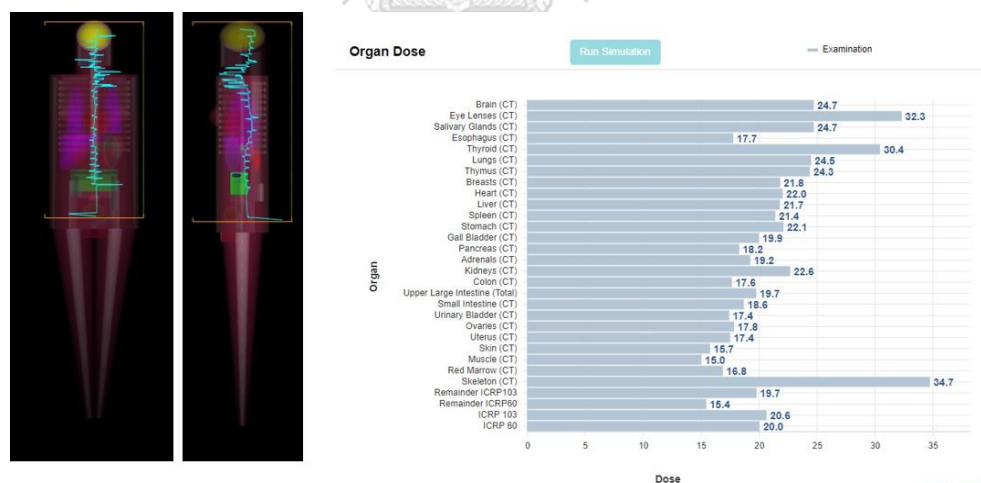


Figure 4.8: The organ dose estimated by the dose monitoring software, Radimetrics™ Enterprise Platform (Bayer HealthCare, Whippany, NJ, USA)

3) Demographic statistics of Thai population

3.1 Baseline rate of cancer

The baseline rate of cancer incidence and mortality rates of gender and age-specific of the unexposed population in Thailand for the year 2020, were provided by CANCER TODAY (WHO) and International Agency for Research on Cancer [4] (Figure 4.9).



Figure 4.9: The baseline rate of cancer provided by CANCER TODAY, WHO

3.2 Survival probability data

The survival function represents the probability of surviving, provided by the life table for the Thai population with age less than one to eighty years old, and obtained from the National Statistical Office of Thailand [50].

4) R Studio software

R Studio is an integrated development environment for R, programming language for statistical computing and graphics. R Studio version 1.4.1103 has been used to calculate the cancer risk, LAR.



5) Stata software

The Stata program, statistical software is commonly used in the field of data science. STATA version 18 was utilized to create a mathematical model to assess the risk of cancer obtained from CTA of the whole aorta examinations.



4.2 Methods

The methods consist of four sections,

4.2.1 Verification of displayed $CTDI_{vol}$

4.2.2 Verification of organ dose

4.2.3 Comparison of the organ dose in Rando phantom and Radimetrics™ Enterprise Platform.

4.2.4 Determination of the Lifetime attributable risk (LAR) of patients

The details will be as follows:

4.2.1 Verification of displayed $CTDI_{vol}$

The $CTDI_{vol}$ was estimated by axial scanning of each PMMA cylindrical phantom with pencil ionization chamber insertions at various kVp values from 80 to 140. The measured and the displayed $CTDI_{vol}$ were compared with the acceptable limit at $\pm 20\%$ [51]. The measurement of $CTDI_{vol}$ followed the IAEA Human Health Series No.19, as follows:

- 1) PMMA phantom was placed on the patient couch. Position the phantom at the center along the scan plane, both vertical and horizontal using CT laser light. Scan projection radiographs (SPR) in both the anterior-posterior and lateral planes to ensure the phantom is centered in both the vertical and horizontal axes. An acceptable level of position accuracy is within a range of ± 1 cm [51].

- 2) The 100 mm pencil chamber was inserted in the center hole of PMMA phantom, then insert the jigs at the other holes.
- 3) The scan parameters were set for the head and body protocols, 100 mA and 1 second rotation time, axial mode, then vary the kVp at 80, 100, 120, and 140. Record the measured dosimeter reading.
- 4) Ion chamber was moved to each peripheral hole of the phantom, record the CTDI values at all positions.
- 5) The measured and displayed $CTDI_{vol}$ on the scanner console were compared. The $CTDI_{vol}$ is calculated using Equations 2.7 and 2.8 of Chapter 2.

4.2.2 Verification of organ dose

The organ doses were obtained from dose monitoring software based, Radimetrics™ Enterprise Platform based on Monte Carlo simulation. The organ doses were verified by exposing the anthropomorphic phantom inserted with glass dosimeters of the clinical protocol technique.

4.2.2.1 Measurement process of RPLGDs

The RPLGDs were annealed before irradiation. Following the irradiation, they were preheated in an oven, and then read out the cumulative value using FGD-1000 reader. The measurement process of glass dosimeters is shown in Figure 4.10.

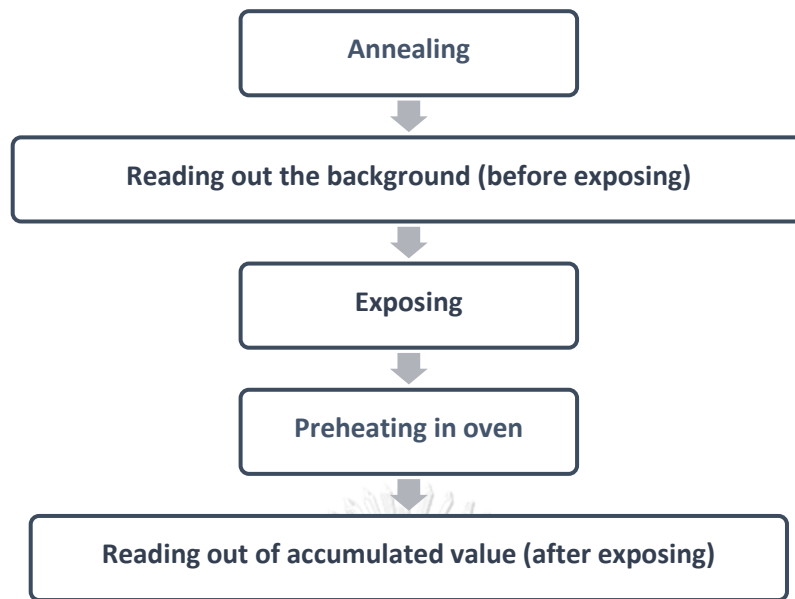


Figure 4.10: Measurement process of RPLGDs

4.2.2.2 Calibration of RPLGDs

The ionization chamber and the RPLGD were set at 150 cm (SDD) from the focal spot with a field size of 5 cm x 5 cm. Each RPLGD was calibrated using diagnostic X-ray beam of 120 kVp (7.7 mm Al HVL). An exposure of 120 kVp and 16 mAs in free air to the IC and RPLDs were displayed in Figure 4.11. 5 RPLGDs in each group at an interval of approximately 1 cm to avoid scatter radiation and exposing 20 groups were set with the same parameter settings. The dose was determined using a calibrated ionizing dosimeter by SSDL Thailand as the gold standard.

Calculation of calibration coefficient

RPLGDs calibration coefficient for a diagnostic X-ray beam of 120 kVp was determined by the following equation.

Calibration coefficient of RPLGD=

$$\frac{\text{Dose value from IC} \times \text{Calibration coefficient of the ionizing dosimeter} \times \text{Correction factor for air density}}{\text{Dose value from RPLGD}}$$



Figure 4.11: Set the SDD for the ionization chamber and RPLGDs at 150 cm for the calibration.

4.2.3 Comparison of the organ dose in Rando phantom and Radimetrics™ Enterprise Platform.

A Rando phantom, inserted with the RPLGD Model GD-352M at the lung, liver, colon, uterus, and breast to determine organ doses, was scanned using chest and abdomen CT protocol. The steps of this process are as follows:

- 1) 100 RPLGDs, 90 RPLGDs were placed at various organs (Table 4.4). Each RPLGD was positioned near the center of the organ. 10 RPLGDs were used to measure background radiation.

Table 4.4: 90 RPLGDs inserted in each tissue or organ.

Organ	Section of anthropomorphic phantom	Number of dosimeters
Breast	Left Breast	8
	Right Breast	8
Lung	11	4
	12	6
	13	6
	14	6
	15	10
	16	10

	17	10
	18	8
	19	6
	20	2
	21	2
Liver	21	3
	22	1
Colon	25	2
	27	1
	28	2
Uterus	29	3
	30	2

2) The phantom was positioned on the CT couch.

3) Rando phantom inserted with the RPLGD was scanned using the protocol for the chest and abdomen using the Siemens Healthineers SOMATOM Force CT scanner. Acquisition parameters and radiation dose for chest and abdomen CT examination are shown in Table 4.5.

Table 4.5: Acquisition parameters and radiation dose for chest and abdomen CT examinations

Acquisition Protocols	Chest and abdomen
Mode	SECT; single energy mode
Tube voltage (kVp)	120
Effective mAs	200
Rotation time (s)	0.5
Scan time (s)	6.53
Pitch	1.2
Detector configuration (mm)	192x0.6
CTDI _{vol} (mGy)	13.4
DLP (mGy.cm)	1141

4) After exposure, the RPLGDs were placed in an oven and preheated before reading out. The net dose for each RPLGDS was determined by subtracting the background radiation and read-out value.

5) Organ absorbed dose in the lung, liver, colon, breast, and uterus were calculated by multiplying the calibrated dose values by the mass energy coefficient ratio of each tissue to air [52-54]. The organ dose was calculated from the following equation.

$$\text{Absorbed organ dose (mGy)} = \frac{(\text{Dose value from RPLGD-Background value}) \times \text{calibration coefficient of RPLGD} \times \left(\frac{\mu_{en}}{\rho}\right)_{med}}{\left(\frac{\mu_{en}}{\rho}\right)_{air}}$$

where $\left(\frac{\mu_{en}}{\rho}\right)_{med}$ and $\left(\frac{\mu_{en}}{\rho}\right)_{air}$ are the mass energy absorption coefficients for the organ and air, which obtained from the ICRU Report 44 (International Commission on Radiological Unit and measurement).

The difference and percent relative difference of organ doses from the phantom to the dose monitoring software, which has a diameter of 228 mm, were compared using the following equation.

$$\% \text{ Relative difference} = \left(\frac{\text{Organ dose from (Radimetrics)(mGy)} - \text{Organ doses from RPLGD measurement(mGy)}}{\text{Organ doses from RPLGD measurement(mGy)}} \right) \times 100$$

CHULALONGKORN UNIVERSITY

4.2.4 Determination of the Lifetime attributable risk (LAR) of patients

The patient aged 15 to 75 years old who underwent CT examinations were collected for a period of five years from January 2018 to December 2022 in the following steps:

1) Patient data (age, gender, body weight, body diameter) and scanning protocols were surveyed at both hospitals from DICOM header, dose monitoring software of patients, obtain

- high dose range, CED at 100 mSv and above in a single day

- low dose range, CED below 100 mSv, from common CT procedures of brain without and with contrast enhanced phase, chest with contrast-enhanced phase, whole abdomen with triphasic phased including without contrast enhanced, arterial and portal phase, and CTA of whole aorta, without contrast, arterial and delayed phase had been acquired. The protocols were designed by the radiologists based on the patient's clinical indications.

Divide the patient data into two age groups: below 40 years old–called young patients, and above 40 years old–called elder patients.

2) Effective dose (mSv) and organ dose (mGy) - such as lung, liver, colon, breast, uterus, and brain were estimated based on Monte Carlo simulation (Radimetrics™ software).

3) LAR was determined according to the BEIR VII report [8] which provided model and parameters for specific organs of each gender including parameters of age at exposure, attained age, organ dose, and dose and dose rate effectiveness factor (DDREF). The LAR of cancer incidence and mortality in each patient was estimated using Equation 2.16 from Chapter 2 and applied to survival probability data of the Thai population.

$$LAR(D, e) = \sum_a^{a_{max}} M(D, e, a) S(a)/S(e)$$

LAR is defined as the summation from a equals $e + L$ to a_{max} , where a is attained age (years), a_{max} is maximum age (80 years), L is a risk-free latent period (5 years for solid cancers), e is the age at exposure (15 to 75 years), D is an organ dose, and $S(a)/S(e)$ is the conditional probability of a person alive and cancer-free at age-at exposure, e , to reach at least an attained age- a , obtained from abridged life table provided by National Statistical Office of Thailand [50].

$M(D, e, a)$ is the excessive cancer risk model, which can be calculated using relative risk transport and absolute risk transport based on the excess relative risk (ERR) model and the excess absolute risk (EAR) model. Models for estimating solid cancer risks and breast cancer: ERR and EAR are in equations 2.13 to 2.15 of Chapter 2. $M(D,$

e, a) was estimated using Equation 2.17 to 2.20 from Chapter 2 and applied to baseline cancer rate of the Thai population.

Excess for cancer incidence risk:

$$M(D, e, a) = EAR(D, e, a)$$

$$M(D, e, a) = ERR(D, e, a)\lambda_I(a)$$

Excess for cancer mortality risk:

$$M(D, e, a) = EAR(D, e, a) \lambda_M(a)/\lambda_I(s, a)$$

$$M(D, e, a) = ERR(D, e, a)\lambda_M(a)$$

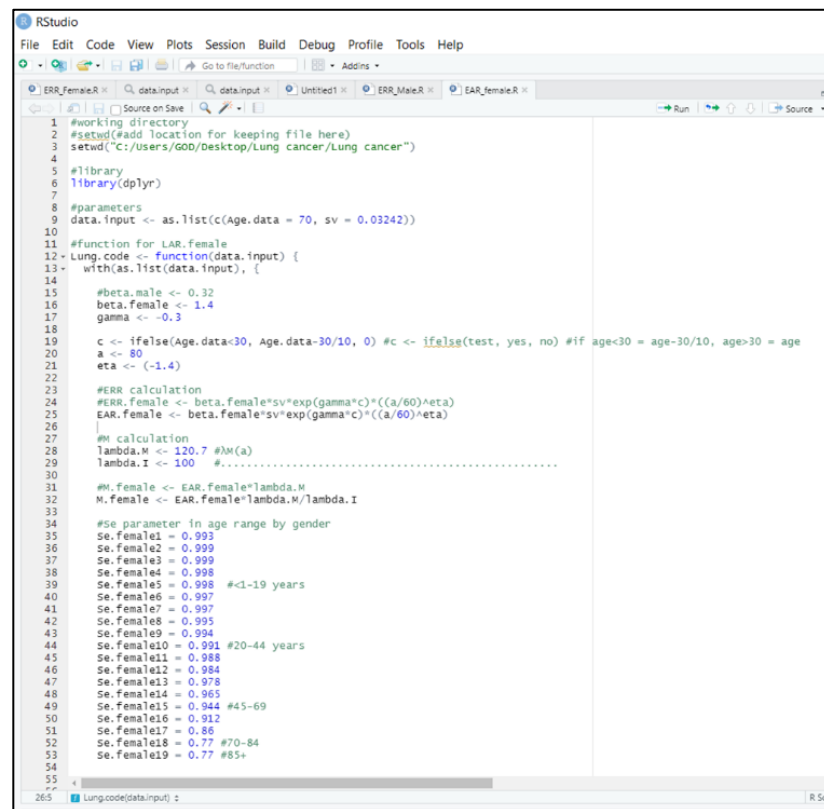
where $\lambda_I(a)$ represents sex and age-specific of baseline cancer incidence rates, whereas the $\lambda_M(a)$ represents sex and age-specific cancer mortality rates obtained from cancer statistics Thailand for the year 2020, published by the World Health Organization (WHO), International Agency for Research on Cancer [4].

For the estimation of LAR, the risk-transfer weight or weighting factor was obtained with EAR and ERR transport models for the site of solid cancers (liver, colon, uterus, and brain), BEIR VII recommended a weighting factor(ω) of 0.7. The weighting factor(ω) of 0.7 was estimated using ERR transport and 0.3 to estimate using EAR transport. For lung cancer, the weighting factor was reversed, 0.7 for the EAR transport and 0.3 for the ERR transport. The LAR of breast cancer was estimated based on the EAR model.

For the LAR estimation, the ERR and EAR models were combined via the weighting factor(ω) and subsequently adjusted by dividing DDREF of 1.5, as suggested by the BEIR VII report.

$$LAR = [(LAR_{ERR})^w \times (LAR_{EAR})^{1-w}]/DDREF$$

For determining LAR, we programmed a library in R studio that contains an application of mathematical functions to calculate LAR based on ERR and EAR (Figure 4.12). Details are illustrated in the appendix.



```

1 #working directory
2 #setwd(Add location for keeping file here)
3 setwd("C:/Users/GOD/Desktop/Lung cancer/Lung cancer")
4
5 #library
6 library(dplyr)
7
8 #parameters
9 data.input <- as.list(c(Age.data = 70, sv = 0.03242))
10
11 #function for LAR.Female
12 Lung.code <- function(data.input) {
13   with(as.list(data.input), {
14
15     #beta.male <- 0.32
16     beta.female <- 1.4
17     gamma <- -0.3
18
19     c <- ifelse(Age.data<30, Age.data-30/10, 0) #c <- ifelse(test, yes, no) #if age<30 = age-30/10, age>30 = age
20     a <- 80
21     eta <- (-1.4)
22
23     #ERR calculation
24     ERR.female <- beta.female*sv*exp(gamma*c)*((a/60)^eta)
25     EAR.female <- beta.female*sv*exp(gamma*c)*((a/60)^eta)
26
27     #M calculation
28     lambda.M <- 120.7 #M(a)
29     lambda.I <- 100 #.....
30
31     #M.female <- EAR.female*lambda.M
32     M.female <- EAR.female*lambda.M/lambda.I
33
34     #se parameter in age range by gender
35     Se.female1 = 0.995
36     Se.female2 = 0.999
37     Se.female3 = 0.999
38     Se.female4 = 0.998
39     Se.female5 = 0.998 #<19 years
40     Se.female6 = 0.997
41     Se.female7 = 0.997
42     Se.female8 = 0.995
43     Se.female9 = 0.994
44     Se.female10 = 0.991 #20-44 years
45     Se.female11 = 0.988
46     Se.female12 = 0.984
47     Se.female13 = 0.978
48     Se.female14 = 0.965
49     Se.female15 = 0.944 #45-69
50     Se.female16 = 0.912
51     Se.female17 = 0.86
52     Se.female18 = 0.77 #70-84
53     Se.female19 = 0.77 #85+
54
55
265 Lung.code(data.input)

```

Figure 4.12: R Studio library development

4). The parameters affected with radiation dose and risk of cancer in CT examinations were identified.

5). Mathematics model/equation has been developed for estimating to estimate the cancer risk from CTA of individual patients with multivariate regression model analysis.

The multivariable prediction model was developed for predicting the individual LAR for cancer incidence and mortality in patients who underwent CTA whole aorta. The process of multiple linear regression involves the application of a linear equation to the data that has been observed in order to figure out the relationship between two or more metric explanatory factors and LAR of cancer incidence and mortality.

4.3 Sample population

4.3.1 Target population

Adult patients underwent CT examination who received CED 100 mSv and above in a single day and common protocols from January 2018 to December 2022 at King Chulalongkorn Memorial Hospital and Songklanagarind Hospital.

4.3.2 Sample size determination

Estimate single proportion, 95% CI of $\pi = p \pm d$

$$n = \frac{z_{\alpha/2}^2 pq}{d^2}$$

Where α : Probability of type I error = 0.005 (2-sided), $Z_{0.025} = 1.96$

p: Estimated proportion, 0.5 (in order to estimate the maximum sample size)

q: $1 - p = 0.5$

d: Margin of error in estimating, 5%

Consequently, the determination of the sample size was 385.

4.3.3 Sample population and eligible criteria

The inclusion criteria

1) The inclusion criteria for primary objective in this study are Thai adult patients of the age 15 to 75 years old and receiving the effective dose at 100 mSv and above in a single day.

2) The inclusion criteria for secondary objective in this study are Thai adult patients with the age 15 to 75 years old and underwent common CT examinations.

The exclusion criterion in this study is patients with incomplete demographic data (e.g., age, gender, body weight).

4.4 Statistical analysis

Descriptive statistics is used and presented as mean, standard deviation, median, percentage mean, standard deviation, frequency and range (min-max). A regression model that provides the relationship between one or more independent variables and dependent variables are used.



CHAPTER 5

RESULTS

5.1 Verification of the displayed $CTDI_{vol}$

The $CTDI_{vol}$ displayed on the monitors of CT scanners was verified by comparing the displayed and measured $CTDI_{vol}$. The percent difference from all CT scanners were within ± 20 [51]. The results at various kVp were displayed in Tables 5.1, 5.2, and 5.3.

5.1.1 Siemens Healthineers CT scanner

Table 5.1: Measured and displayed $CTDI_{vol}$ on the Siemens CT monitor in head and body phantoms.

$CTDI_{vol}$ (mGy) in 16 cm head phantom (5 mm slice thickness)			
kVp	Measured $CTDI_{vol}$	Displayed $CTDI_{vol}$	% Difference
100	7.79	7.21	7.45
120	12.50	11.57	7.44
140	17.80	17.01	4.44
$CTDI_{vol}$ (mGy) in 32 cm body phantom (5 mm slice thickness)			
100	3.59	3.46	3.62
120	5.99	5.82	2.84
140	8.76	8.65	1.26

5.1.2 GE CT scanner

Table 5.2: Measured and displayed $CTDI_{vol}$ on the GE CT monitor in head and body phantoms.

$CTDI_{vol}$ (mGy) in 16 cm head phantom (5 mm slice thickness)			
kVp	Measured $CTDI_{vol}$	Displayed $CTDI_{vol}$	% Difference
80	6.86	8.21	19.68
100	12.62	14.88	17.91
120	19.72	22.75	15.37

140	27.70	32.00	15.52
CTDI _{vol} (mGy) in 32 cm body phantom (5 mm slice thickness)			
80	3.16	3.74	18.35
100	5.98	6.94	16.05
120	9.56	10.87	13.70
140	13.67	15.49	13.31

5.1.3 Canon CT scanner

Table 5.3: Measured and displayed CTDI_{vol} on the Canon CT monitor in head and body phantoms.

CTDI _{vol} (mGy) in 16 cm head phantom (8 mm slice thickness)			
kVp	Measured CTDI _{vol}	Displayed CTDI _{vol}	% Difference
80	9.28	10.00	7.76
100	16.60	18.30	10.24
120	27.12	28.1	3.61
135	35.74	37.10	3.81
CTDI _{vol} (mGy) in 32 cm body phantom (8 mm slice thickness)			
80	4.05	4.40	8.64
100	8.58	9.00	4.90
135	19.10	20.40	6.81

5.2 Verification of organ dose

5.2.1 Calibration of RPLGDs

The mean \pm S.D. of the air kerma measured by the ionization chamber was 307.17 \pm 0.08 μ Gy. The mean \pm S.D. of the air kerma measured by 100 RPLGDs was 303.80 \pm 9.59 μ Gy as shown in Table 5.4. The readout value for 100 RPLGDs is displayed in Figure 5.1. The outlier is excluded.

Table 5.4: Air kerma measurement from 100 RPLGDs

Descriptive statistics	Mean	S.D.	CV(%)	Maximum	Minimum
Air kerma value from RPLGDs (μ Gy)	303.80	9.59	3.17	318	240

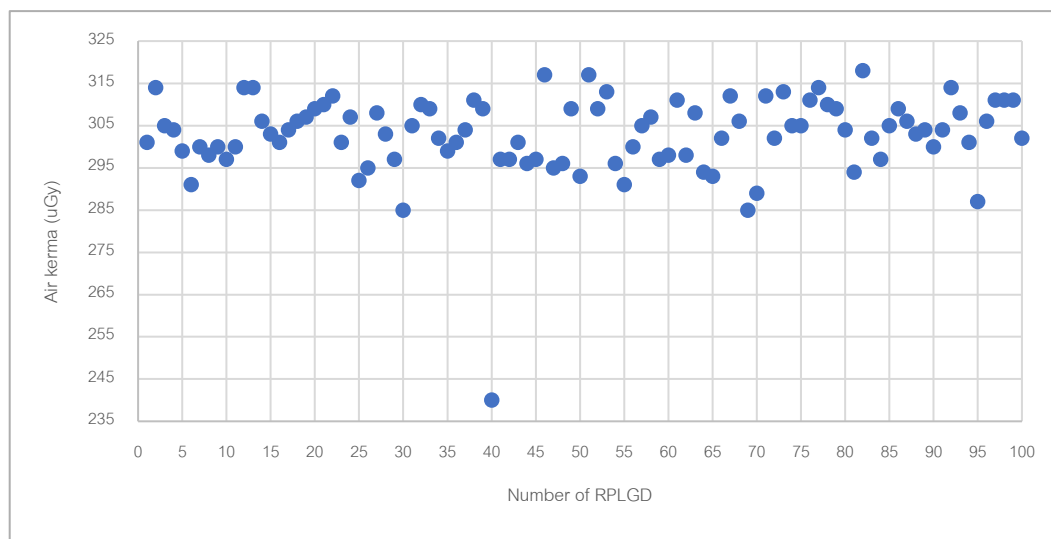


Figure 5.1: Air kerma measurement from 100 RPLGDs

5.3 Comparison of organ doses from measurements and Radimetrics

The 90 RPLGDs were inserted in 5 organs in the Rando phantom. The other 10 were used to measure the background. Organ doses measured by RPLGDs were compared to the organ doses calculated by Radimetrics. The results show the difference in mGy and the percent relative difference in Table 5.5 and Figure 5.2.

Table 5.5: Comparison of organ doses using RPLGD measurement and Radimetrics

Organ	Organ doses (RPLGD) (mGy)	Organ dose (Radimetrics) (mGy)	The difference, mGy and (% relative difference)
Breast	15.3	21.8	6.5 (42)
Lung	23.6	24.5	0.9 (3.8)
Liver	26.2	21.7	4.5 (17.2)
Colon	24.2	17.6	6.6 (27.3)
Uterus	18.9	17.4	1.5 (7.9)

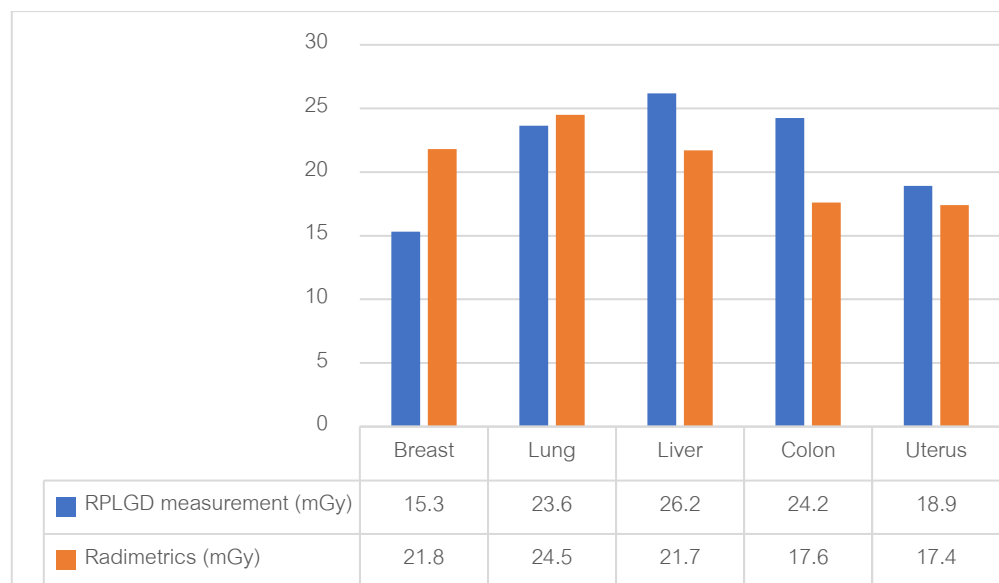


Figure 5.2: The comparison of 5 organ doses measured by RPLGD and calculated by Radimetrics

5.4 Patient study on CT examinations

For a period of five years, 285,286 CT examinations were collected from two academic centers. CT examinations were CT chest (27.2 percent), whole abdomen (20.3 percent), brain (13.3 percent), and vascular (9.0 percent). The rest were extremities, spine, cardiac, and neck. (30.2 percent).

5.4.1 Patient radiation dose from CT examinations with CED 100 mSv and above

The number of patients who underwent CT examinations in a single day with CED 100 mSv and above was 27, or 0.009 percent of 285,286 CT examinations. The median CED was 113 mSv for females (n=15) and 114 mSv for males (n=12), as shown in Figure 5.3. There is no significant difference in the median CED between females and males. The maximum CED from CT abdomen examination was 160 mSv from male patient, and the maximum CED from CT angiography at the thoracic aorta was 139 mSv from female patient.

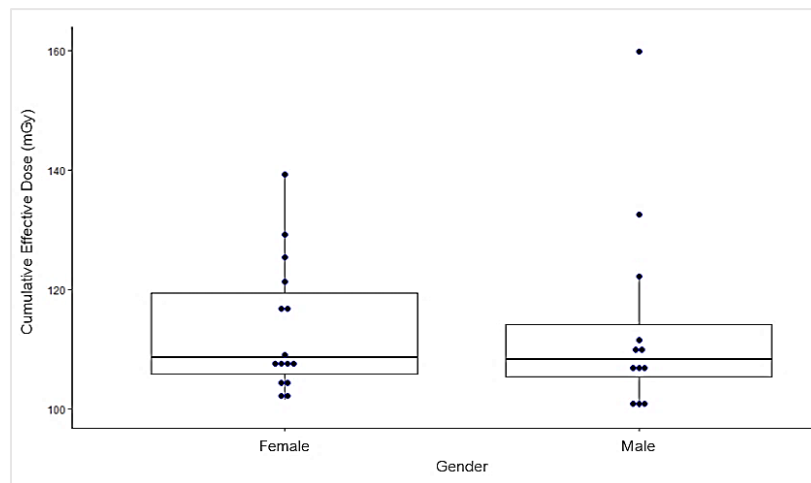


Figure 5.3: 27 patients with high CED in a single day (15 females and 12 males).

The acquisition protocols for 27 patients following the multiple CT scans in 6 cases were

- CT C-spine, whole abdomen, CTA neck, and CTA chest
- brain, neck, and whole abdomen
- brain, C-spine, and whole abdomen
- brain, C-Spine, CTA run off of upper extremity
- shoulder, chest and whole abdomen
- CTA run off of lower extremity, chest, and whole abdomen

6 cases of whole abdomen

3 cases of chest and whole abdomen

3 cases of angiography of the thoracic aorta

9 cases of a single protocol

Seven of 27 (3 females, 4 males) were young patients with an age below 40 years old, and 20 of 27 (12 females, 8 males) were elder patients, with an age above 40 years old. For the groups of young and elder patients, the descriptive statistics of patient demographics and radiation dose were shown in Tables 5.6 and 5.7, respectively. The maximum organ dose of 201 mGy at the colon was received by a young patient and the maximum organ dose 313 mGy at the lung was received by an elderly patient.

Table 5.6: Patient demography and radiation dose from CT examinations in young patients with the high dose

Descriptive Statistics: Among the young age group receiving high dose (n=7)				
	Mean	S.D.	Minimum	Maximum
Age at the exam (year)	32	7	22	39
Patient Weight (kg)	112	46	55	188
Cumulative effective dose, CED (mSv)	108.4	6.7	100.2	121.4
Organ dose (mGy);				
Lung	100.4	53.2	37.0	180.0
Liver	151.9	16.5	133.2	183.1
Colon	123.9	48.8	36.7	201.2
Breast	103.9	79.2	12.5	151.5
Uterus	100.8	93.1	7.4	193.7
Brain	17.2	44.1	0.1	117.2

Table 5.7: Patient demography and radiation dose from CT examinations in elder patients with the high dose

Descriptive Statistics: Among the young age group receiving high dose (n=20)				
	Mean	S.D.	Minimum	Maximum
Age at the exam (year)	61	9	46	73
Patient Weight (kg)	82	30	50	160
Cumulative effective dose, CED (mSv)	115.7	15.2	101.5	160.0
Organ dose (mGy);				
Lung	152.7	78.5	38.7	313.4
Liver	164.0	38.6	120.7	246.4
Colon	105.4	62.3	5.8	226.8
Breast	147.8	76.5	16.1	306.0
Uterus	79.8	57.7	1.5	166.1
Brain	19.9	39.6	0.1	153.3

Table 5.8 presents the patient demographic information of the age at exam, gender, body weight, clinical indications, CT protocols, CED (mSv), and organ doses (mGy) of seven young patients, aged between 22 and 39 years. Patient No. 3 underwent

multiple CT examinations, and all organ doses were higher than 100 mGy. Patient No. 4, underwent CT abdomen examination, all organs received over 100 mGy except the brain.

Table 5.8: Patient demography and organ dose from CT examinations in young patients with the high dose

Patient No.	Age(yr)/gender	BW (kg)	Clinical indications	CT Protocols	CED (mSv)	Organ dose (mGy)					
						Lung	Liver	Colon	Breast	Uterus	Brain
1	38/Female	73	Cryptogenic cirrhosis for liver transplantation	Upper abdomen	121.3	37.0	183.1	201.2	12.5	193.7	0.2
2	35/Female	55	Takayasu arteritis with severe aortic regurgitation	CTA thoracic aorta with gated	103.8	179.9	159.0	36.7	151.5	7.4	2.5
3	22/Male	80	Motorcycle accident	Brain/ C-spine/ CTA Run off arterial upper extremity	110.4	160.4	133.2	112.6	-	-	117.2
4	22/Female	188	R/O renal mass	Whole abdomen	109.1	111.8	149.8	112.9	147.6	101.3	0.4
5	35/Male	122	Fatty liver and R/O renal calculi	Whole abdomen	107.2	69.4	155.9	142.5	-	-	0.1
6	31/Male	135	R/O KUB stone	KUB	106.7	85.8	142.7	130.7	-	-	0.2
7	39/Male	130	F/U of KUB	KUB	100.2	58.6	139.3	130.9	-	-	0.1

* R/O: Rule Out (usually refers to a diagnosis or condition that your provider is actively trying to figure out if you do not have), * F/U: Follow-up

Table 5.9: Patient demography and organ dose from CT examinations in elder patients with the high dose

Pt. No.	Age (yr) /gender	BW (kg)	Clinical indications	CT Protocols	CED (mSv)	Organ dose (mGy)					
						Lung	Liver	Colon	Breast	Uterus	Brain
1	60/ Female	80	Rule out lymphoma	Chest and abdomen	116.1	128.8	154.6	115.2	165.8	99.5	0.6
2	52/ Female	160	Hypermenorrhea with anemia	Whole abdomen	101.6	38.7	140.5	170.5	16.1	166.1	0.1
3	57/ Female	67	F/U Aortic dissection	CTA of thoracic aorta	139.3	270.8	213.9	22.5	245.8	6.0	2.6
4	72/ Female	75	Dermatomyositis	Brain/ Neck/ Abdomen	105.0	109.3	129.5	95.0	125.7	73.7	153.3
5	56/ Female	50	Rheumatic heart disease	CTA coronary	129.2	313.4	165.0	5.8	306.0	1.5	0.6
6	46/ Female	55	Abdominal bleeding	Chest and abdomen	102.9	144.0	127.3	75.9	128.2	43.6	43.0
7	69/ /Male	62	Aortic aneurysm	CTA of thoracic aorta	122.2	286.7	246.4	24.0	-	-	1.0
8	73/ /Male	70	Staghorn renal stones	Whole abdomen	101.5	66.2	147.4	150.3	-	-	0.1
9	61/ /Male	59	Coronary Artery Bypass Grafting	CTA coronary	106.7	267.4	220.2	12.6	-	-	0.6
10	47/ /Male	73	Aortic root aneurysm	CTA whole aorta	109.4	178.6	155.1	106.0	-	-	22.0
11	54/ /Male	117	Epidural abscess and psoas abscess	Brain/C-spine / Abdomen	101.5	122.6	152.9	139.7	-	-	0.3
12	73/ Female	57	severe stenosis coronary artery disease	CTA coronary and CTA whole aorta	108.6	196.2	131.5	54.3	185.1	40.8	24.8
13	55/ Female	57	F/U symptoms	Shoulder/Chest and abdomen	125.4	101.7	170.3	161.4	89.7	155.2	1.4
14	46/ Female	83	F/U symptoms	Chest and abdomen	117.6	182.3	139.7	56.5	186.7	16.7	93.6
15	70/ Female	110	F/U groin nodes	Whole abdomen	107.7	82.4	142.7	138.9	106.3	131.7	0.2
16	60/ Female	61	F/U advanced stage CRC	CTV Lower Extremity/ Chest and abdomen	106.8	113.1	120.7	112.7	99.5	109.0	50.0
17	61/ Female	77	Renal artery stenosis	CTA abdominal aorta	107.7	130.4	131.8	115.3	118.7	113.8	0.4
18	73/ /Male	80	High mechanism trauma	C-spine//CTA Chest/Abdomen	132.6	94.8	199.7	199.1	-	-	0.8

/CTA neck											
19	66/ /Male	92	Arch aneurysm	CTA whole aorta	111.6	148.8	151.6	125.0	-	-	3.1
20	70/ /Male	145	Perirenal abscess	Whole abdomen	159.9	77.4	239.5	226.8	165.8	99.5	0.1

As indicated before, most patients who received a high dose, specifically 6 out of 27, underwent CT whole abdomen examinations with four-phase protocol. The mean CED \pm S.D. (range) of 6 patients was 114.5 ± 22.5 (101.5–160.0) mSv. The mean organ dose \pm S.D. (range) of the lung was 74.3 ± 23.8 (38.9–111.8) mGy, liver, 162.7 ± 38.1 (140.5–239.5) mGy, colon, 156.9 ± 38.9 (112.9–226.8) mGy, female breast, 89.9 ± 67.3 (16.1–147.6) mGy, and female uterus, 133.1 ± 32.4 (101.3–166.1) mGy, as shown in Figure 5.4.

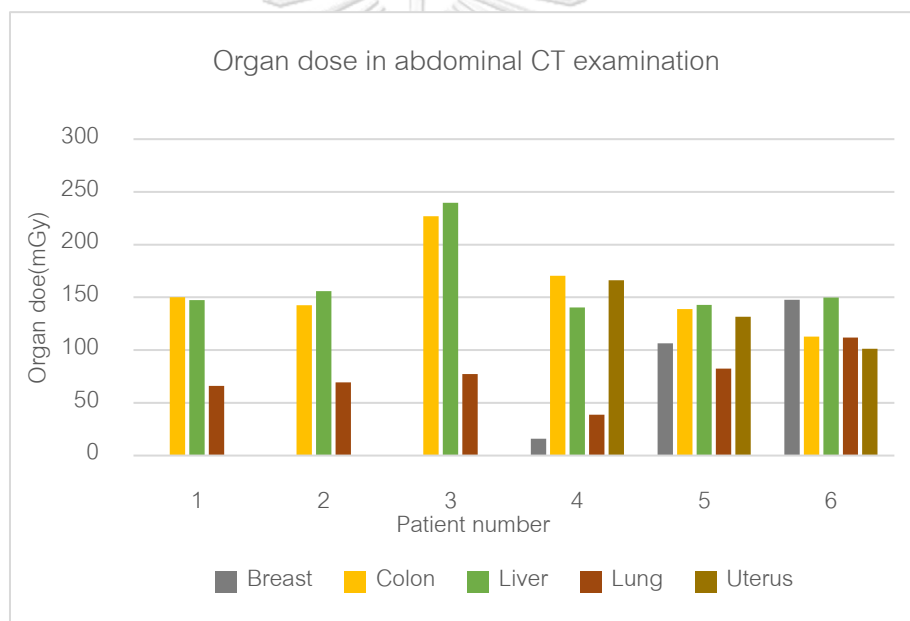


Figure 5.4: Organ doses obtained from CT abdomen examination in six patients.

5.4.2 Patient radiation dose from CT examinations with CED below 100 mSv

The patient data and CED (mSv) classified by gender in common CT protocols following CT brain without and with contrast-enhanced phase (n=802), chest with contrast-enhanced phase (n=1207), abdomen with triphasic phased including without contrast-enhanced, arterial, portal phase (n=391) and CTA of whole aorta, without contrast, arterial phase, and delayed phase (n=694) were shown in Table 5.10. The mean \pm SD of organ dose (mSv), from common CT protocols in young and elder patients, as shown in Table 5.11.

Table 5.10: Patient demography and CED (mSv) from common CT protocols

CT Protocols	CED (mSv)	Age at exposure (yr)	Body weight (kg)	WED
Brain				
Female (n=683)	5.4 \pm 0.6	53 \pm 13	58.1 \pm 12.6	158.5 \pm 6.1
Male (n=119)	6.1 \pm 1.0	52 \pm 16	69.0 \pm 16.2	166.2 \pm 7.0
Chest				
Female (n=759)	10.4 \pm 2.8	51 \pm 14	55.6 \pm 12.5	238.1 \pm 28.2
Male (n=448)	8.6 \pm 2.2	53 \pm 16	58.5 \pm 11.9	242.2 \pm 24.2
Whole abdomen				
Female (n=188)	28.6 \pm 8.3	55 \pm 15	58.2 \pm 14.2	259.4 \pm 29.9
Male (n=203)	26.1 \pm 9.0	56 \pm 14	64.6 \pm 12.7	260.5 \pm 27.2
CTA of the whole aorta				
Female (n=147)	37.5 \pm 13.9	58 \pm 15	57.0 \pm 10.1	248.5 \pm 25.9
Male (n=547)	33.8 \pm 12.7	56 \pm 15	68.0 \pm 15.4	262.7 \pm 28.4

Table 5.11: Mean organ dose (mGy) in common CT protocols from all patients

Organ	CT protocols							
dose (mGy)	Brain		Chest		Whole abdomen		CTA of the whole aorta	
Age group: ≤ 40 years old								
Gender	Female	Male	Female	Male	Female	Male	Female	Male
	(n=118)	(n=25)	(n=180)	(n=89)	(n=33)	(n=30)	(n=21)	(n=97)
Lung	0.9±0.2	1.0±0.2	18.1±4.6	18.9±4.9	18.8±11.1	14.0±6.9	47.5±15.7	52.3±15.2
Liver	0.1±0.01	0.08±0.01	15.1±3.8	16.5±4.2	46.2±14.1	39.8±13.7	44.4±15.6	48.0±14.2
Colon	0.01±0.001	0.01±0.002	2.5±1.7	3.2±1.9	43.4±16.3	34.8±11.6	35.0±15.7	35.1±12.0
Breast	0.3±0.04	-	16.2±4.6	-	11.8±14.0	-	44.5±15.8	-
Uterus	0.01±0.002	-	0.5±0.3	-	38.5±15.9	-	31.5±16.5	-
Brain	105.7±10.7	100.2±11.2	0.2±0.1	0.1±0.1	0.03±0.02	0.01±0.01	7.5±7.3	7.6±5.6
Age group: > 40 years old								
Gender	Female	Male	Female	Male	Female	Male	Female	Male
	(n=565)	(n=94)	(n=579)	(n=359)	(n=142)	(n=150)	(n=126)	(n=450)
Lung	0.9±0.2	1.1±0.3	19.4±4.9	19.1±4.7	19.5±9.6	16.6±8.7	44.8±16.6	48.5±20.3
Liver	0.08±0.01	0.07±0.02	16.2±4.0	16.7±4.0	46.3±12.6	46.2±14.7	44.9±16.6	46.8±17.2
Colon	0.01±0.001	0.01±0.002	2.6±1.7	3.1±1.9	41.2±11.4	40.1±12.1	36.8±16.5	36.8±15.7
Breast	0.25±0.04	-	17.4±4.8	-	10.2±8.9	-	44.4±17.6	-
Uterus	0.01±0.002	-	0.6±0.33	-	35.1±10.8	-	33.2±17.3	-
Brain	105.3±9.1	97.6±12.6	0.2±0.13	0.1±0.1	0.03±0.03	0.02±0.01	5.6±7.7	4.47±5.9

5.4.3 Lifetime attributable risk (LAR) at 5 organs for incident and mortality cancers in high dose

Box plots display the median, and IQR values of LAR for solid cancer incidence (top) and mortality (bottom) per 100,000 exposed patients from high CED categorized by gender across 27 patients, (15 females, 12 males) as shown in Figure 5.5. The median LAR of the lung in female and liver in male were higher than other solid cancers.

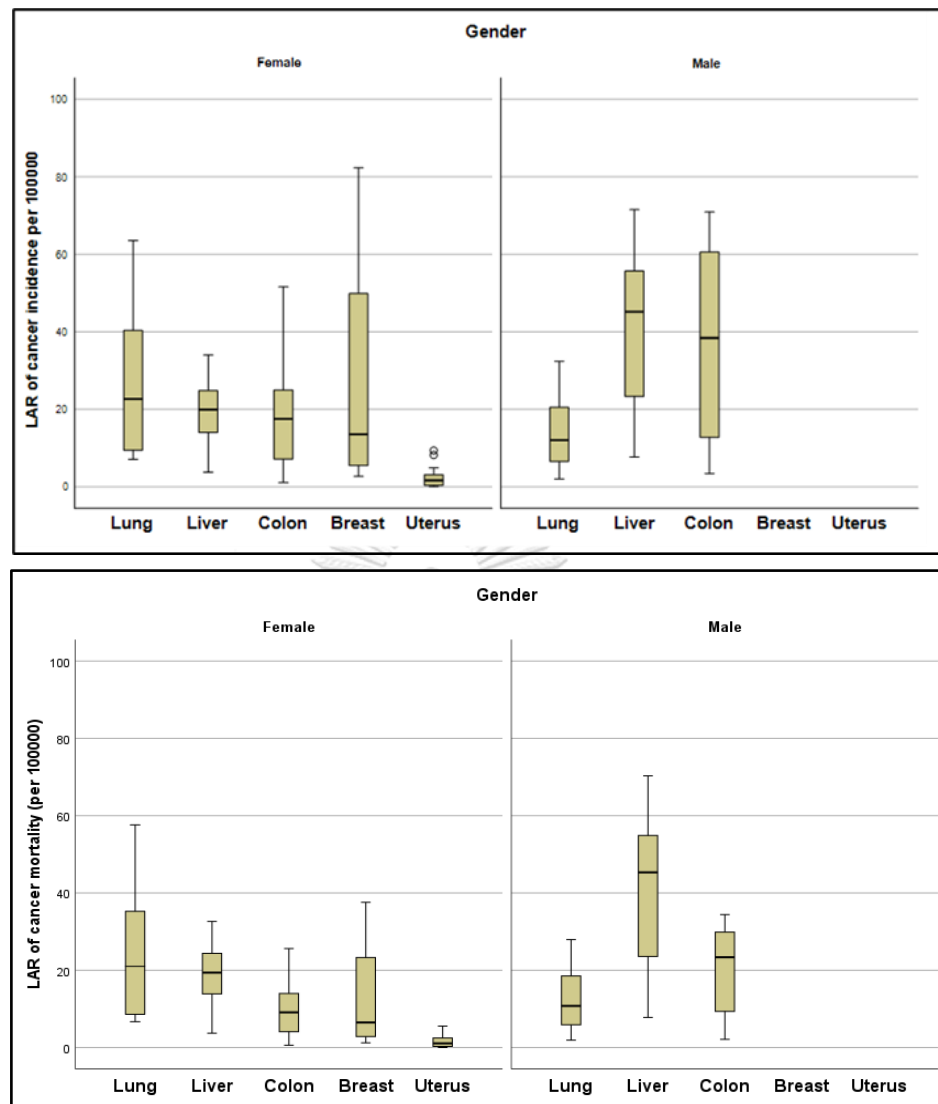


Figure 5.5: LAR for incidence (top) and mortality (bottom) of 5 cancer sites from high CT dose for both genders among 27 patients.

Table 5.12 shows the LAR of cancer incidence and mortality from CT examinations for each young patient per 100,000 at 6 organs, along with 7 patients. LAR for breast cancer incidence and mortality were 82 and 35 per 100,000, respectively, the highest among young females. The incidence and mortality rates for liver cancer were 72 and 34 per 100,000, respectively, the highest among young males. In both cases, the patient's age was 22 years old.

Table 5.13 and 5.14 display the LAR of cancer incidence and mortality in young and elderly patients.

Table 5.12: LAR of cancer incidence and mortality from CT examinations for each young patient

Patient No.	Age (yr) /gender	LAR of cancer incidence*						LAR of cancer mortality*					
		Lung	Liver	Colon	Breast	Uterus	Brain	Lung	Liver	Colon	Breast	Uterus	Brain
1	38/Female	9.2	30.9	51.6	6.1	9.4	0.01	8.0	30.0	25.6	2.7	5.5	0.01
2	35/Female	45.0	27.3	9.6	77.2	0.4	0.3	39.2	26.4	4.7	34.0	0.2	0.2
3	22/Male	32.4	71.5	70.9	-	-	16.9	28.0	70.3	34.4	-	-	14.1
4	22/Female	38.1	34.1	39.9	82.4	8.2	0.1	32.9	32.7	19.5	35.4	4.2	0.1
5	35/Male	10.4	62.7	67.0	-	-	0.01	9.0	61.7	32.9	-	-	0.01
6	31/Male	12.7	57.6	61.4	-	-	0.02	11.0	56.7	30.0	-	-	0.01
7	39/Male	8.6	53.8	59.7	-	-	0.01	7.5	53.1	29.7	-	-	0.01

* LAR per 100000 exposed patients

Table 5.13: LAR of cancer incidence and mortality from CT examinations to 7 young patients

	N	Mean	S.D.	Median	Minimum	Maximum
LAR for incidence cancer						
Lung	7	22.3	15.6	12.7	8.6	45.0
Liver	7	48.3	17.4	53.8	27.3	71.5
Colon	7	51.5	21.1	59.7	9.6	70.9
Breast	3	55.2	42.6	77.2	6.1	82.4
Uterus	3	5.9	4.9	8.2	0.4	9.4
Brain	7	2.5	6.4	0.02	0.01	16.9
LAR for mortality cancer						
Lung	7	19.4	13.5	11.0	7.6	39.2
Liver	7	47.3	17.4	53.1	26.4	70.3
Colon	7	25.3	10.3	29.7	4.7	34.4
Breast	3	24.0	18.5	33.9	2.7	35.4
Uterus	3	3.3	2.8	4.2	0.2	5.5
Brain	7	2.1	5.3	0.01	0.01	14.10

* LAR per 100000 exposed patients

Table 5.14: LAR of cancer incidence and mortality from CT examinations to 20 elder patients

	N	Mean	S.D.	Median	Minimum	Maximum
LAR for incidence of cancer						
Lung	20	21.0	16.7	18.4	2.1	63.5
Liver	20	21.4	13.3	20.7	3.8	52.3
Colon	20	17.9	14.4	16.0	1.1	50.2
Breast	12	23.9	24.9	13.2	2.7	81.4
Uterus	12	1.6	1.6	1.3	0.04	4.9
Brain	20	0.8	1.7	0.03	0.0004	6.9
LAR for mortality cancer						
Lung	20	19.1	15.1	17.1	1.9	57.6
Liver	20	21.3	13.3	20.2	3.7	51.9
Colon	20	10.6	7.9	9.8	0.6	27.1
Breast	12	11.5	11.4	6.4	1.2	37.6
Uterus	12	1.3	1.2	1.0	0.03	3.6
Brain	20	0.7	1.5	0.03	0.0004	6.3

* LAR per 100000 exposed patients

Table 5.15: LAR of cancer incidence and mortality from CT whole abdomen with the high dose

Patient No.	Age(y) /gender	BW, (kg)	LAR per 100,000 of cancer incidence					LAR per 100,000 of cancer mortality				
			Lung	Liver	Colon	Breast	Uterus	Lung	Liver	Colon	Breast	Uterus
1	52/Female	160	8.3	19.7	35.2	2.7	4.9	7.4	19.2	18.6	1.2	3.6
2	73/Male	70	2.1	7.7	10.9	-	-	1.9	7.8	8.0	-	-
3	70/Female	110	7.7	8.1	10.3	4.8	1.1	7.3	8.1	7.6	3.0	0.9
4	22/Female	188	38.1	34.6	40.0	82.4	8.2	32.9	32.7	19.5	35.4	4.2
5	35/Male	122	10.4	62.7	67.0	-	-	9.0	61.7	32.9	-	-
6	70/Male	145	4.6	25.0	33.2	-	-	4.2	25.2	24.3	-	-

* LAR per 100000 exposed patients

5.4.4 Lifetime attributable risk (LAR) at 6 organs for incident and mortality cancers in low dose

Table 5.16 shows the LAR for cancer incidence and mortality of young and elder patients of both genders. A significant difference between males and females was observed in LAR for lung, liver, and colon cancer incidence and mortality from CT brain and CTA of the whole aorta ($p<0.05$), except for LAR of brain cancer incidence and mortality. LAR of all solid cancers from CT whole abdomen and chest were significantly different between females and males, ($p<0.05$). Table 5.17: Lifetime attributable risk per 100,000 of cancer incidence and mortality of the elder patients with both genders in common CT protocols.

Table 5.16: Lifetime attributable risk per 100,000 of cancer incidence and mortality of the young patients with both genders in common CT protocols

CT Protocols	Brain		Chest		Whole abdomen		CTA of the whole aorta	
	Female	Male	Female	Male	Female	Male	Female	Male
	(n=123)	(n=28)	(n=180)	(n=89)	(n=33)	(n=30)	(n=21)	(n=97)
LAR for incidence cancer;								
Lung	0.2±0.1	0.2±0.1	5.0±1.4	3.4±1.0	5.3±3.6	2.3±1.1	13.5±4.8	8.8±2.8
Liver	0.01±0.003	0.04±0.01	2.8±0.8	7.9±2.3	8.7±2.9	17.7±6.1	8.5±2.9	21.7±7.8
Colon	0.003±0.001	0.006±0.002	0.7±0.5	1.8±1.0	12.6±4.9	18.2±6.4	10.2±4.1	18.6±7.1
Breast	0.13±0.02	-	8.4±2.4	-	6.2±7.4	-	23.2±7.6	-
Uterus	0.001±0.0001	-	0.03±0.02	-	2.4±1.1	-	1.9±0.9	-
Brain	12.7±4.3	13.2±5.7	0.03±0.01	0.01±0.01	0.004±0.003	0.001±0.001	1.0±1.1	0.9±0.7
LAR for mortality cancer;								
Lung	0.2±0.1	0.2±0.1	4.3±1.2	3.0±0.9	4.6±3.1	2.0±0.9	11.7±4.1	7.6±2.4
Liver	0.01±0.003	0.04±0.01	2.7±0.7	7.82±2.3	8.4±2.8	17.4±6.0	8.2±2.8	21.4±7.7
Colon	0.002±0.0003	0.003±0.001	0.3±0.2	0.9±0.6	6.2±2.4	8.9±3.9	5.0±2.0	9.1±3.4
Breast	0.06±0.01	-	3.7±1.0	-	2.7±3.2	-	10.1±3.4	-
Uterus	0.0003±0.0001	-	0.02±0.01	-	1.3±0.6	-	1.0±0.5	-
Brain	10.7±3.2	11.0±4.3	0.02±0.01	0.01±0.001	0.003±0.003	0.001±0.001	0.87±0.92	0.7±0.6

Table 5.17: Lifetime attributable risk per 100,000 of cancer incidence and mortality of the elder patients with both genders in common CT protocols

CT Protocols	Brain		Chest		Whole abdomen		CTA of the whole aorta	
Gender	Female (n=565)	Male (n=94)	Female (n=579)	Male (n=359)	Female (n=155)	Male (n=173)	Female (n=126)	Male (n=450)
<i>LAR for incidence cancer;</i>								
Lung	0.2±0.1	0.1±0.1	3.5±1.4	1.9±0.9	3.1±2.0	1.5±1.0	6.5±4.0	4.4±2.8
Liver	0.01±0.004	0.02±0.01	1.9±0.7	3.5±1.9	4.6±2.3	9.2±5.6	4.1±2.7	8.8±6.3
Colon	0.002±0.001	0.003±0.001	0.4±0.3	0.8±0.7	5.8±3.1	10.3±5.8	4.8±3.6	8.8±6.1
Breast	0.05±0.04	-	3.2±2.8	-	1.5±2.3	-	6.0±7.5	-
Uterus	0.0002±0.0001	-	0.01±0.01	-	0.7±0.5	-	0.6±0.6	-
Brain	4.70±2.37	3.51±1.98	0.01±0.01	0.03±0.003	0.001±0.001	0.0006±0.0005	0.2±0.3	1.2±0.3
<i>LAR for mortality cancer;</i>								
Lung	0.1±0.1	0.10±0.04	3.2±1.2	1.7±0.7	2.8±1.8	1.4±0.9	5.9±3.6	4.0±2.5
Liver	0.01±0.003	0.02±0.01	1.8±0.8	3.5±1.9	4.5±2.2	9.2±5.5	4.1±2.6	8.8±6.2
Colon	0.001±0.0004	0.002±0.001	0.2±0.2	0.5±0.3	3.4±1.5	5.9±2.9	2.8±1.9	5.2±3.2
Breast	0.02±0.02	-	1.5±1.2	-	0.7±1.1	-	2.9±3.4	-
Uterus	0.0002±0.0001	-	0.01±0.01	-	0.5±0.3	-	0.5±0.4	-
Brain	4.4±2.1	3.3±1.8	0.01±0.01	0.003±0.003	0.001±0.001	0.0005±0.0004	0.2±0.3	0.2±0.3

5.4.5 LAR, organ dose and related patient parameters in common CT protocols

The Pearson Correlation Coefficient (r) has been used to quantify the degree of two associated variables. The correlation between LAR of cancer incidence and patient parameters of various protocols is displayed in Table 5.19-5.28.

Table 5.18: Correlation of patient parameters and LAR in common CT protocols

Protocol	
CT Chest	lung cancer incidence
CT Abdomen	breast cancer incidence
	liver cancer incidence
	colon cancer incidence
	uterus cancer incidence
CTA whole aorta examination	lung cancer incidence
	liver cancer incidence
	colon cancer incidence
	breast cancer incidence
	uterus cancer incidence

Table 5.19: Correlation of LAR for lung cancer incidence and patient parameters: CT Chest examination

	LAR for lung cancer incidence	Organ dose: Lung	Age at exam	Bodyweight	WED
Organ dose: Lung	0.4547*	1.0000			
Age at exam	-0.6838*	0.0561	1.0000		
Bodyweight	0.2653*	0.5185*	-0.0844*	1.0000	
WED	0.2570*	0.6664*	0.0630*	0.8371*	1.0000

**P* value<0.05

From the table above, there was a positive moderate correlation between LAR for lung cancer incidence and organ dose with statistically significant, $r = 0.45$, $p < 0.05$. A negative moderate correlation was found between LAR for lung cancer incidence and age at the exam with statistically significant, $r = -0.68$, $p < 0.05$. There was a moderate correlation between lung dose and body weight and water equivalent diameter with statistical significance, $r = 0.52$, $p < 0.05$ and $r = 0.67$, $p < 0.05$, respectively.

Table 5.20: Correlation of LAR for breast cancer incidence and patient parameters: CT Chest examination

	LAR for breast cancer incidence	Organ dose: Breast	Age at exam	Bodyweight	WED
Organ dose: Breast	0.2834*	1.0000			
Age at exam	-0.8323*	0.0676	1.0000		
Bodyweight	0.3302*	0.6288*	-0.0844*	1.0000	
WED	0.2446*	0.7658*	0.0630*	0.8371*	1.0000

**P* value<0.05

A negative moderate correlation between LAR for breast cancer incidence and age at exam was found with statistical significance, $r = -0.83$, $p < 0.05$. A moderate correlation was observed between breast dose and body weight and water equivalent diameter, $r = 0.63$, $p < 0.05$, and $r = 0.77$, $p < 0.05$, respectively.

Table 5.21: Correlation of LAR for liver cancer incidence and patient parameters: CT Abdomen examination

	LAR for liver cancer incidence	Organ dose: Liver	Age at exam	Bodyweight	WED
Organ dose: Liver	0.2895*	1.0000			
Age at exam	-0.7160*	0.1333*	1.0000		
Bodyweight	0.2828*	0.5679*	0.0537	1.0000	
WED	0.1819*	0.7190*	0.1613*	0.8307*	1.0000

* P value<0.05

There was a negative moderate correlation between LAR for liver cancer incidence and age at exam with statistical significance, $r = -0.72$, $p < 0.05$. A statistically significant moderate correlation was observed between liver dose and body weight, and water equivalent diameter, $r = 0.57$, $p < 0.05$ and $r = 0.72$, $p < 0.05$, respectively.

Table 5.22: Correlation of LAR for colon cancer incidence and patient parameters: CT Abdomen examination

	LAR for colon cancer incidence	Organ dose: Colon	Age at exam	Bodyweight	WED
Organ dose: Colon	0.3187*	1.0000			
Age at exam	-0.7581*	0.0950	1.0000		
Bodyweight	0.2964*	0.5835*	0.0537	1.0000	
WED	0.2101*	0.7374*	0.1613*	0.8307*	1.0000

* P value<0.05

There was a negative moderate correlation between LAR for colon cancer incidence and age at exam with statistical significance, $r = -0.76$, $p < 0.05$. A moderate correlation between colon dose and body weight, and water equivalent diameter was found with statistical significance, $r = 0.58$, $p < .05$ and $r = 0.74$, $p < 0.05$, respectively.

Table 5.23: Correlation of LAR for uterus cancer incidence and patient parameters:

Abdomen examination

	LAR for uterus cancer incidence	Organ dose: Uterus	Age at exam	Bodyweight	WED
Organ dose: Uterus	0.4349*	1.0000			
Age at exam	-0.8985*	-0.0477	1.0000		
Bodyweight	0.2647*	0.5913*	0.0537	1.0000	
WED	0.2027*	0.6818*	0.1613*	0.8307*	1.0000

**P* value<0.05

A statistically significant positive moderate correlation was observed between LAR for uterus cancer incidence and organ dose, $r = 0.43$, $p < 0.05$. The negative strong correlation between LAR for uterus cancer incidence and age at the exam was statistically significant, $r = -0.90$, $p < 0.05$. There was a moderate correlation between uterus dose and body weight, and water equivalent diameter with statistical significance, $r = 0.59$, $p < .05$ and $r = 0.68$, $p < 0.05$, respectively.

Table 5.24: Correlation of LAR for lung cancer incidence and patient parameters: CTA whole aorta examination

	LAR for lung cancer incidence	Organ dose: Lung	Age at exam	Bodyweight	WED
Organ dose: Lung	0.5689*	1.0000			
Age at exam	-0.7652*	-0.1212*	1.0000		
Bodyweight	0.1741*	0.1520*	-0.2195*	1.0000	
WED	0.2063*	0.1865*	-0.2017*	0.6981*	1.0000

**P* value<0.05

The positive moderate correlation between LAR for lung cancer incidence and organ dose was statistically significant, $r = 0.57$, $p < 0.05$. The negative strong correlation between LAR for lung cancer incidence and age at the exam was statistically significant, $r = -0.77$, $p < .05$.

Table 5.25: Correlation of LAR for liver cancer incidence and patient parameters: CTA whole aorta examination

	LAR for liver cancer incidence	Organ dose: Liver	Age at exam	Bodyweight	WED
Organ dose: Liver	0.4821*	1.0000			
Age at exam	-0.8133*	0.0803*	1.0000		
Bodyweight	0.3952*	0.2624*	-0.2195*	1.0000	
WED	0.4096*	0.4180*	-0.2017*	0.6981*	1.0000

* P value < 0.05

There was a positive moderate correlation between LAR for liver cancer incidence and organ dose, body weight, and water equivalent diameter with statistically significant, $r = 0.48$, $r = 0.40$, and $r = 0.40$ respectively. The negative strong correlation between LAR for liver cancer incidence and age at the exam was statistically significant, $r = -0.81$, $p < 0.05$. A moderate correlation between liver dose and water equivalent diameter was statistically significant, $r = 0.42$, $p < .05$.

Table 5.26: Correlation of LAR for colon cancer incidence and patient parameters: CTA whole aorta examination

	LAR for colon cancer incidence	Organ dose: colon	Age at exam	Bodyweight	WED
Organ dose: Uterus	0.4779*	1.0000			
Age at exam	-0.7690*	0.0189	1.0000		
Bodyweight	0.3615*	0.1506*	-0.2195*	1.0000	
WED	0.3766*	0.2752*	-0.2017*	0.6981*	1.0000

* P value < 0.05

A positive moderate correlation between LAR for colon cancer incidence and organ dose was statistically significant, $r = 0.48$, $p < .05$. The negative moderate correlation between LAR for colon cancer incidence and age at the exam was statistically significant, $r = -0.77$, $p < .05$.

Table 5.27: Correlation of LAR for breast cancer incidence and patient parameters: CTA whole aorta examination

	LAR for breast cancer incidence	Organ dose: Breast	Age at exam	Bodyweight	WED
Organ dose: Breast	0.3713*	1.0000			
Age at exam	-0.8960*	-0.0334	1.0000		
Bodyweight	0.3361*	0.4653*	-0.2195*	1.0000	
WED	0.2654*	0.5390*	-0.2017*	0.6981*	1.0000

**P* value<0.05

The negative strong correlation between LAR for breast cancer incidence and age at the exam was statistically significant, $r = -0.90$, $p < .05$. There was a moderate correlation between breast dose and body weight, and water equivalent diameter with statistically significant, $r = 0.47$, $p < 0.05$ and $r = 0.54$, $p < 0.05$, respectively.

Table 5.28: Correlation of LAR for uterus cancer incidence and patient parameters: CTA whole aorta examination

	LAR for uterus cancer incidence	Organ dose: Uterus	Age at exam	Bodyweight	WED
Organ dose: Uterus	0.4897*	1.0000			
Age at exam	-0.8450*	-0.0132	1.0000		
Bodyweight	0.2953*	0.1822*	-0.2195*	1.0000	
WED	0.2032*	0.1837*	-0.2017*	0.6981*	1.0000

**P* value<0.05

There is a positive moderate correlation between LAR for uterus cancer incidence and organ dose with statistically significant, $r = 0.49$, $p < 0.05$. A negative moderate correlation between LAR for uterus cancer incidence and age at the exam was found with statistical significance, $r = -0.85$, $p < .05$.

5.4.6 Risk Model for incident cancer risk from CTA examinations

Multivariate regression risk model for incident cancer risk from CTA examinations includes the following;

- 1) LAR for lung cancer incidence
- 2) LAR for liver cancer incidence
- 3) LAR for colon cancer incidence
- 4) LAR for breast cancer incidence
- 5) LAR for uterus cancer incidence

1) Model for LAR for lung cancer incidence

- Normal distribution of the variable

We used Shapiro-Wilk test to check the normality of the data, ($P > 0.001$). The LAR for lung cancer incidence conformed to a normal distribution when LAR was represented in square root form. The organ dose of the lung was under normal distribution. The histogram in age at exam data shows non-normally distributed, it is obvious that the variable displacement is skewed to the right. Hence, we categorize the data based on age at exam; Age group 1: age at exam ≤ 40 , 2: age at exam 41-60, 3: age at exam 61-70, 4: age at exam 71-75 years old.

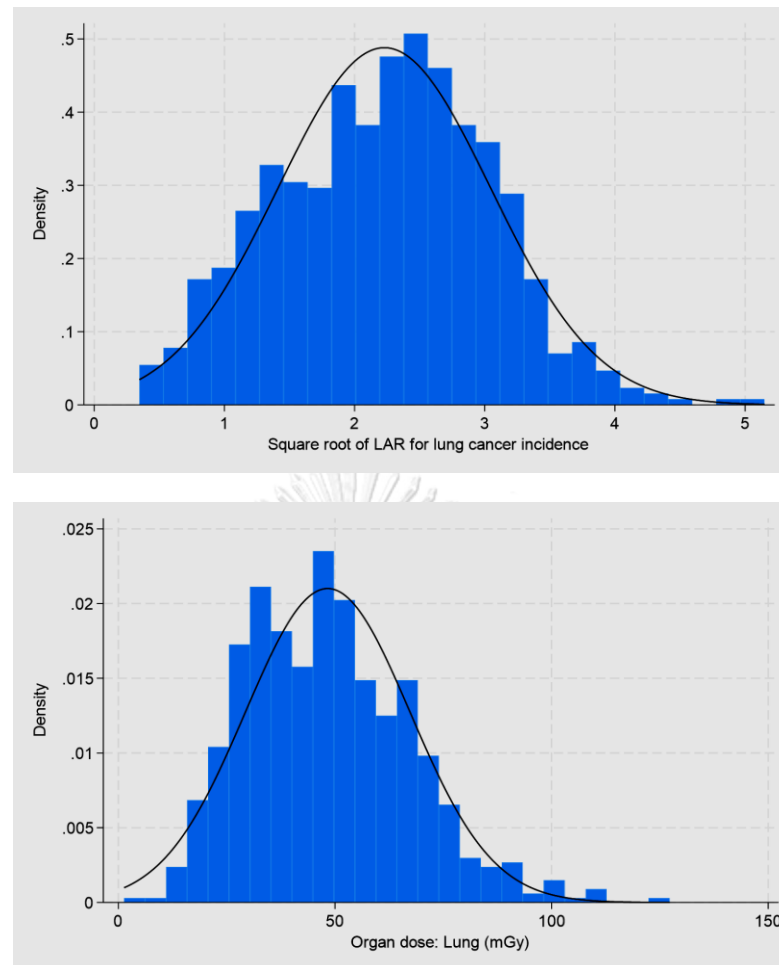


Figure 5.6: The normal distributed square root form of LAR (Top) and dose in the lung (Bottom)

- Univariate linear regression

Simple linear regression analysis revealed the p-value was below the significance level of $P < 0.001$. This indicates that the predictor variables, organ dose in the lung, age at exam, and gender, had a statistically significant association with the LAR for lung cancer incidence. Therefore, the variables are being added to the multiple linear regression model (Table 5.29).

Table 5.29: Univariate linear regression of LAR for lung cancer incidence

Univariate linear regression	Standardize Coefficient (β)	95% CI	P-value
Organ dose in the lung	0.02	0.02–0.03	<0.001
Age group; 1:<=40 yr (ref)			
2:41-60 yr	-0.41	-0.52–(-0.29)	<0.001
3:61-70 yr	-1.04	-1.16–(-0.92)	<0.001
4:71-75 yr	-1.83	-1.97–(-1.71)	<0.001
Gender; Female (ref)			
Male	-0.46	-0.60–(-0.31)	<0.001

Significance level: *** $p < 0.001$

- Multivariate Linear Regression

The multiple linear regression model is used to predict the LAR, the summary output is provided below.

Table 5.30: Multiple linear regression of LAR for lung cancer incidence

Linear regression

Number of obs

=

694

F(8, 685)

=

730.58

Prob > F

=

0.0000

R-squared

=

0.9093

Root MSE

=

.24752

sqrt_LAR	β	Robust				
	Coefficient	std. err.	t	P> t	[95% conf. interval]	

agegr01						
2	-.3520255	.1028428	-3.42	0.001	-.5539505	-.1501005
3	-.6114648	.1109667	-5.51	0.000	-.8293405	-.3935891
4	-1.057818	.1180392	-8.96	0.000	-1.289581	-.8260563
Lung dose	.027605	.0019164	14.40	0.000	.0238422	.0313677
agegr01#c.Lung dose						
2	-.0006651	.0020332	-0.33	0.744	-.0046572	.0033271
3	-.0073138	.0022393	-3.27	0.001	-.0117105	-.002917
4	-.0136418	.0024753	-5.51	0.000	-.0185019	-.0087817
1.male	-.6090101	.0281845	-21.61	0.000	-.6643485	-.5536717
_cons	2.130729	.099274	21.46	0.000	1.935811	2.325647

There is an equation for multiple linear regression.

$$\begin{aligned}
 \text{sqrt LAR for lung cancer incidence (per100000)} \\
 = 2.13 + \beta_1(\text{age group}) + \beta_2(\text{Lung dose(mGy)}) + \beta_3(\text{male}) \\
 + \beta_4(\text{agegr01\#c.Lung dose})
 \end{aligned}$$

From the obtained multiple linear regression, residuals had a normal distribution, (Figure 5.7) and there was no evidence of multicollinearity, with mean VIF=1.57. Additionally, the R^2 value was relatively high, 0.91 and very low Root MSF, 0.24. A scatterplot displays the relationship between actual and predicted value while line plots represent regression of the actual data. As can be seen in Figure 5.8.

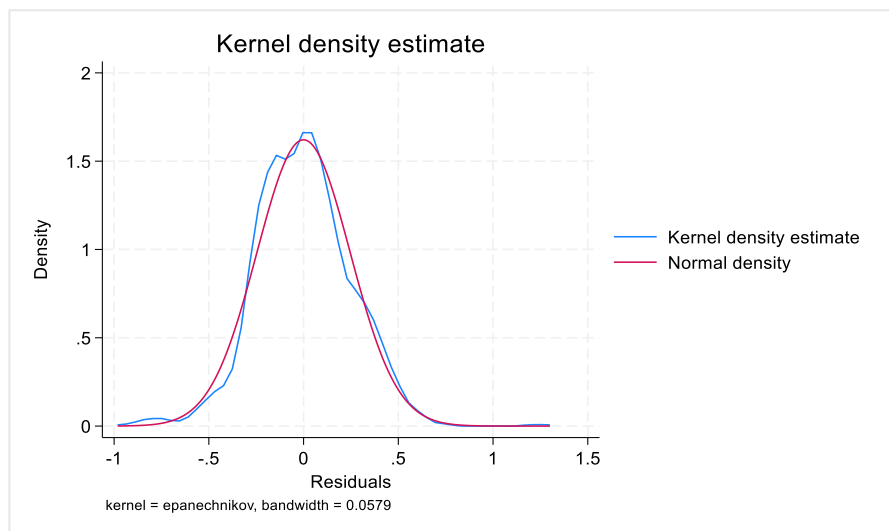


Figure 5.7: Kernel density estimation of residuals follow normal distribution in multiple linear regression analysis (Blue)

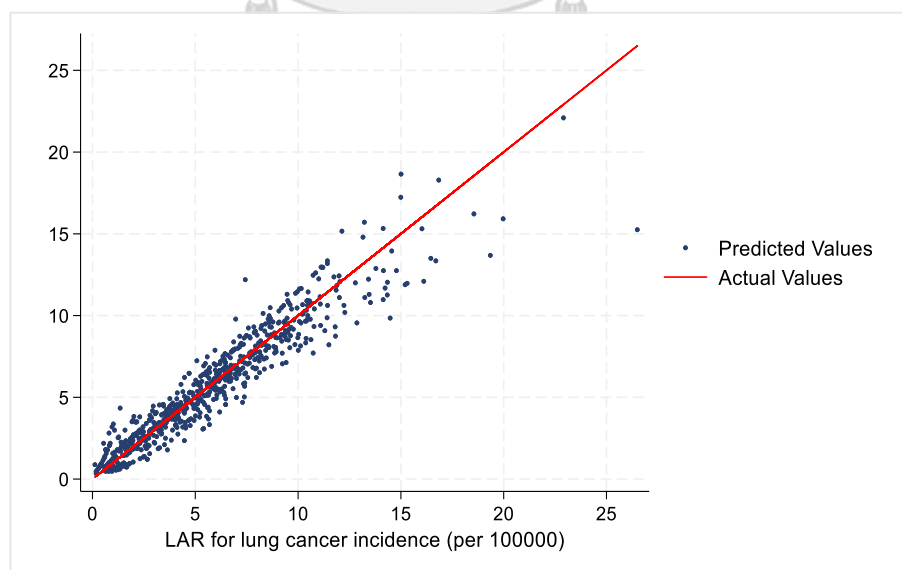


Figure 5.8: Two-way scatterplot with a linear regression line of LAR for lung cancer incidence

Risk Model for 2) - 5) will be included in the Appendix.

- 2) LAR for liver cancer incidence
- 3) LAR for colon cancer incidence
- 4) LAR for breast cancer incidence
- 5) LAR for uterus cancer incidence



CHAPTER 6

DISCUSSION

Lifetime attributable risk (LAR) of radiation-induced cancer incidence and mortality was studied among patients undergoing CT examinations. Patients who received a high dose ($CED \geq 100$ mSv) from recurrent CT in a single day and a low dose, ($CED < 100$ mSv) obtained from common CT examinations, especially on CTA whole aorta were included in this study. The BEIR VII model was used to evaluate the risk of site-specific solid cancers of the lung, liver, colon, breasts, and uterus, as a function of age at exposure, attained age, organ dose, life table data, and baseline cancer incidence and mortality rates of the Thai population. In order to obtain the accurate LAR at each cancer site, the displayed CT dose and the organ doses had been verified.

6.1 Verification of the displayed $CTDI_{vol}$

The $CTDI_{vol}$ displayed on the CT scanner monitor has been compared to the measured values from both PMMA phantoms and the pencil ion chamber. The percentage differences from GE were highest among three CT scanners. (Table 5.1-5.3). The similar results were the highest difference recorded from the low kVp of both phantoms and then reduced at higher kVp. Siemens CT scanner showed the lowest difference especially from body phantom. Canon scanners showed the medium difference and not really according to kVp in head phantom.

6.2 Verification of organ dose

6.2.1 Calibration of RPLGDs

The mean air kerma measured by RPLGDs was 1.1 percent lower than the mean measurement by an ion chamber. The lowest read out by RPLGD no. 40 at 21 percent difference, had been excluded from the study.

6.2.2 The organ doses from measurements and Radimetrics

The measured organ doses by RPLGDs were compared to the readouts from Radimetrics. The measured breast and lung doses were lower than Radimetrics readouts, while the measured liver, colon and uterus were higher than Radimetrics as shown in Table 5.5.

6.2.3 Comparison of the organ doses to other studies

Iriuchijima A et al. [55] compared the organ doses from CT examinations using Monte Carlo simulation of Radimetrics, to female Rando phantom inserted by RPLGD model 352 M in different organs. The CT chest and abdomen were scanned by Siemens SOMATOM Definition Flash and GE LightSpeed VCT. The scanning parameters and results from Siemens were 120 kVp, 330 mA, and a rotation time 0.5 seconds, $CTDI_{vol}$ was 20 mGy. The organ dose measured by RPLGD were lower from Radimetrics software in breast while the other 4 organ doses were higher.

This study supported our results. The organ doses measured by RPLGD were lower than Radimetrics at the breast and lung while liver, colon and uterus were higher than Radimetrics as shown in Table 6.1.

Table 6.1: Comparison of the organ doses from Iriuchijima A et al. and our study

Organ	Iriuchijima A et al			Our study		
	Measurement (mGy)	Radimetrics (mGy)	The difference, mGy and (% relative difference)	Measurement (mGy)	Radimetrics (mGy)	The difference, mGy and (% relative difference)
Breast	25.4	32.7	7.3(28.7)	15.3	21.80	6.5 (42.5)
Lung	41.8	36.6	5.2(12.4)	23.6	24.50	0.9 (3.8)
Liver	42	32.7	9.3(22.1)	26.2	21.70	4.5 (17.2)
Colon	31.8	28.9	2.9(9.2)	24.2	17.60	6.6 (27.3)
Uterus	29.9	27.9	2(6.7)	18.9	17.40	1.5 (7.9)

Guberina N et al [56] verified the organ doses from Radimetrics, based on Monte Carlo Simulation in thoracic CT protocols and from the measurement of a phantom inserted by TLD. The inter-modality comparison demonstrated a strong correlation between Monte Carlo, Radimetrics and measured by TLD as in Table 6.2.

Table 6.2: Comparison of the organ doses from Guberina N et al. and our study

Organ	Guberina N et al			Our study		
	Measurement (mGy)	Radimetrics (mGy)	The difference, mGy and (% relative difference)	Measurement (mGy)	Radimetrics) (mGy)	The difference, mGy and (% relative difference)
Breast	2.2	2.5	0.3(13.6)	15.3	21.80	6.5 (42.5)
Lung	2.7	2.8	0.1(3.7)	23.6	24.50	0.9 (3.8)
Liver	2.3	1.7	0.6 (26.1)	26.2	21.70	4.5 (17.2)
Colon	0.07	0.06	0.01(14.3)	24.2	17.60	6.6(27.3)
Uterus	n/a	n/a	n/a	18.9	17.40	1.5 (7.9)

The organ doses from the breast and lung measured by TLD were lower than the Radimetrics. While the measured organ dose for the liver and colon were higher. This agreed with our study, breast dose was lower while lung, liver, colon and uterus were higher even though the dosimeters were different.

The minimal difference between the two methods is observed in the lung dose, with a difference value of 0.9 for our study, and 0.1 for Guberina N et al. For the lung region, RDLPGs were placed in the central axis of the organ in every slab to obtain more dose distribution information (Figure 6.1). However, the other organs such as colon did not have clear boundaries. The identification of organ locations remain uncertain, especially in uniform tissue-equivalent materials [57] .



Figure 6.1: RPLGDs were inserted into the holes along the central axis of the lungs.

The difference in organ dose values between the two methods results from differences in phantom types, Rando phantom and the Radimetrics software (stylized phantom). This discrepancy is further influenced by the calculating algorithms utilized by Radimetrics and the positioning of glass dosimeters within the Rando phantom slab.

6.3 Patient study on CT examinations

6.3.1 Patient radiation dose from CT examinations with CED 100 mSv and above

The number of patients receiving CED 100 mSv and above in a single day was 27 or 0.009% of the total of 285,286 patients who performed CT scans during five years. They underwent multiple CT exams, and whole abdomen. The sources of high CED are the patient's size, clinical protocols involving multiple phases, and frequent or repeated scanning.

The age distribution of 27 patients could be separated into 3 groups:

1. 37 percent (10 patients) was less than 50 (23-50) years old
2. 33 percent (9 patients) was 51–65 years old, and
3. 30 percent (8 patients) was over 65 y

The age distribution from other published studies were as the following:

Brambilla M et al. [58] reported the number of patients receiving CED 100 mSv and above in a single day was 70 of the total of 28,780 patients underwent CT examinations from 2017 to 2018. The mean age was 67 ± 13 years, of 51 males and 19 females. The age distribution of 70 patients was as following: 14 percent (10 patients) ≤ 50 years old; 21 percent (15 patients) aged 51-65 years; and 64 percent (45 patients) aged > 65 years.

Rehani MM et al.[40] reported high dose, 100–200 mSv frequently encountered in older age groups at greater than 60 years old. While Zewde N. et al. [9] showed a large distribution of patients receiving CED above 100 mSv were between 55 and 84 years old.

The patient age from our study were uniformly distributed among three groups from young to middle age of 23-50 years at 10 patients, middle to elder age 51-65 years at 9 patients and the eldest at higher than 65 years at 8 patients. Therefore, the risk estimation among three groups are necessitated according to organ dose, gender, age at the CT scan, for the cancer incidence and mortality.

The acquisition protocols resulted in high radiation doses including multiple CT scans (6 patients) and whole abdomen (6 patients). The median CED was 113 mSv for females and 114 mSv for males. Two patients received the maximum CED from CT angiography and CT abdomen according to the following information:

A 57-year-old female with the clinical indication of aortic graft replacement from the ascending aorta to the aortic arch underwent CT angiography at the thoracic aorta with 3 scanning phases. A Dual-Energy CT with retrospective ECG-gated technique was applied to scan almost the entire length of the thoracic aorta. The motion artifact in the aortic root and ascending segment can be minimized by the data from an ECG-gated system. She received the maximum CED at 139 mSv. [27].

A 70-year-old male patient underwent the 4 phases CT abdomen examination. His demography was 145 kg body weight, with abdominal diameter at 409 mm. In order to maintain sufficient image quality for clinical interpretation, the acquisition protocols

were: tube voltage (kVp) at 140 and the mean tube current-time (mAs) at 530. He received maximum CED of 160 mSv.

Similar study from Moghadam N et al who reported the CED from CT examinations of 75,252 patients over one-year period. 7 patients (0.009%) received a CED > 100 mSv from CT abdomen. The highest CED was 129 mSv received by a 23-year-old male who underwent 3 phases of CT abdomen. His abdominal diameter was 491 mm. The patient size and number of phases are major parameters of high CED of CT abdomen.

The organ doses from high CED patients were as high as 300 mGy (Table 5.8 and 5.9). Similar results reported by Zewde N. et al. [7] for most organ doses in excess of 100 to 200 mGy.

Six of the 27 patients in our study underwent CT whole abdomen examinations with four-phase protocol. The mean CED \pm S.D. (range) was 114.5 \pm 22.5 (101.5–160.0) mSv. Most patients were heavy weight, with the age under 40 years old. In addition, the organ dose for the colon and liver were over 200 mGy in patient No.3 (Figure 5.4).

Two patients who received highest breast dose were patient no.4 in the young adult group (Table 5.8), who underwent CT abdomen, a breast dose was 147 mGy. Another patient no.17 in the older age group (Table 5.9), who underwent CTA abdominal aorta, received a breast dose of 118.7 mGy. In large patients, the scan setting could be influenced by the overlapped of the breast and abdomen regions, and the patient's breathing pattern.

6.3.2 Patient radiation dose from CT examinations with CED below 100 mSv

Among 4 CT protocols of brain, chest, whole abdomen and CTA of the whole aorta, the organ doses among gender and age groups were considered from Table 5.11. For CT brain protocol, the brain doses were approximately 100 mGy for both gender and age groups. Female brain doses were a little higher than male. For CTA of the whole aorta, the lung and liver organ doses in male were higher than female in both

age groups. Furthermore, the female breast doses were highest among 4 CT protocols. For CT chest: the lung dose was similar in both genders but little higher at old age. For CT whole abdomen, young female liver and colon doses were higher than male doses and similar to old age group. The uterus dose was higher than dose from CTA protocol in female.

6.3.3 Lifetime attributable risk (LAR) at 5 organs for incident and mortality cancers in high dose

LAR for incident and mortality cancers was estimated by considering the frequent cancer sites, such as lung, liver, breast, colon, and uterus in Thai population[4, 5]. In both young and old patient groups, the LAR for cancer incidence of the lung, liver, and uterus are slightly higher than cancer mortality. Meanwhile, the LAR for cancer incidence of the colon and breast is nearly twice LAR for mortality cancer. LAR for cancer incidence and mortality in young patients are higher than the old group (Table 5.13 and Table 5.14).

The high LAR for cancer incidence and mortality in female patient belongs to patient no.4, who underwent CT whole abdomen, 188 kg body weight, age at CT exam of 22 years old (Table 5.8, 5.12). LAR for breast cancer incidence and mortality were 82 and 35 per 100,000, respectively.

The high LAR for cancer incidence and mortality in male patients belongs to patient no. 3 who underwent multiple CT examination, 80 kg body weight, age at CT exam of 22 years old (Table 5.8, 5.12). LAR for liver and colon cancer incidence and mortality were 71.5, 70.9 and 70.3, 34.4 per 100,000, respectively.

The upper evidence agreed with the epidemiological principle reported by BEIR VII that radiation exposure in younger patients is associated with a dose-related increase in the rates of cancer, with a higher lifetime risk of cancer compared to the aged patients.

Bosch de Basea M. et al [17] estimated of the organ dose and LAR for organs in the scanning regions such as the stomach, colon and rectum, pancreas, liver, and kidneys from CT abdomen. Meanwhile, Khan NA et al. [14] determined the organ dose and LAR in organs exposed to scattered radiation.

Our study estimated the organ dose and LAR not only within the scan area, but also in the periphery, for example from CT abdomen, 6 patients receiving high dose, $CED \geq 100$ mSv, the average organ dose of the lung was 74.3 ± 23.8 (38.9–111.8) mGy while female breast was 89.9 ± 67.3 (16.1–147.6) mGy.

6.3.4 Lifetime attributable risk (LAR) at 6 organs for incident and mortality cancers in low dose

In common CT examinations, the LAR of the young patient's organ is also higher than in the old patient for all cancer sites (Tables 5.16 and 5.17). The high LAR for cancer incidence in male obtained from CTA of the whole aorta (Tables 5.16), with high organ dose was compared to other examination. The maximum average LAR for breast cancer incidence in young female was 23 per 100,000 while for liver cancer incidence in male patients was 22 per 100,000 from CTA whole aorta.

The LAR of the radiation sensitive organ outside the scan area was also estimated. The organ dose and LAR were significantly low. For CT chest, the organ dose at uterus was 0.5 ± 0.3 mGy (Table 5.11), the LAR for uterus cancer incidence was 0.03 ± 0.02 per 100,000 (Table 5.16). Therefore, the estimation of LAR of the organs situated outside the CT scan region based on the scattered radiation, were very low and negligible.

As the CT chest was performed at 27.2 percent of our study and higher than other CT examinations, the average LAR for lung cancer incidence was estimated and the average LAR for female was higher than males. Table 5.16 shows CT chest examination, it can be observed that the trend in the data is illustrated in Figure 6.2, showing that the LAR of lung cancer incidence in younger females was higher than

males and decreased with increasing exposure age. This is consistent with the results of the estimated cancer incidence provided by BEIR VII, in Table 12D-1 (Figure 6.3), LAR for lung cancer incidence in females is higher than in males and decreases with age.

The average lung dose in female was 18.1 ± 4.6 mGy and males, 18.9 ± 4.9 mGy whereas the parameter of ERR and EAR model derived from BEIR VII report of females was greater than males. The mean \pm S.D. of LAR for lung cancer incidence of young females and males from CT chest examinations was 5.0 ± 1.4 and 3.4 ± 1.0 per 100,000 respectively. Although the amount of LAR per 100,000 is relatively low, it is necessary to consider the potential cancer risk resulting from radiation especially in young adults who may receive recurrent CT scans from follow-up or diagnose their diseases, the risk of cancer may increase significantly.

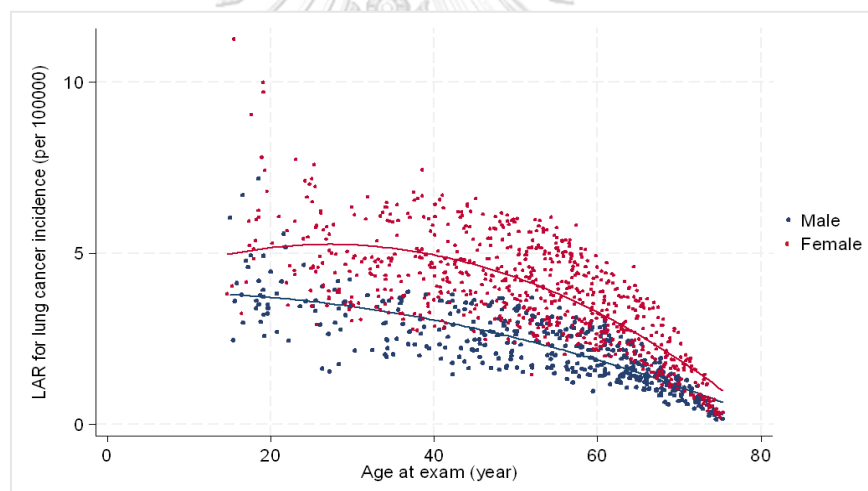


Figure 6.2: LAR for lung cancer incidence from CT chest examination

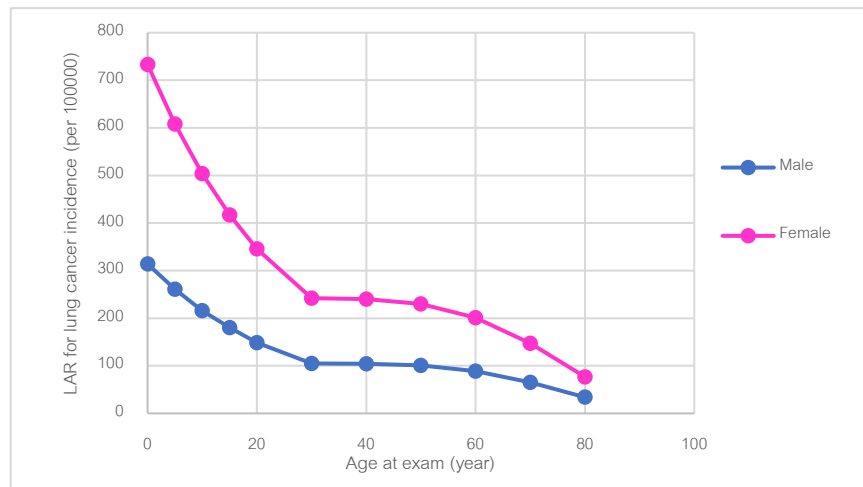


Figure 6.3: The LAR for lung cancer incidence per 100,000 persons (BEIR VII)

For the CT abdomen, LAR for colon cancer incidence has a higher average value than other cancer sites. From the graph (Figure 6.4), it can be seen that the trend of LAR data for colon cancer incidence in male is higher than that in female, and the LAR decreases with increasing age. This is consistent with the results of LAR for colon cancer incidence from Table 12D1 in the BEIR VII report (Figure 6.5).

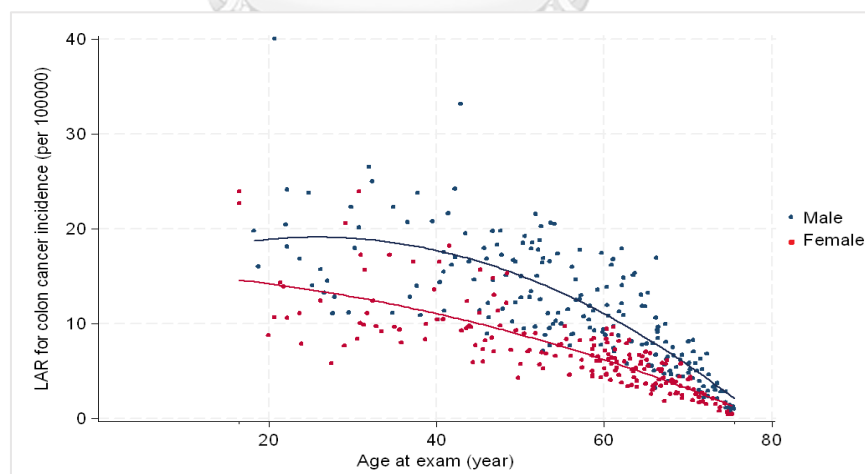


Figure 6.4: LAR for colon cancer incidence from CT abdomen examination

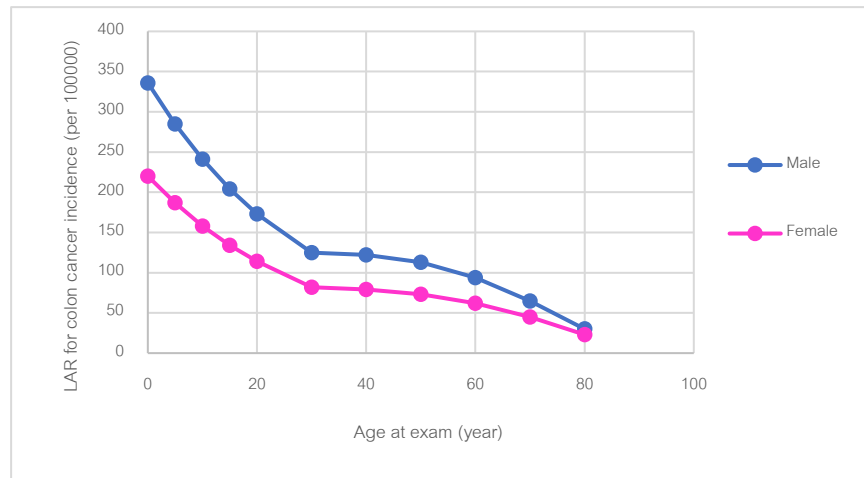


Figure 6.5: The LAR for colon cancer incidence per 100,000 persons (BEIR VII)

According to epidemiological data from the LSS cohort, radiation-induced breast cancer rates were high, especially in young adult [12]. In our study, the average LAR for breasts cancer incidence of patients performing CTA of the whole aorta was 23 in 100,000 (Table 5.16).

Bosch de Basea M. et al. [17] determined the lifetime cancer risk for young patients from CT scans, providing useful data to promote radiation protection, particularly in the young cohorts. It is beneficial to categorize the levels of cancer risk associated with radiation exposure according to the procedures, age group, and gender in order to justify the health risks, benefits and optimized parameter settings.

6.3.5 LAR, organ dose and related patient parameters in common CT protocols

For the common CT examinations which the CED was lower than 100 mSv, the correlation between LAR and patient parameters such as: patient size, age at exposure, and organ dose has been expressed as Pearson Correlation Coefficient (r). LAR of cancer incidence has a strong negative correlation with the age at exposure with statistically significant $p < 0.05$ (Table 6.3).

Table 6.3: Correlation of LAR for lung cancer incidence and age at exposure

Protocol	LAR	<i>r</i>
CT Chest	lung cancer incidence	-0.6838
CT Abdomen	breast cancer incidence	-0.8323
	liver cancer incidence	-0.7160
	colon cancer incidence	-0.7581
	uterus cancer incidence	-0.8985
CTA whole aorta examination	lung cancer incidence	-0.7652
	liver cancer incidence	-0.8133
	colon cancer incidence	-0.7690
	breast cancer incidence	-0.8960
	uterus cancer incidence	-0.8450

LAR for cancer incidence has a positive moderate to low correlation with the organ dose with statistically significant, $p < 0.05$ as shown in Table 6.4.

Table 6.4: Correlation of LAR for lung cancer incidence and organ dose

Protocol	LAR	<i>r</i>
CT Chest	lung cancer incidence	0.45
CT Abdomen	breast cancer incidence	0.28
	liver cancer incidence	0.29
	colon cancer incidence	0.32
	uterus cancer incidence	0.43
CTA whole aorta examination	lung cancer incidence	0.57
	liver cancer incidence	0.48
	colon cancer incidence	0.48
	breast cancer incidence	0.37
	uterus cancer incidence	0.49

The relationship between organ dose and water-equivalent diameter (WED), appears to have varying degrees of correlation, ranging from 0.18 to 0.76, with statistical significance.

6.3.6 Risk Model for incident cancer risk from CTA examinations

As the LAR calculations for each cancer site are not simple, the mathematical model to predict cancer risk has been established. The risk model/equation for the multiple linear regression is:

sqrt LAR for lung cancer incidence (per100000)

$$= 2.13 + \beta_1(\text{age group}) + \beta_2(\text{Lung dose(mGy)}) + \beta_3(\text{male}) + \beta_4(\text{agegr01\#c.Lung dose})$$

The residuals follow a normal distribution (Figure 5.7). There is no evidence of multicollinearity, as demonstrated by a mean Variance Inflation Factor (VIF) of 1.57. R^2 value was relatively high, 0.91, indicating that this set of variables can explain 91% of the LAR for lung cancer incidence.

M Ali RMK et al [59] studied on the mathematical model of radiation-induced cancer risk from breast screening by mammography, multiple linear regression equations were employed to assess the lifetime risk. Various factors such as organ dose, gender, age, and the frequency of screenings were considered. The obtained R^2 value of 0.870 indicates that the multiple linear regression models can be useful for predicting radiation-induced cancer risks from screening programs.

From our study and M Ali RMK et al., it could be confirmed that the equations can predict cancer risk effectively and be useful information for clinicians, referrers, and screening clients.

6.4 Limitations

There are limitations in this study. First, the BEIR VII method is implemented to estimate the risk of cancer based on the linear dose-risk relationship. The risk coefficients and risk-transfer weights were adopted to calculate LAR for each cancer

site, while these factors were obtained from the cohort of Japanese and U.S. populations. Consequently, the uncertainty of this issue should be considered and mentioned. Second, LAR has been calculated using the maximum age of 80 years in this study, based on the average typical life expectancy for both genders of Thai subjects [39]. Due to Thailand's demographic life table showed a limited probability of surviving longer than 80 years. While CT scans were performed in the general population aged 0 to 100 years or higher. Third, the baseline rates for cancer incidence and mortality were based on data from the World Health Organization (WHO) for Thailand in the year 2020. The estimation of cancer rates may introduce some uncertainty into our study.



CHAPTER 7

CONCLUSION

This study was aimed to evaluate the organ doses and lifetime attributable risk (LAR) for cancer incidence and mortality from CT examinations at high dose ($CED \geq 100$ mSv) in a single day to low dose ($CED < 100$ mSv) from the common CT procedures including CTA whole aorta. BEIR VII model and abridged life table data as well as baseline cancer incidence and mortality rates for the Thai population had been applied.

The number of patients underwent CT examinations receiving a high dose, $CED \geq 100$ mSv and above in a single day was 27, accounting for 0.009 percent of 285,286 CT examinations. 7 of 27 were young patients with the age below 40 years old, and 20 of 27 were elder patients, with the age above 40 years old. The median CED of male and female was 114 and 113 mSv respectively. The male patient received the maximum CED from CT abdomen examination at 160 mSv, and the female patient received the maximum CED from CTA of the thoracic aorta at 139 mSv. Six patients received high dose from multiple CT scans (22.2 percent), and another six patients received high dose from CT whole abdomen with four-phase protocol (22.2 percent). The mean $CED \pm S.D.$ (range) was $114.5 \pm 22.5 (101.5 - 159.9)$ mSv received by the heavy weight patients with a mean body weight of 133 kg.

Some patients received the organ dose at the lung, liver, and colon exceeded 200 mGy, and over 300 mGy for the breast. LAR for breast cancer incidence of 22 years old female who underwent CT whole abdomen was 82 in 100,000 with a breast dose of 148 mGy. LAR of liver cancer in 22 years old male patients underwent multiple CT scans was 72 in 100,000 with a liver dose of 133 mGy. Both LARs were higher than other cancer sites.

The average range of LAR for cancer incidence and mortality in the common CT procedures of the brain, chest, whole abdomen, and CTA whole aorta in young patients, were 0.0003–13.2, 0.01–8.4, 0.001–18.2, and 0.7–23.2 per 100,000, respectively. While elder patients were 0.0002–4.70, 0.003–3.49, 0.0005–10.32, 0.16–8.84 per 100000.

Although the LAR was a small amount per 100,000, the estimation of radiation-attributable cancer risk of the patient who received CED below 100 mSv in the common procedure or over 100 mSv in a single day, should not be negligible, especially in young adults, which the risk of cancer in later life may significantly increase. It is necessary to consider the appropriate parameter settings, particularly the impact on cancer risk. It is recommended to justify the health risks and benefits of clinical outcomes in order to increase awareness of the use of medical radiation. The patient dose of the CED at 100 mSv and above should be recorded and monitored individually for justification, optimization, and dose reduction with recurrent CT imaging in a particular young adult patient.

The patient age at exposure is a strong negative correlation with LAR for cancer incidence with statistically significant, $p < 0.05$. The organ dose is positive moderate to weak correlation with LAR for cancer incidence and with statistically significant, $p < 0.05$. In the multiple linear regression equation, R^2 value of 0.91 and residuals had a normal distribution have shown that mathematical modelling can efficiently predict cancer risk.

Finally, it can be concluded that, our findings confirm the research hypothesis as follow:

- The percentage of patients receiving CED from recurrent CT in a single day at 100 mSv and above is *less than 0.01 per total CT examination in five years*.

- LAR of cancer incidence and mortality of major internal organs are *less than 300 per 100,000 patients* from recurrent CT in a single day at 100 mSv and above.



RECOMMENDATIONS

- Unique considerations for children: they are considerably more sensitive to radiation than adults, they have a longer life expectancy than adults, they may receive a higher radiation dose than necessary if CT settings are not adjusted for their smaller body size. The risk for developing a radiation-related cancer can be several times higher for a young child compared with an adult exposed to an identical CT scan. Minimizing radiation exposure from pediatric CT, whenever possible, will reduce the projected number of CT-related cancers.
- A national survey is highly recommended to establish a national diagnostic reference level for CTA. A CTA procedure is operator-dependent. Therefore, continuous training in CTA use and safety is crucial. Special concern is recommended in justifying CTA procedures for young female patients. Comprehensive justification of examinations is highly recommended, and repetition of examinations should be avoided.

REFERENCES

1. National Council on Radiation Protection and Measurements. Medical radiation exposure of patients in the United States. NCRP Report 184. Bethesda, Maryland: NCRP; 2019.
2. Mettler FA, Jr., Mahesh M, Bhargavan-Chatfield M, Chambers CE, Elee JG, Frush DP, et al. Patient Exposure from Radiologic and Nuclear Medicine Procedures in the United States: Procedure Volume and Effective Dose for the Period 2006-2016. *Radiology*. 2020;295:418-27.
3. Brenner DJ, Hall EJ. Computed tomography--an increasing source of radiation exposure. *N Engl J Med*. 2007;357:2277-84.
4. World Health Organization (WHO). Global Cancer Observatory: Cancer Today 2020 [1 April 2022]. Available from: <https://gco.iarc.fr/today>.
5. Virani S, Bilheem S, Chansaard W, Chitapanarux I, Daoprasert K, Khuanchana S, et al. National and Subnational Population-Based Incidence of Cancer in Thailand: Assessing Cancers with the Highest Burdens. *Cancers (Basel)*. 2017;9.
6. Bushberg JT SJ, Leidholt EM Jr, Boone JM,. The essential physics of medical imaging. 4th ed. Philadelphia: Lippincott William and Wilkins; 2021.
7. ICRP. The 2007 Recommendations of the International Commission on Radiological Protection. ICRP Publication 103. Ann. ICRP. ed2007.
8. National Research Council. Health Risks from Exposure to Low Levels of Ionizing Radiation: BEIR VII Phase 2. Washington, DC: The National Academies Press; 2006.
9. Zewde N, Ria F, Rehani MM. Organ doses and cancer risk assessment in patients exposed to high doses from recurrent CT exams. *Eur J Radiol*. 2022;149:110224.
10. Lee S, Kim J, Han S. A Comparative Review of Radiation-induced Cancer Risk Models. *J Radiat Prot Res*. 2017;42:130-40.
11. U.S EPA (Environmental Protection Agency). Radiogenic Cancer Risk Models and Projections for the U.S. Population. 402-R-11-001 ER, editor. Washington, DC: U.S.

Environmental Protection Agency; 2011.

12. World Health Organization. Health risk assessment from the nuclear accident after the 2011 Great East Japan earthquake and tsunami, based on a preliminary dose estimation. Geneva: World Health Organization; 2013.
13. Adeleye B, Chetty N. Radiation dose and cancer risk estimates in helical CT for pulmonary tuberculosis infections. *Open Physics*. 2017;15:769-76.
14. Khan AN, Khosa F, Nikolic B, Shuaib W, Lin PJ, Khan MK. Cancerogenesis Risks between 64 and 320 Row Detector CT for Coronary CTA Screening. *J Clin Imaging Sci*. 2014;4:18.
15. Lim H, Choi J, Kim JH, Cheong HK, Ha M. Estimation of Cancer Incidence and Mortality Risks Attributed to Diagnostic Medical Radiation Exposure in Korea, 2013. *J Korean Med Sci*. 2018;33:e211.
16. Harbron RW, Chapple CL, O'Sullivan JJ, Best KE, Berrington de González A, Pearce MS. Survival adjusted cancer risks attributable to radiation exposure from cardiac catheterisations in children. *Heart*. 2017;103:341-6.
17. Bosch de Basea M, Moriña D, Figuerola J, Barber I, Muchart J, Lee C, et al. Subtle excess in lifetime cancer risk related to CT scanning in Spanish young people. *Environ Int*. 2018;120:1-10.
18. Huang B, Li J, Law MW, Zhang J, Shen Y, Khong PL. Radiation dose and cancer risk in retrospectively and prospectively ECG-gated coronary angiography using 64-slice multidetector CT. *Br J Radiol*. 2010;83:152-8.
19. Mettler FA, Jr., Bhargavan M, Faulkner K, Gilley DB, Gray JE, Ibbott GS, et al. Radiologic and nuclear medicine studies in the United States and worldwide: frequency, radiation dose, and comparison with other radiation sources--1950-2007. *Radiology*. 2009;253:520-31.
20. UNSCEAR. Sources, effects and risks of ionizing radiation. United Nations Scientific Committee on the Effects of Atomic Radiation - UNSCEAR 2020/2021 - Report to the UN General Assembly with Scientific Annexes. New York; 2022.
21. Guberina N, Suntharalingam S, Naßenstein K, Forsting M, Theysohn J, Wetter A, et

- al. Clinical evaluation of a dose monitoring software tool based on Monte Carlo Simulation in assessment of eye lens doses for cranial CT scans. *Neuroradiology*. 2016;58:955-9.
22. Dance DR, Christofides S, Maidment ADA, McLean ID, Ng KH. *Diagnostic Radiology Physics: A Handbook for Teachers and Students*. Vienna: International Atomic Energy Agency; 2014.
 23. Gao Y, Quinn B, Mahmood U, Long D, Erdi Y, St Germain J, et al. A comparison of pediatric and adult CT organ dose estimation methods. *BMC Med Imaging*. 2017;17:28.
 24. Maxwell S, Fox R, McRobbie D, Bulsara M, Doust J, O'Leary P, et al. How have advances in CT dosimetry software impacted estimates of CT radiation dose and cancer incidence? A comparison of CT dosimetry software: Implications for past and future research. *PLoS One*. 2019;14:e0217816.
 25. De Mattia C, Campanaro F, Rottoli F, Colombo PE, Pola A, Vanzulli A, et al. Patient organ and effective dose estimation in CT: comparison of four software applications. *Eur Radiol Exp*. 2020;4:14.
 26. Hsieh J. *Computed tomography; principles, design, artifacts, and recent advances*. 2 ed: Book News, Inc.; 2010.
 27. Manna C, Silva M, Cobelli R, Poggese S, Rossi C, Sverzellati N. High-pitch dual-source CT angiography without ECG-gating for imaging the whole aorta: intraindividual comparison with standard pitch single-source technique without ECG gating. *Diagn Interv Radiol*. 2017;23:293-9.
 28. Booi R, Budde RPJ, Dijkshoorn ML, van Straten M. Technological developments of X-ray computed tomography over half a century: User's influence on protocol optimization. *Eur J Radiol*. 2020;131:109261.
 29. Hammerstingl RM, Vogl TJ. Abdominal MDCT: protocols and contrast considerations. *Eur Radiol*. 2005;15 Suppl 5:E78-90.
 30. Raju S, Ghosh S, Mehta AC. Chest CT Signs in Pulmonary Disease: A Pictorial Review. *Chest*. 2017;151:1356-74.

31. Croft M, Lim W, Lavender N, Gormly K. Optimising CT-chest protocols and the added value of venous-phase contrast timing; Observational case-control. *J Med Imaging Radiat Oncol.* 2022;66:768-75.
32. Fleischmann D. CT angiography: injection and acquisition technique. *Radiol Clin North Am.* 2010;48:237-47, vii.
33. Ion CT, John AE, Adrian U, Malcolm John U, Ionel D. *New Approaches to Aortic Diseases From Valve to Abdominal Bifurcation.* London, United Kingdom: Academic Press; 2018.
34. Latson LA, Jr., DeAnda A, Jr., Ko JP. Imaging of the Postsurgical Thoracic Aorta: A State-of-the-Art Review. *J Thorac Imaging.* 2017;32:1-25.
35. Bossone E, Eagle KA. Epidemiology and management of aortic disease: aortic aneurysms and acute aortic syndromes. *Nat Rev Cardiol.* 2021;18:331-48.
36. van Bogerijen GHW, van Herwaarden JA, Conti M, Auricchio F, Rampoldi V, Trimarchi S, et al. Importance of dynamic aortic evaluation in planning TEVAR. *Annals of cardiothoracic surgery.* 2014;3:300-6.
37. Holloway BJ, Rosewarne D, Jones RG. Imaging of thoracic aortic disease. *Br J Radiol.* 2011;84 Spec No 3:S338-54.
38. McCollough CH, Leng S, Yu L, Cody DD, Boone JM, McNitt-Gray MF. CT dose index and patient dose: they are not the same thing. *Radiology.* 2011;259:311-6.
39. Ulanowski A, Kaiser JC, Schneider U, Walsh L. Lifetime radiation risk of stochastic effects - prospective evaluation for space flight or medicine. *Ann ICRP.* 2020;49:200-12.
40. Rehani MM, Heil J, Baliyan V. Multicentric study of patients receiving 50 or 100 mSv in a single day through CT imaging-frequency determination and imaging protocols involved. *Eur Radiol.* 2021;31:6612-20.
41. Suksancharoen W, Lowong T, Krisanachinda A. Assessment of patient radiation dose from recurrent ct examinations. *MEDICAL PHYSICS INTERNATIONAL.* 2021;9:93-6.
42. Einstein AJ, Henzlova MJ, Rajagopalan S. Estimating risk of cancer associated with

- radiation exposure from 64-slice computed tomography coronary angiography. JAMA. 2007;298:317-23.
43. Shubayr N, Alashban Y. Estimation of radiation doses and lifetime attributable risk of radiation-induced cancer in the uterus and prostate from abdomen pelvis CT examinations. Front Public Health. 2022;10:1094328.
 44. Ghatti C, Ortenzia O, Maddalo M, Altabella L, Sverzellati N. Dosimetric and radiation cancer risk evaluation of high resolution thorax CT during COVID-19 outbreak. Phys Med. 2020;80:119-24.
 45. Kim JS, Park BR, Yoo J, Ha W-H, Jang S, Jang WI, et al. Measurement uncertainty analysis of radiophotoluminescent glass dosimeter reader system based on GD-352M for estimation of protection quantity. Nuclear Engineering and Technology. 2022;54:479-85.
 46. Matsubara K, Yoshida S, Hirosawa A, Chusin T, Furukawa Y. Characterization of Small Dosimeters Used for Measurement of Eye Lens Dose for Medical Staff during Fluoroscopic Examination. Diagnostics (Basel). 2021;11.
 47. AGC TECHNO GLASS CO. Dose Ace Technical Guide. 2013. p. 1-4.
 48. Gharbi S, Labidi S. Radiation dose optimization in computed tomography with current modulation and iterative reconstruction 2017. 220-3 p.
 49. Bayer HealthCare Medical Care. CT Organ Dose Calculations in Radimetrics™ Enterprise Platform. Indianola: Bayer Pharma AG; 2016.
 50. National Statistical Office Thailand. Abridged life table for population in Thailand, 2005-2006 2006 [Available from: www.nso.go.th].
 51. Dance DR CS, Maidment ADA, McLean ID, Ng KH.,. Dosimetry in Diagnostic Radiology: An International Code of Practice. Vienna: INTERNATIONAL ATOMIC ENERGY AGENCY; 2007.
 52. Matsubara K, Sugai M, Toyoda A, Koshida H, Sakuta K, Takata T, et al. Assessment of an organ-based tube current modulation in thoracic computed tomography. J Appl Clin Med Phys. 2012;13:3731.
 53. Hörnlund M, Bernhardsson C, editors. Organ doses determined using a RANDO

phantom for different radionuclide depositions and photon energies 2013.

54. Chang W, Koba Y. Evaluation of Organ Doses for Pediatric Computed Tomography Using a Newly Designed Radiophotoluminescence Glass Dosimeter and Comparison with a Monte Carlo Simulation-based Dose Calculator. *Health Phys.* 2021;120:288-95.
55. Iriuchijima AF, Y. Ogura, A.,. Comparison of Organ Dose Calculation Using Monte Carlo Simulation and In-phantom Dosimetry in CT Examination. *Nihon Hoshasen Gijutsu Gakkai Zasshi.* 2018;74:166-71.
56. Guberina N, Suntharalingam S, Naßenstein K, Forsting M, Theysohn J, Wetter A, et al. Verification of organ doses calculated by a dose monitoring software tool based on Monte Carlo Simulation in thoracic CT protocols. *Acta Radiol.* 2018;59:322-6.
57. Zhang D, Li X, Gao Y, Xu XG, Liu B. A method to acquire CT organ dose map using OSL dosimeters and ATOM anthropomorphic phantoms. *Med Phys.* 2013;40:081918.
58. Brambilla M, Cannillo B, D'Alessio A, Matheoud R, Agliata MF, Carriero A. Patients undergoing multiphase CT scans and receiving a cumulative effective dose of ≥ 100 mSv in a single episode of care. *Eur Radiol.* 2021;31:4452-8.
59. RMK MA, England A, Mercer C, Tootell A, Walton L, Schaake W, et al. Mathematical modelling of radiation-induced cancer risk from breast screening by mammography. *Eur J Radiol.* 2017;96:98-103.

APPENDIX I

Quality Control of Multi-Detector Computed Tomography System

Canon CT scanner:

1. Position dependence and S/N ratio of C.T. numbers

Method:

Place the C.T. head phantom at the center of the gantry. Acquire a single scan with a 1 cm slice thickness using the typical head technique. Select a circular region of interest measuring approximately 400 sq. mm. Record the mean C.T. number and standard deviation for each of positions 1 through 5.

Technique: 120 kV, 300 mA, 1 second, 250 mm. FOV

Results

Position	Mean C.T.	S.D.	C.V.
1	89.2	10.0	0.112
2	88.9	9.9	0.111
3	87.8	10.4	0.118
4	88.8	10.7	0.120
5	89.3	11.4	0.128

*CV = Standard deviation/mean CT number

Tolerance: The coefficient of variation of mean CT numbers of the four scans should be less than 0.2.

Comment: Pass

2.Reproducibility of C.T. Numbers

Method:

Using the same setup and technique as in the position dependence study, conduct three scans. Utilize the same region of interest (ROI) as employed in the position dependence study at location 5, which corresponds to the center of the phantom, to retrieve mean C.T. numbers for each scan.

Results:

Run Number	1	2	3
Mean C.T	88.9	89.2	88.9
Mean Global C.T Number	88.9		
Standard Deviation	0.13		
Coefficient of variation	0.001		

Tolerance: The coefficient of variation of mean C.T. numbers of the four scans should be less than 0.002

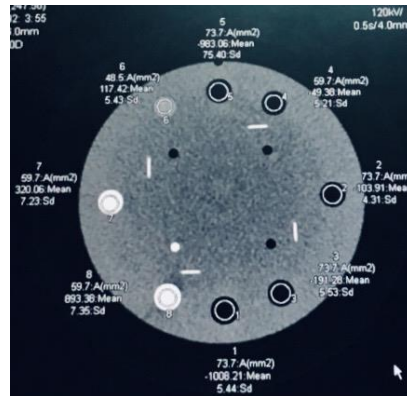
Comment: Pass

3. Linearity of C.T. Numbers

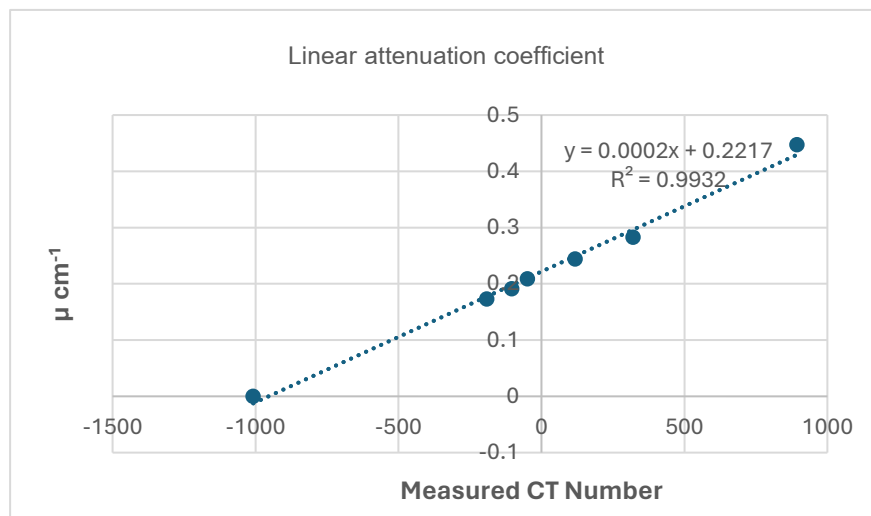
Method:

Set up the CATPHAN performance phantom as described in beam alignment. Select the section containing the test objects of different C.T. numbers. Select the head technique and perform a single transverse scan. Select a region of interest (ROI) of sufficient size to cover the test objects. Place the ROI in the middle of each test object and record the mean C.T. number.

Results



Material	Expected CT #	Measured CT #
Acrylic	120	117.42
Polystyrene	-35	-49.38
LDPE	-100	-103.91
PMP	-200	-191.28
Delrin	340	320.06
Teflon	990	893.38
Air (inferior)	-1000	-1008.2
Air (superior)	-1000	-983.06



Tolerance: R-square between measured CT number and linear attenuation coefficient

(μ) more than 0.9

Comment: Pass

4. High contrast resolution

Set up the Catphan phantom in beam alignment. Select the section containing the high-resolution test object. (CTP528 21-line pair high-resolution Module). Select the head technique and perform a single transverse scan. Select the area containing the high-resolution test objects. Select the appropriate window and level for the best visualization of the test objects.

Results



Slice Thickness in mm	Resolution	Gap size
4 mm	7 lp/mm	0.071 cm

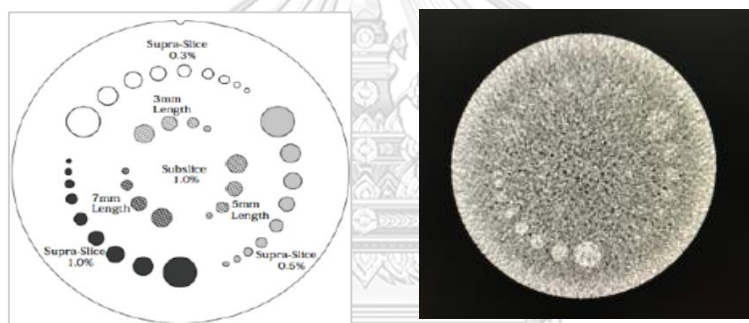
Tolerance: > 5 lp/cm visible

Comment: Pass

5.Low contrast resolution

Method:

Set up the Catphan 600 phantom in beam alignment. Select the section containing the low-resolution test object CTP515 Sub-slice and supra-slice low contrast Module. Select the head technique and perform a single transverse scan. Select the area containing the low-resolution test objects. Select the appropriate window and level for the best visualization of the test objects. Record the smallest test object visualized.



Slice thickness in mm	Smallest target(spokes) diameter (mm)					
	Contrast level of supra-slice			Length of sub-slice 1.0%		
	1.00%	0.50%	0.30%	7 mm	5 mm	3 mm
4 mm	7	4	4	4	4	3

Tolerance: The smallest target diameter at 0.5% contrast level of supra-slice should be seen 4 spokes.

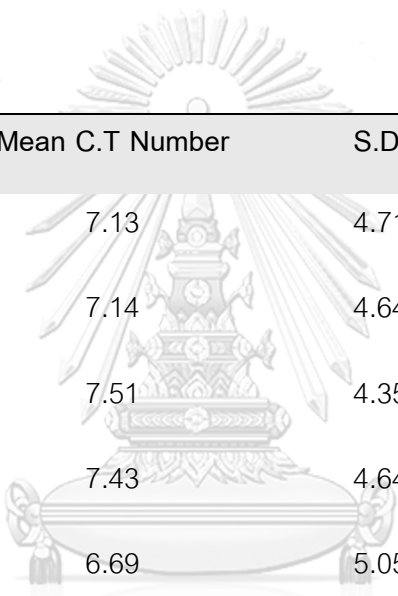
Comment: Pass

6. Image uniformity

Method:

Set up the Catphan phantom as described in beam alignment. Select the CTP486 solid image uniformity module. Select the head technique and perform a single transverse scan. Select a region of interest (ROI) of sufficient size to cover the test objects. Place the ROI in the middle of each test object and record the mean C.T. number.

Results:



Position	Mean C.T Number	S.D.	Difference (HU)
1	7.13	4.71	0.44
2	7.14	4.64	0.45
3	7.51	4.35	0.82
4	7.43	4.64	0.74
5	6.69	5.05	

Different = |CT number center – CT number peripheral|

Tolerance: Less than 5 HU

Comment: Pass

7. Measurement of Computed Tomography Dose Index (CTDI) in air (CTDI_{air})

Method:

Position the 100 mm pencil chamber at the isocenter of the CT bore. The scan parameters for the head protocol were set at 100 mAs and 1 second scan time. Perform axial mode scanning and vary the kilovoltage settings at 80, 100, 120, and 140. CTDI free in air is measured and recorded in mGy units. The calculation CTDI₁₀₀ in air according to equation 2.6 in Chapter 2.

Results

1) Siemens Healthineers CT scanner

Table I. 1: The measured CTDI free in air (mGy) for head protocol

CTDI free in air (mGy) for head protocol with 180 mm FOV(s)				
kVp	80	100	120	140
Detector configuration (mm)				
1X5	0.065	0.117	0.182	0.259

2) GE CT scanner

Table I. 2: The measured CTDI free in air (mGy) for head protocol

CTDI free in air (mGy) for head protocol with 180 mm FOV(s)				
kVp	80	100	120	140
Detector configuration (mm)				
1.25 X 4	0.134	0.227	0.336	0.461
0.625 X 64	0.091	0.154	0.228	0.313

3) Canon CT scanner

Table I. 3: The measured CTDI free in air (mGy) for head protocol

CTDI free in air (mGy) for head protocol with 180 mm FOV(s)				
kVp	80	100	120	135
Detector configuration (mm)				
1 X 1	0.513	0.849	1.282	1.729
2 X 4	0.171	0.281	0.414	0.534



APPENDIX II

Measurement process of RPLGDs

1. Annealing

For the annealing process, place the glass dosimeter on the tray. The annealing process takes about 20 minutes at 400 °C using an annealing oven (Figure 4.11). After annealing, observe the temperature to ensure it is not higher than 40°C before removing the tray.



Figure II. 1: Annealing RPLGDs

2. Reading out the background (before exposing)

Read out the background using a standard read-out magazine before irradiation. The value should be ranged from 10 to 30 μGy .

3. Exposing

Place the RPL Glass Dosimeter into holders and make sure the cap is securely closed before exposing.

4. Preheating in oven

Position the RPL Glass Dosimeter into the preheat tray and set the preheating environment to 70 °C for 30 minutes. After that, allow the dosimeter to cool to room temperature.

5. Reading out of accumulated value (after exposing)

Detach the glass parts from the holders after the dosimeter elements cooled. Then, put them into the magazine, set the mode, and read out the parameter using FGD-1000 software (AGC Techno Glass Co., LTD, Shizuoka, Japan), (Figure 4.12).

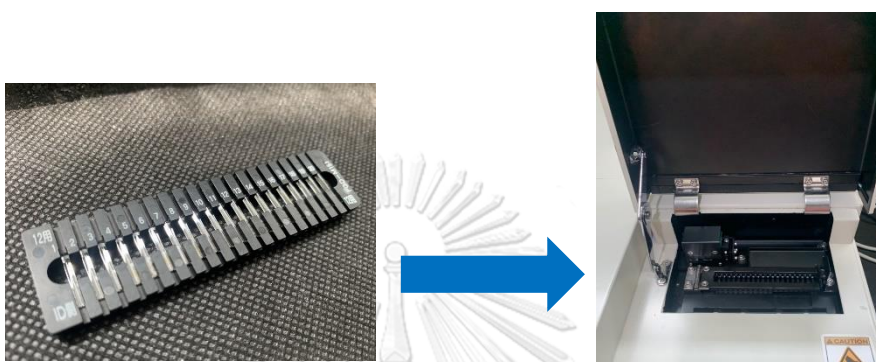


Figure II. 2: The reading-out process utilizing the FGD-1000 reader.

Calibration of RPLGDs

From the experimental results of the calibration of RPLGDs in section 5.2.1, air kerma was measured three times by the ionization chamber as shown in Table II.1. Air kerma measurement from 100 RPLGDs as shown in Table II.2. Which can be observed that RPLGD No. 40 has a lower air kerma value than the others. The Figure II.1 displays the RGLGDs' calibration coefficient.

Table II. 1: Air kerma measurement from ionization chamber (IC)

Measurement	Air kerma measured by IC: (μGy)
1	307.17
2	307.26
3	307.07
Average	307.17

Table II. 2: Air kerma measurement from 100 RPLGDs

Number of RPLGDs	Air kerma (uGy)	Number of RPLGDs	Air kerma (uGy)
1	301	51	317
2	314	52	309
3	305	53	313
4	304	54	296
5	299	55	291
6	291	56	300
7	300	57	305
8	298	58	307
9	300	59	297
10	297	60	298
11	300	61	311
12	314	62	298
13	314	63	308
14	306	64	294
15	303	65	293
16	301	66	302
17	304	67	312
18	306	68	306
19	307	69	285
20	309	70	289
21	310	71	312
22	312	72	302
23	301	73	313
24	307	74	305
25	292	75	305
26	295	76	311
27	308	77	314
28	303	78	310
29	297	79	309
30	285	80	304
31	305	81	294
32	310	82	318
33	309	83	302
34	302	84	297
35	299	85	305
36	301	86	309
37	304	87	306
38	311	88	303

39	309	89	304
40	240	90	300
41	297	91	304
42	297	92	314
43	301	93	308
44	296	94	301
45	297	95	287
46	317	96	306
47	295	97	311
48	296	98	311
49	309	99	311
50	293	100	302

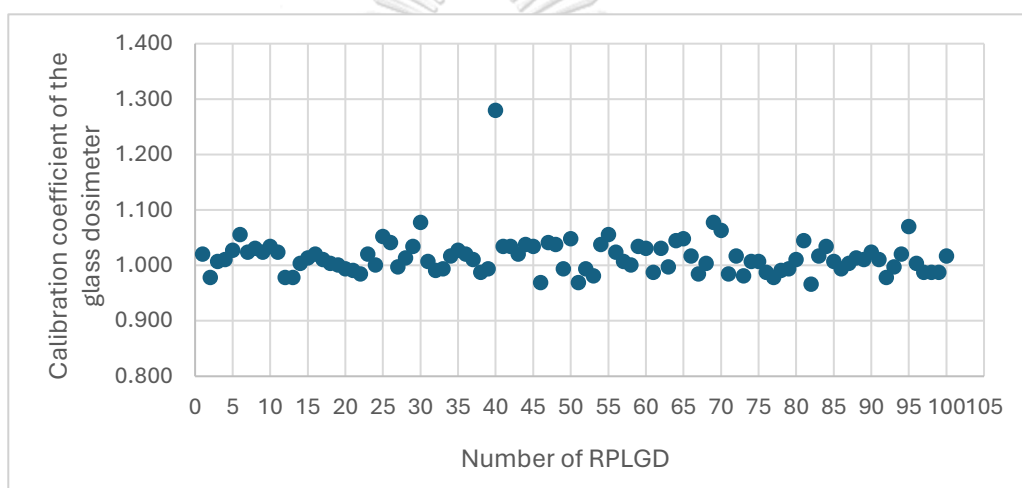


Figure II. 3: The calibration coefficient of the RGLGDs

APPENDIX III

Lifetime attributable risk (LAR)

1) LAR in high dose for each elder patient

Lifetime attributable risk (LAR) at 5 organs for incident and mortality cancers in high dose of 20 patients with aged above 40 years old, CED at 100 mSv and above in a single day, as shown in Table III. 1.

Table III. 1: LAR of cancer incidence and mortality from CT examinations for each older patient

Patient No.	Age (yr) /gender	LAR per 100,000 of cancer incidence						LAR per 100,000 of cancer mortality					
		Lung	Liver	Colon	Breast	Uterus	Brain	Lung	Liver	Colon	Breast	Uterus	Brain
1	60/Female	23.4	17.6	18.5	19.2	2.0	0.02	21.6	17.4	10.8	9.5	1.7	0.02
2	52/Female	8.3	19.7	35.2	2.7	4.9	0.01	7.4	19.2	18.6	1.2	3.6	0.01
3	57/Female	53.3	26.8	4.1	33.4	0.14	0.1	48.5	26.3	2.3	16.0	0.11	0.12
4	72/Female	7.1	4.9	4.7	3.8	0.4	1.5	6.7	4.9	3.5	2.4	0.4	1.5
5	56/Female	63.5	21.4	1.1	43.8	0.04	0.03	57.6	21.0	0.6	20.8	0.03	0.03
6	46/Female	33.7	19.9	17.8	55.9	1.6	3.16	29.8	19.4	9.1	25.8	1.1	2.9
7	69/Male	16.3	25.2	3.4	-	-	0.01	15.2	25.5	2.4	-	-	0.01
8	73/Male	2.0	7.7	11.0	-	-	0.0004	1.9	7.8	8.0	-	-	0.0004
9	61/Male	28.7	47.2	3.6	-	-	0.02	26.3	47.6	2.1	-	-	0.02
10	47/Male	24.8	52.3	43.7	-	-	1.4	21.8	51.9	22.4	-	-	1.3
11	54/Male	15.6	43.2	50.2	-	-	0.01	14.0	43.0	27.1	-	-	0.01
12	73/Female	9.7	3.8	2.0	4.2	0.2	0.2	9.2	3.7	1.5	2.6	0.15	0.2
13	55/Female	21.2	22.8	31.5	13.5	4.0	0.1	19.1	22.4	17.1	6.4	3.1	0.1
14	46/Female	42.6	21.8	13.2	81.4	0.6	6.9	37.7	21.3	6.8	37.6	0.4	6.2
15	70/Female	7.7	8.1	10.3	4.8	1.1	0.003	7.3	8.1	7.6	3.0	0.9	0.003

16	60/Female	20.5	13.8	18.1	11.5	2.2	2.0	19.0	13.6	10.6	5.7	1.8	1.9
17	61/Female	22.7	14.3	17.5	12.8	2.1	0.01	21.0	14.2	10.4	6.5	1.8	0.01
18	73/Male	2.9	10.5	14.5	-	-	0.01	2.7	10.6	10.6	-	-	0.01
19	66/Male	11.4	21.6	24.4	-	-	0.07	10.6	21.9	16.0	-	-	0.06
20	70/Male	4.5	25.0	33.2	-	-	0.002	4.2	25.2	24.3	-	-	0.002

2) Organ dose and LAR of whole aorta with dual energy CT protocol

CTA protocol includes 3 phases including non-contrast, arterial phase and a delay. Dual-Energy CT conducted in arterial Phase of CT whole aorta. The Independent Samples t-test was used to compare the means of organ dose in male and female patients. The results indicate that there were no statistically significant differences between the two groups, with a P value greater than 0.05 (Table III. 2). The highest LAR for breast cancer incidence in young female was 17 per 100,000 exposed patients, with a breast dose of 36 mGy at the age of the exam being 44 years old, body weight 95 kg, and WED 311 mm. The highest LAR for colon cancer incidence in male patients was 20 per 100,000, with a colon dose of 55 mGy at the age of the exam being 56 years old, body weight 102 kg, and WED 341 mm (Figure III. 1).

Table III. 2: Mean organ dose (mGy) in common CT protocols from all patients

	Gender	
	Female	Male
Organ dose (mGy)	(n=255)	(n=54)
Lungs	29.4±7.6	31.4±9.9
Liver	27.1±6.8	28.3±8.5
Colon	23.0±5.7	23.8±6.6
Breast	28.9±8.6	
Uterus	21.9±5.4	

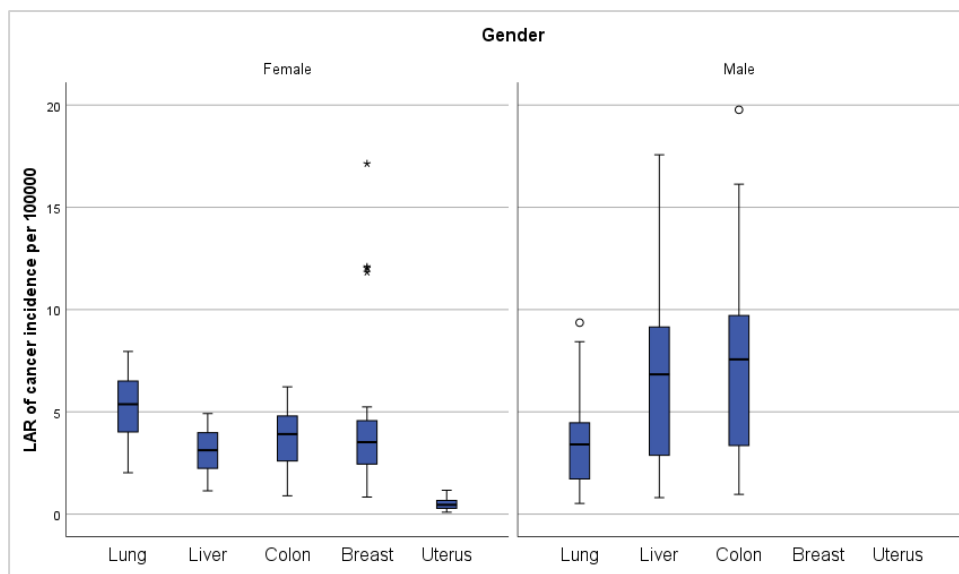


Figure III. 1: LAR of whole aorta with dual energy CT protocol



3) Risk Model for incident cancer risk from CTA examinations

In the section 5.36 (Chapter 5) Risk Model for incident cancer risk from CTA examinations Multivariate regression risk model for incident cancer risk from CTA examinations includes the following

- 2) LAR for liver cancer incidence
- 3) LAR for colon cancer incidence
- 4) LAR for breast cancer incidence
- 5) LAR for uterus cancer incidence

2) Model for LAR for liver cancer incidence

- Normal distribution of the variable

The LAR for liver cancer incidence conformed to a normal distribution when LAR was represented in square root form. The distribution of organ dose in the liver was normal. The histogram in age at exam data shows non-normally distributed, we categorize the data based on age at exam; Age group 1: age at exam ≤ 40 , 2: age at exam 41-60, 3: age at exam 61-70, 4: age at exam 71-75 years old.

- Univariate linear regression

Univariate linear regression analysis revealed that the p-value was below the significance level of $P < 0.05$. This indicates that the predictor variables, organ dose in the liver, age at exam, and gender, had a statistically significant association with the LAR for liver cancer incidence. Therefore, the variables are being added to the regression model.

● Multiple Linear Regression

Linear regression

Number of obs = 694
 F(8, 685) = 801.37
Prob > F = **0.0000**
R-squared = **0.9087**
Root MSE = **.37366**

		β	Robust				
srlarincliver	Coefficient	std. err.	t	P> t	[95% conf. interval]		
agegr01							
2	-.2392218	.1777557	-1.35	0.179	-.5882332	.1097895	
3	-.6766941	.1753464	-3.86	0.000	-1.020975	-.3324132	
4	-1.283971	.19917	-6.45	0.000	-1.675028	-.8929137	
Liver dose	.0491369	.0038542	12.75	0.000	.0415694	.0567045	
agegr01#c.liver dose							
2	-.0121602	.0041411	-2.94	0.003	-.020291	-.0040294	
3	-.0237788	.0040913	-5.81	0.000	-.0318118	-.0157459	
4	-.0313195	.0046755	-6.70	0.000	-.0404994	-.0221395	
1.male	.8635288	.0387213	22.30	0.000	.7875022	.9395554	
_cons	1.256385	.1577105	7.97	0.000	.9467306	1.566039	

Multiple linear regression equation with interaction term:

$$\text{LAR for liver cancer incidence (per 100000)} = 1.26 + \beta_1(\text{age group}) + \beta_2(\text{Liver dose (mGy)}) + \beta_3(\text{male}) + \beta_4(\text{agegr01\#c.Liver dose})$$

From the obtained multiple linear regression equation, residuals had a normal distribution and there was no evidence of multicollinearity, (mean VIF=1.56). Additionally, the R^2 value was relatively high, indicating that this set of variables can explain 91% of the LAR for liver cancer incidence. The Root MSF, 0.37 was low indicating that the original values and predicted values are close to each other. A scatterplot displays the relationship between actual and predicted value while line plots represent regression of the actual data (Figure III. 2).

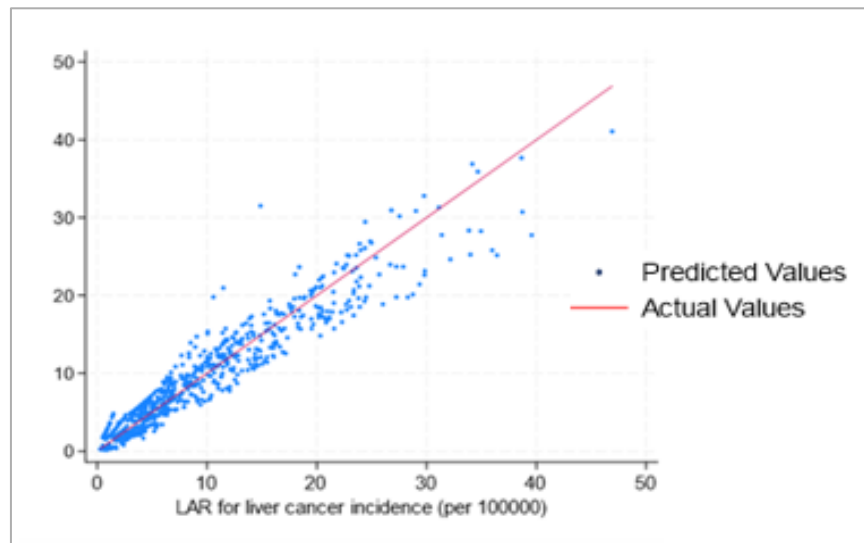


Figure III. 2: Two-way scatterplot with a linear regression line of LAR for liver cancer incidence

3) Model for LAR for colon cancer incidence

- Normal distribution of the variable

The LAR for colon cancer incidence conformed to a normal distribution when LAR was represented in square root form. The distribution of organ dose in the colon was normal.

- Univariate linear regression

Univariate linear regression analysis revealed that the p-value was below the significance level of $P < 0.05$. This indicates that the predictor variables, organ dose in the colon, age at exam, and gender, had a statistically significant association with the LAR for colon cancer incidence. Therefore, the variables are being added to the regression model.

- Multiple Linear Regression

Multiple linear regression equation with interaction term:

```
. reg srlarinccolon b1.agegr01#c.colonsvmc b0.male,robust
```

Linear regression	Number of obs	=	694
	F(8, 685)	=	875.86
	Prob > F	=	0.0000
	R-squared	=	0.9089
	Root MSE	=	.34614

		Robust					
srlarinccolon		Coefficient	std. err.	t	P> t	[95% conf. interval]	

agegr01							
2		-.3329248	.1378236	-2.42	0.016	-.6035322	-.0623174
3		-.7910097	.1364032	-5.80	0.000	-1.058828	-.5231911
4		-1.400251	.1590283	-8.81	0.000	-1.712493	-1.08801
Colon dose		.0542264	.0038911	13.94	0.000	.0465864	.0618664
agegr01#c.colondose							
2		-.0096897	.0042371	-2.29	0.023	-.018009	-.0013704
3		-.0219241	.0042133	-5.20	0.000	-.0301965	-.0136516
4		-.0319288	.0048437	-6.59	0.000	-.041439	-.0224186
1.male		.7588918	.031535	24.07	0.000	.696975	.8208087
_cons		1.519085	.1201268	12.65	0.000	1.283224	1.754946

LAR for colon cancer incidence (per100000)=1.52+ β_1 (age group)+ β_2 (colon dose(mGy)+ β_3 (male)+ β_4 (agegr01#c.Colon dose)

From the obtained multiple linear regression equation, residuals had a normal distribution and there was no evidence of multicollinearity,(mean VIF=1.56). Additionally, the R^2 value was relatively high, indicating that this set of variables can explain 91% of the LAR for colon cancer incidence. The Root MSF, 0.35 was very low indicating that the original values and predicted values are close to each other. A scatterplot displays the relationship between actual and predicted value while line plots represent regression of the actual data (Figure III. 3).

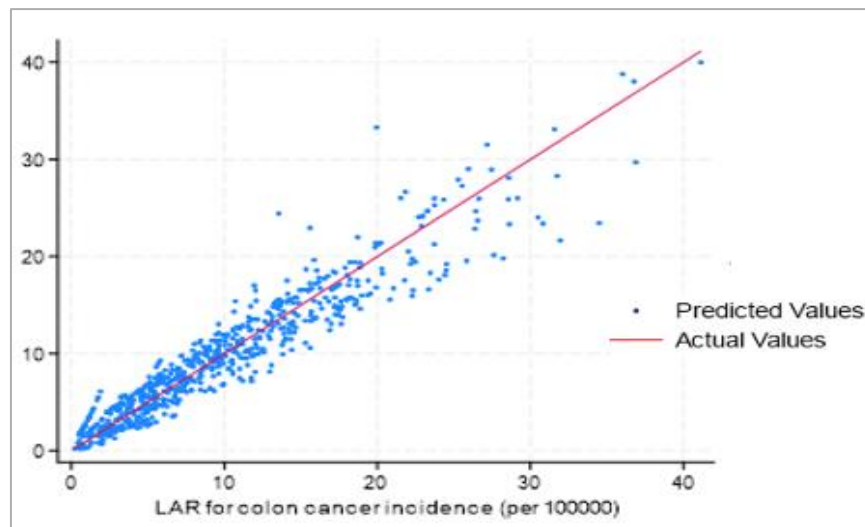


Figure III. 3: Two-way scatterplot with a linear regression line of LAR for colon cancer incidence

4) Model for LAR for breast cancer incidence

- Normal distribution of the variable

The LAR for breast cancer incidence conformed to a normal distribution when LAR was represented in square root form. The distribution of organ dose in the breast was normal.

- Univariate linear regression

Univariate linear regression analysis revealed that the p-value was below the significance level of $P < 0.05$. This indicates that the predictor variables, organ dose in the breast, and age at exam had a statistically significant association with the LAR for breast cancer incidence. Therefore, the variables are being added to the regression model.

● Multiple Linear Regression

Linear regression

Number of obs = 147
 F(5, 141) = 256.35
Prob > F = **0.0000**
R-squared = **0.9229**
Root MSE = **.41973**

		β	Robust				
	srlarincbreast	Coefficient	std. err.	t	P> t	[95% conf. interval]	
	agegrbreast						
	2	-1.392945	.2830686	-4.92	0.000	-1.952553	-.8333381
	3	-1.99989	.2924638	-6.84	0.000	-2.578071	-1.421709
	breastdose	.0394929	.0064235	6.15	0.000	.0267942	.0521916
	agegrbreast#c.breast dose						
	2	-.0180244	.0067671	-2.66	0.009	-.0314026	-.0046462
	3	-.0262771	.006965	-3.77	0.000	-.0400464	-.0125078
	_cons	2.683854	.2671671	10.05	0.000	2.155683	3.212025

Multiple linear regression equation with interaction term:

$$LAR \text{ for breast cancer incidence (per100000)} = 2.68 + \beta_1(\text{age group}) + \beta_2(\text{breast dose(mGy)}) + \beta_3(\text{agegr01\#c.breast dose})$$

From the obtained multiple linear regression equation, residuals had a normal distribution and there was no evidence of multicollinearity, (mean VIF=1.33). Additionally, the R^2 value was relatively high, indicating that this set of variables can explain 92% of the LAR for breast cancer incidence. The Root MSF, 0.42 was very low indicating that the original values and predicted values are close to each other. A scatterplot displays the relationship between actual and predicted value while line plots represent regression of the actual data (Figure III. 4).

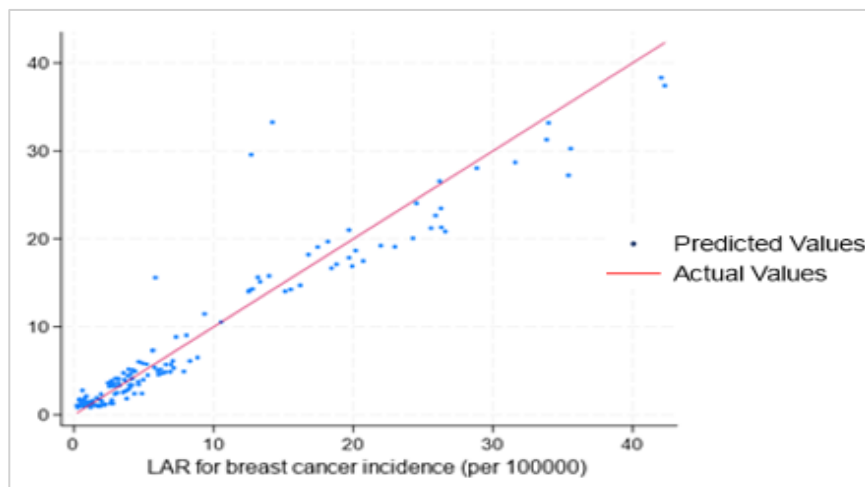


Figure III. 4: Two-way scatterplot with a linear regression line of LAR for liver cancer incidence

5) Model for LAR for uterus cancer incidence

- Normal distribution of the variable

The LAR for uterus cancer incidence conformed to a normal distribution when LAR was represented in square root form. The distribution of organ dose in the uterus was normal.

- Univariate linear regression

Univariate linear regression analysis revealed that the p-value was below the significance level of $P < 0.05$. This indicates that the predictor variables, organ dose in the uterus, and age at exam had a statistically significant association with the LAR for uterus cancer incidence. Therefore, the variables are being added to the regression model.

- Multiple Linear Regression

Linear regression

Number of obs = 147
 F(5, 141) = 194.57
Prob > F = 0.0000
R-squared = 0.8775
Root MSE = .14287

		Coefficient	Robust std. err.	t	P> t	[95% conf. interval]	
srlarincuterus							
agegruterus							
	2	-.3353623	.0742058	-4.52	0.000	-.482062	-.1886625
	3	-.5567481	.0738838	-7.54	0.000	-.7028113	-.4106848
Uterus dose		.0137107	.0014952	9.17	0.000	.0107548	.0166666
agegruterus#c.uterusdose							
	2	-.002908	.0017924	-1.62	0.107	-.0064514	.0006354
	3	-.0066499	.0017692	-3.76	0.000	-.0101474	-.0031524
_cons		.7748857	.0665383	11.65	0.000	.6433441	.9064274

Multiple linear regression equation with interaction term:

$$LAR \text{ for uterus cancer incidence (per100000)} = 0.77 + \beta_1(\text{age group}) + \beta_2(\text{uterus dose(mGy)}) + \beta_3(\text{agegr01\#c.uterus dose})$$

From the obtained multiple linear regression equation, residuals had a normal distribution and there was no evidence of multicollinearity, (mean VIF=1.32). Additionally, the R^2 value was relatively high, indicating that this set of variables can explain 88% of the LAR for uterus cancer incidence. The Root MSF was very low indicating that the original values and predicted values are close to each other. A scatterplot displays the relationship between actual and predicted value while line plots represent regression of the actual data (Figure III. 5).

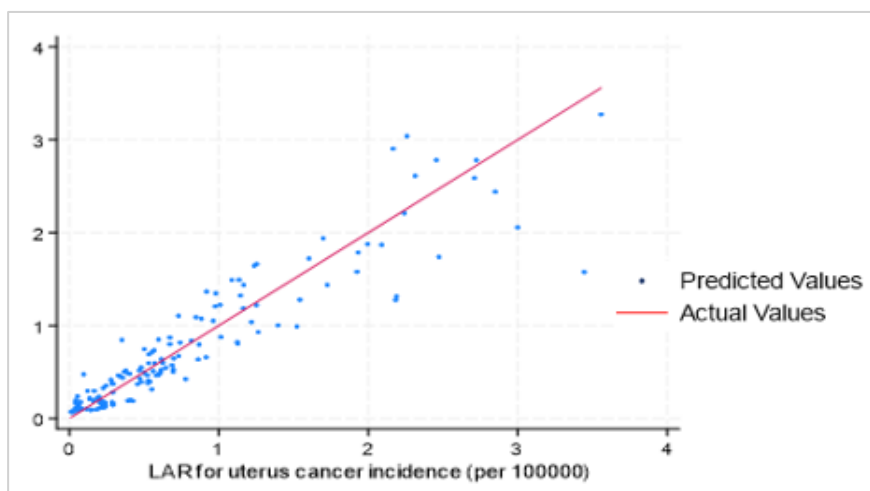


Figure III. 5: Two-way scatterplot with a linear regression line of LAR for liver cancer incidence



4) R command for computing LAR

```
library(dplyr)
```

```
LAR ESTIMATION
```

```
#beta.male <- 0.32
```

```
beta.female <- 1.4
```

```
gamma <- -0.3
```

```
c <- ifelse(Age.data<30, (Age.data-30)/10, 0) #c <- ifelse(test, yes, no) #if age<30 = age-30/10, age>30 = age
```

```
a <- if(Age.data<76){seq(from = Age.data+5, to = 80,by = 1)}else{Age.data+5}
```

```
a.start <- Age.data
```

```
eta <- (-1.4)
```

```
ERR.female <- beta.female*sv*exp(gamma*c)*((a/60)^eta)
```

```
#M calculation
```

```
lambda.M15 = 0.09
```

```
lambda.M20 = 0.64
```

```
lambda.M25 = 0.92
```

```
lambda.M30 = 1.5
```

```
lambda.M35 = 3.1
```

```
lambda.M40 = 6.5
```

```
lambda.M45 = 11.3
```

```
lambda.M50 = 18.5
```

```
lambda.M55 = 29.9
```

```
lambda.M60 = 45.6
```

```
lambda.M65 = 63.2
```

```
lambda.M70 = 86.7
```

```
lambda.M75 = 123.3
```

```
lambda.lung.M <- ifelse(between(a,15,19),lambda.M15, ifelse(between(a,20,24),lambda.M20,ifelse(between(a,25,29),lambda.M25,ifelse(between(a,30,34),lambda.M30
```

```
,ifelse(between(a,35,39),lambda.M35, ifelse(between(a,40,44),lambda.M40, ifelse(between(a,45,49),lambda.M45
```

```
,ifelse(between(a,50,54),lambda.M50, ifelse(between(a,55,59),lambda.M55, ifelse(between(a,60,64),lambda.M60
```

```
,ifelse(between(a,65,69),lambda.M65, ifelse(between(a,70,74),lambda.M70, lambda.M75))))))))))
```



```

M.female <- ERR.female*lambda.lung.M

#Se parameter in age range by gender
Se.female5 = 0.99965 #<1-19 years
Se.female6 = 0.99891
Se.female7 = 0.99446
Se.female8 = 0.99421
Se.female9 = 0.98616
Se.female10 = 0.98614 #20-44 years
Se.female11 = 0.98600
Se.female12 = 0.98781
Se.female13 = 0.95821
Se.female14 = 0.93886
Se.female15 = 0.90184 #45-69
Se.female16 = 0.85888
Se.female17 = 0.79194 #75-79
Se.female18 = 0.79194 #70-84
Se.female19 = 0.79194 #85+

age<- if(Age.data<76){seq(from = Age.data+5, to = 80,by = 1)}else{Age.data+5}
#Note that if e+5 = 80 is maximum cannot calculate for 76+ years, however age max can be 84 based on Se != 0

#do not vary, using at a.start
Se <- ifelse(a<1, Se.female1, ifelse(between(a.start,1,4),(Se.female2),ifelse(between(a.start,5,9),(Se.female3),ifelse(bet
ween(a.start,10,14),(Se.female4),
      ifelse(between(a.start,15,19),(Se.female5),ifelse(between(a.start,20,24),(Se.female6),ifelse(between(a.star
t,25,29),(Se.female7),
      ifelse(between(a.start,30,34),(Se.female8),ifelse(between(a.start,35,39),(Se.female9),ifelse(between(a.star
t,40,44),(Se.female10),
      ifelse(between(a.start,45,49),(Se.female11),ifelse(between(a.start,50,54),(Se.female12),ifelse(between(a.s
tart,55,59),(Se.female13),
      ifelse(between(a.start,60,64),(Se.female14),ifelse(between(a.start,65,69),(Se.female15),ifelse(between(a.s
tart,70,74),(Se.female16),
      ifelse(between(a.start,75,79),(Se.female17),ifelse(between(a.start,80,84),(Se.female18),(Se = Se.female1
9)))))))))))))))))

```

```

ifelse(a>80,Se==0.77,Se)

Sa <-ifelse(age<1,Se.female1, ifelse(between(age,1,4),(Se.female2),ifelse(between(age,5,9),(Se.female3),ifelse(between(age,10,14),(Se.female4),
  ifelse(between(age,15,19),(Se.female5),ifelse(between(age,20,24),(Se.female6),ifelse(between(age,25,29),(Se.female7),
    ifelse(between(age,30,34),(Se.female8),ifelse(between(age,35,39),(Se.female9),ifelse(between(age,40,44),(Se.female10),
      ifelse(between(age,45,49),(Se.female11),ifelse(between(age,50,54),(Se.female12),ifelse(between(age,55,59),(Se.female13),
        ifelse(between(age,60,64),(Se.female14),ifelse(between(age,65,69),(Se.female15),ifelse(between(age,70,74),(Se.female16),
          ifelse(between(age,75,79),(Se.female17),ifelse(between(age,80,84),(Se.female18),(Sa=Se.female19))))))))))))))
)))

ifelse(age>80,Sa==0.77,Sa)

LAR.female_function <- function(M.female,Sa,Se){

  LAR.female <- M.female*Sa/Se #LAR equation

  #print(LAR.female) #individual LAR

  LAR.sum <- sum(LAR.female) #LAR summation
  return(LAR.sum)
}

LAR.female_function(M.female,Sa,Se)

}} }

```

VITA

NAME	Mrs.Saowapark Poosiri
DATE OF BIRTH	24 March 1990
PLACE OF BIRTH	Phattalung, Thailand
INSTITUTIONS ATTENDED	Bachelor of Science in Radiological Technology, Faculty of Medical Technology, Mahidol University, 2011 Master of Science in Medical Imaging, Department of Radiology, Faculty of Medicine Chulalongkorn University, 2016
HOME ADDRESS	92 Phanangtung Sub-district, Khuan Khanun District, Phatthalung Province, Thailand 93150
PUBLICATION	Conference abstract 1. Evaluation of patient radiation dose and risk of cancer from CT examination (Oral presentation), IUPESM World Congress on Medical Physics and Biomedical Engineering, 2022. Online 2. Evaluation of the lifetime attributable risk of cancer from CT examinations in Thai population (Oral presentation), 21st South East Asian Congress of Medical Physics (SEACOMP) and 6th Pertemuan Ilmiah Tahunan Fisika Medis dan Biofisika (PIT-FMB) 2023, Indonesia Original article Poosiri, S., Krisanachinda, A. Khamwan, K. Evaluation of patient radiation dose and risk of cancer from CT examinations. Radiol Phys Technol, 2023. https://doi.org/10.1007/s12194-023-00763-w